Towards the activity
of the antimicrobial peptide PGLa
in cell membranes

Solid state ^{19}F-NMR studies of PGLa and magainin 2

Zur Erlangung des akademischen Grades eines

DOKTORS DER NATURWISSENSCHAFTEN
(Dr. rer. nat.)

der Fakultät für Chemie und Biowissenschaften der
Universität Karlsruhe (TH)

vorgelegte

DISSERTATION

von
Diplom-Biologe Marco Ieronimo
aus Baden-Baden

Dekan: Prof. Dr. Stefan Bräse

Referent: Prof. Dr. Anne S. Ulrich

Korreferent: Prof. Dr. Reinhard Fischer

Tag der mündlichen Prüfung: Montag, 4. Februar 2008

Not because it is difficult, we don´t dare to do it, but because we don´t dare to do it, it is difficult.

(Socrates)

Die vorliegende Arbeit wurde am Institut für Organische Chemie, Lehrstuhl Biochemie der Universität Karlsruhe (TH) unter der Leitung von Prof. Anne S. Ulrich im Zeitraum von November 2004 bis Dezember 2007 durchgeführt.

Acknowledgments

Ich erkläre hiermit wahrheitsgemäß, dass ich die vorliegende Arbeit selbstständig angefertigt und keine Hilfsmittel, außer den bereits angegebenen, benutzt habe. Diese Arbeit wurde weder an dieser, noch an einer anderen Hochschule als Prüfungsschrift eingereicht.

Karlsruhe, 19.12.2007

Table of contents

1 Motivation

Living organisms are constantly exposed to potentially harmful pathogenes (Reddy 2004). Evolutionary old endogenous peptides act as a first line defence. They are ubiquitous among all eukaryots and are one of the most important components of their innate immunity (Kamysz 2003). These antimicrobial peptides (AMPs) usually consist of 10 to 50 amino acids and exhibit an amphipathic spatial distribution of polar (usually cationic) and hydrophobic residues in their secondary structure. AMPs are assumed to interact with membranes of invaders according to their amphipathicity, selecting for example the negatively charged lipids of bacteria, and permeabilize their cellular membranes.

Such AMPs are promising compounds for the development of new therapeutics to treat the growing world problem of microbial resistance against conventional antibiotics. In particular, these AMPs have the potential not to be affected by the bacterial resistence mechanism (Otvos 2005; Reddy 2004). To modulate the activity of these AMPs in order to enhance their selectivity against bacteria, knowledge of their mechanism of action is crucial.

The α-helical peptides PGLa and magainin 2 from the African clawed frog *Xenopus laevis* show significant bactericidal, but low hemolytic activity (Soravia 1988). Synergy in action between these two peptides has been demonstrated (Westerhoff 1995). For each peptide separately and together as a synergetic pair, toroidal pore formation is proposed as an explanation of the permeabilizing activity. By solid state NMR spectroscopy, PGLa has been shown to adopt different alignment states in synthetic lipid bilayers, dependent on peptide concentration (Strandberg 2006; Glaser 2005) and presence of equimolar quantity of magainin 2 (Tremouilhac 2006a). These results were used to explain the effects of PGLa structurally.

Do these alignment states of PGLa (S, T and I) only occure in synthetic lipid bilayers or can they be identified in cell membranes of bacteria and eukaryots? How does the complexity of real biomembranes in terms of composition and thus phase behaviour influence the peptide alignment? Can real biomembranes be employed for solid state NMR investigations of that kind at all? To answer these fundamental questions for future investigations towards a clarification of the situation in vivo, the present study is a desicive contribution.

2   Theoretical background

2.1 Biological membranes

2.1.1 Functions

The cell is the fundamental unit of life for all organisms. The ability to regulate and coordinate vital biochemical processes is strictly bound to a cell. The function of a cell in turn is essentially connected to the occurrence and structure of biological membranes. In cells different types of membranes exist. All cells possess a cytoplasmic membrane that spatially defines the cell. The cytoplasmic membrane acts as a selective barrier for substances, separating the outside and the inside of the cell. It enables the cell to maintain a highly ordered chemical system. In eukaryotic cells additional intracellular membranes define compartments of specific function, separating reaction processes and maintaining defined physical and chemical environments. Membranes regulate the distribution of substances, carry enzymes for chemical reactions and energy conversions, and are involved in signal transductions and in recognition processes (Voet 2002; Alberts 2004; Nultsch 1996).

2.1.2 Composition

Despite their various functions, biological membranes possess a common structure principle (Voet 2002; Alberts 2004; Nultsch 1996). They are basically lamellar bilayers made up mainly of lipids and proteins. Lipids are a class of bio-amphiphiles that self-assemble in aqueous environments with their hydrophilic polar head groups directed to the surrounding medium and their hydrophobic tails forming the interior of the structure. Lipid bilayers of cells are usually 6 to 10 nm thick, depending on the length of the hydrophobic tails. According to the currently accepted fluid mosaic model (Singer 1972) the lipid bilayer of a membrane forms the fluid matrix in which proteins are either integrally or unilaterally embedded, or to which they are extrinsically associated. From a reductionist point of view the structural basis for each membrane is lipids forming fluid bilayers (Katsaras 2001).
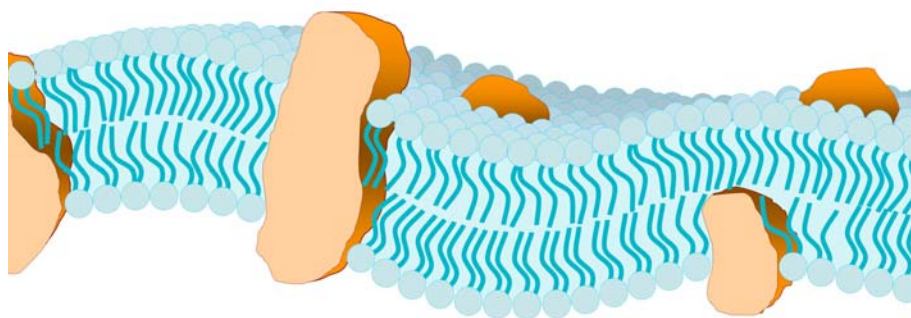
Figure 2.1 The Nicholson-Singer "fluid mosaic model". It is the standard conceptualization of membrane architecture. Lipids self-assemble to form bilayers as a matrix in which proteins are embedded.

Membranes differ significantly in their lipid composition as well as in their protein/lipid ratio (Evans 1991; Graham 1998; Hanke 1997). The exact composition of a biological membrane depends strongly on its origin, i.e. the organism, the organ or tissue, the type of cell and the type of membrane in a particular cell. Among the various lipid classes in biological membranes the most abundant are glycerophospholipids and sphingolipids (glycolipids) (Stryer 1999). Table 2.1 and Table 2.2 show examples for the variation in cytoplasmic membrane composition.

Table 2.1 Protein and lipid content of different cytoplasmic membranes as percentage of dry weight [% dw]. (Graham 1998; Hanke 1997; Afonin 2003a)

Source	Protein	Lipid
Bacillus (Gram-positive)	75	25
Micrococcus (Gram-positive)	70	30
Escherichia coli (Gram-negative)	75	25
Amoeba (Protozoa/Eukaryot)	54	42
Erythrocyte (Eukaryot)	49	44
Hepatocyte (Eukaryot)	50	50
Enterocyte (Eukaryot)	85	15
Myelin cell (Eukaryot)	20	80

Typically, the cytoplasmic membrane of prokaryots (*Bacteria* and *Archaea*) has a higher protein content compared to eukaryots (*Eukarya*). This is due to the fact that physiological processes, which are distributed over several compartments and membranes in eukaryots, e.g. the endoplasmatic reticulum, mitochondria or plastids, take place at the single membrane in prokaryots. Eukaryotic cell membranes typically contain sterols, e.g. cholesterol in animals and ergosterol in plants, but bacterial cell membranes do not. Bacterial membranes have a

3

higher content of glycerophospholipids, but only traces of glycolipids, which appear to be ubiquitous in the outer layer of animal cell membranes.

Table 2.2 Lipid composition of cytoplasmic membranes from human erythrocytes and bacterial protoplasts [% dw]. (Evans 1991)

Source	Phospholipids	Glycolipids	Cholesterol
Human erythrocyte	61	11	22
Bacterial protoplast	80 – 90	traces	0

Lipid head groups determine the charge of a membrane. Anionic phosphatidylglycerol and net uncharged phosphatidylethanolamin make up the highest percentage of glycerophospholipids in bacterial cell membranes. Animal cell membranes characteristically possess high amounts of net uncharged phosphatidylcholine. Typical phospholipids of cytoplasmic membranes are depicted in Figure 2.2.
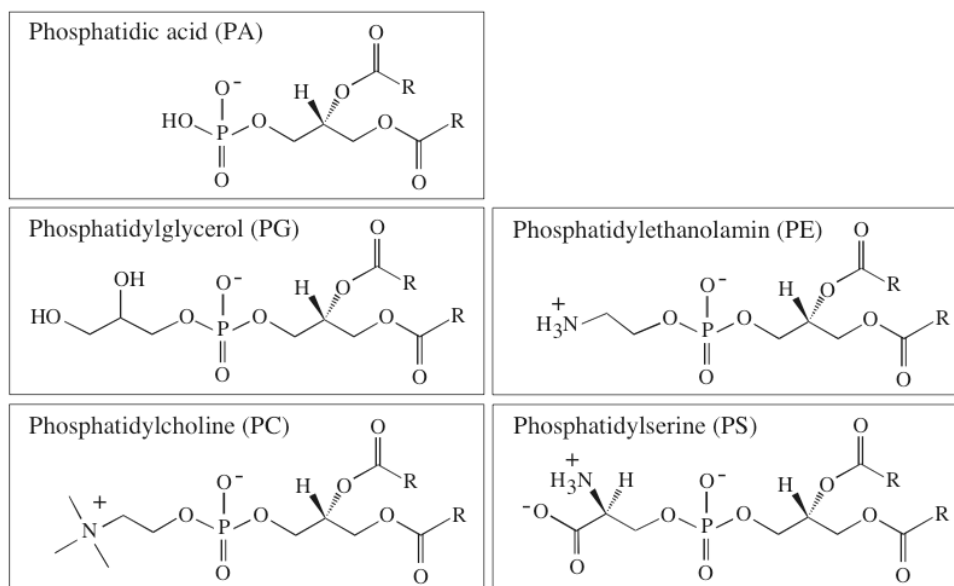
Figure 2.2 Typical phospholipids of cytoplasmic membranes and their charge at physiological conditions. R=acyl chains

The composition of hydrophobic acyl chains of phospholipids in biomembranes shows a significant diversity (Voet 2002; Yawata 2003; Denich 2003). Animal cell membranes contain high amounts of unsaturated fatty acids with up to 6 double bonds. Acyl chains are usually 16 to 24 carbon atoms in length, most common are 16 and 18 carbon atoms. Bacterial cell membranes contain only a low degree of unsaturated fatty acids, but are enriched in polyunsaturated ones. Their acyl chains are typically 12 to 24 carbon atoms in length, most

commonly 14 to 20. Additionally, Gram-positive bacteria, like *Bacillus* or *Micrococcus*, often possess unusual acyl chains like branched or cyclopropanated ones. Bacteria are known to adapt their cytoplasmic membrane lipid composition to the environmental conditions, like temperature, medium composition and the growth phase of a microbial culture. Modification of acyl chains or head group alters the packing of lipids within the bilayer and thereby its fluidity.

2.1.3 Asymmetry

Constituents of biological membranes are usually not distributed regularly, but exhibit lateral as well as transversal asymmetry.

Biological membranes contain a variety of regions containing specific proteins and lipids assembled to carry out specialized functions. These domains of distinct composition vary greatly in size as well as in life span (Tamm 2005; Somerharju 1999; Welby 1996; Lommerse 2004; Subczynski 2000).

Apical membranes of epithelial cells, cell-surface or cell-cell adhesion domains are among the largest and most stable cell membrane compartments (Tamm 2005; Subczynski 2000). The desmosome, a cellular organelle shared by two adhering cells, can be as large as 10 μm in diameter and the lifetime of the assembly may be longer than the doubling time of the cell in the range of hours.

The cytoskeleton contributes to partitioning of a cell membrane into compartments of 30 to 230 nm in size (Tamm 2005; Lommerse 2004; Voet 2002). The part of the cytoskeleton linked to the membrane by actin-associated proteins is actually considered part of the cell membrane. The skeleton forms a diffusion barrier for integral proteins throughout the cell membrane ("fence"). Other integral proteins can be anchored to the skeleton ("pickets") and thereby effectively confine virtually all membrane components, even phospholipids in the outer layer.

"Raft domains" are transient and highly dynamic microdomains of sphingolipids and cholesterol (Tamm 2005; Voet 2002; Alberts 2004). They represent a time-dependent phase separation in the fluid lipid bilayer with their size varying in the range of nanometers. They serve to accumulate and organize specific proteins for subsequent vesicle transport or signal transduction processes, for instance specific receptors like GPI-anchored receptors (glycosyl-phosphatidylinositol), or cytoplasmic signaling molecules, anchored to the cytoplasmic layer of the cell membrane via saturated alkyl chains.

Oligomers of proteins, like dimers of G-protein-coupled proteins, or proteins specifically interacting with surrounding lipids via polar head groups or hydrophobic acyl chains contribute to the heterogeneous distribution of membrane constituent on the smallest scale (Subczynski 2000; Voet 2002).

Transbilayer lipid asymmetry has been observed in *Bacteria* and *Eukarya*, in cytoplasmic and intracellular membranes (Sandra 1978; Herbette 1984). It is actively established and maintained via ATP-dependent transbilayer lipid transport. In *Bacteria*, membrane lipids play an essential metabolic function, as they are employed as transporters for components in the synthesis of polymers outside the cytoplasmic membrane, like peptidoglycan (Schlegel 1992) or lipomannan (Pakkiri 2004; 2.1.7). In erythrocytes, improved membrane mechanical stability is achieved by transbilayer lipid asymmetry and interaction of phosphatidylserine with the cytoskeleton (Manno 2002). The asymmetric distribution of lipids in human erythrocyte cell membranes is shown in Table 2.3.

Table 2.3 Asymmetric distribution of lipids in thee inner and outer leaflet of human erythrocyte cell membranes [% dw]. (Graham 1998)

Type of lipid	Inner leaflet	Outer leaflet
Sphingomyelin	17	83
Phosphatidylcholine	26	74
Phosphatidylethanolamine	77	23
Phosphatidylserine	95	< 5
Glycolipids	< 5	95

Due to the heterogeneous composition and the irregular distribution of constituents, real biomembranes cannot be described as a homogeneous system with bulk phase physical properties (Welby 1996).

2.1.4 Lipid polymorphism

The ratio between the cross-sectional area of a lipid head group and its acyl chain determines its overall molecular shape and classifies it as bilayer or non-bilayer forming lipid. Depending on the molecular shape, the supramolecular structure formed in solution by an isolated type of lipid shows a characteristic morphology (polymorphism) (Cullis 1986, Seddon 1990; Katsaras 2001).
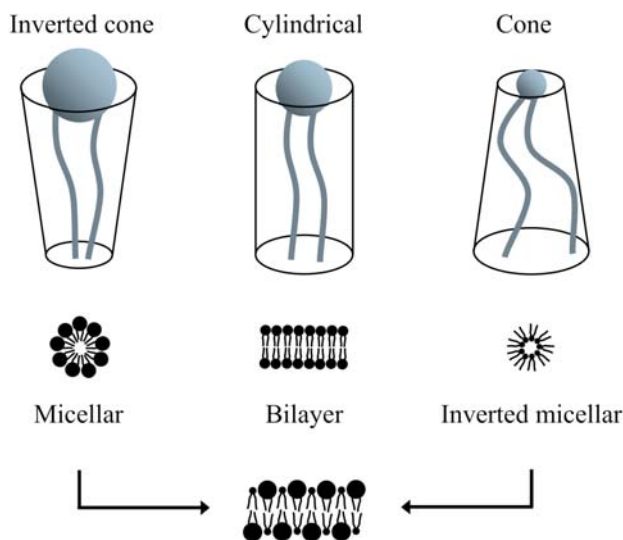
Figure 2.3 Molecular shapes of lipids and respective structures of lipid assemblies in aqueous solution. A bilayer can be formed by mixtures of cone shaped and inverted cone shaped lipids (complementary effect). (See text for a further specification of the phases exhibited by non-bilayer forming lipids either in water (type I) or in oil (type II).)

Bilayer forming lipids possess overall cylindrical molecular shape and in aqueous solution, i.e. oil-in-water (type I), result in a stable lamellar (L) bilayer conformation (L_I phase). Non-bilayer forming lipids possess conical overall molecular shape with either their head group or acyl chains having a bigger cross-sectional area. Non-bilayer forming lipids in solution assemble to micellar (M) or hexagonal (H) structures. The inverted hexagonal phase (H_{II}) (water-in-oil) represents laterally stacked cylinders, while the hexagonal phase (H_I) (oil-in-water) can be present as individual cylindrical micelles. PE is abundant in cell membranes of eukaryots and Gram-negative bacteria, and is an example of a lipid that can spontaneously form the inverted hexagonal phase (Seddon 1990).

Within the lamellar phase, several temperature-dependent (thermotropic) phases are discriminated. Two important types of lamellar phase are the gel phase (L_β) and the fluid phase (L_α). L_β is characterized by highly ordered all-trans acyl chains, which are tilted with regard to the membrane normal. The lateral diffusion of lipids here is relatively slow. Upon an increase in temperature above a melting point (the transition temperature T_m), order and packing of acyl chains is reduced and mobility increased. Acyl chains are present in cis-conformation. This state is the fluid lamellar phase L_α. The volume of the hydrophobic core is increased, and the bilayer thickness is reduced, compared to L_β. Many inter-related factors control membrane fluidity and thus the value of T_m. It is primarily related to lipid packing within the membrane. Lipid packing is determined by shape, which in turn is generally

determined by the balance of attractive forces between the acyl chains due to the hydrophobic effect and the preference of the hydrophilic head groups to associate with water. A higher degree of acyl chain unsaturation results in higher fluidity and lower T_m. Shorter acyl chains, on the other hand, allow for higher ordering of lipids and result in less fluidity and higher T_m. However, there are other factors which may affect membrane packing of lipids, such as water, protein and carbohydrate content. Temperature, pH, presence of cations or ionic strength will also affect packing of phospholipids (Denich 2003).

The biologically relevant lipid phase is the fully hydrated high-temperature fluid state L_α (Katsaras 2001; Denich 2003). The local presence of non-bilayer forming lipids, however, which modify many of the properties of the bilayer, like thickness, permeability and deformability, appears to be of fundamental relevance for many processes taking place in, on, or through biomembranes. Modification of the properties of the lipid matrix has been shown to affect the function and activity of membrane proteins, for instance of mitochondrial proteins, of Ca-ATPase or of the lactose permease of *Escherichia coli* (Seddon 1990; Zhang 2000).

Under normal physiological conditions, the majority of phospholipids in the bacterial membrane are bilayer forming lipids in the lamellar fluid phase L_α. Bacterial cytoplasmic membranes can compensate for the alteratin of growth conditions by homeophasic adaptation, for instance by adjustment of lipid composition, so that the membrane can remain in the fluid phase even as the environment changes. On the other hand, *Escherichia coli* and *Acholeplasma laidlawii* have been shown to tolerate a wide range of fluidities. Up to 50% and 80 to 90% of their lipids, respectively, may be in the gel phase without affecting their growth (Denich 2003).

Sterols are essential constituents of eukaryotic membranes, with cholesterol being the most common one in animal membranes (Katsaras 2001; Voet 2002). On the one hand, the rigid sterol system reduces fluidity of membranes as it inhibits the mobility of acyl chains upon increase in temperature. On the other hand, sterols inhibit ordering of acyl chains upon decrease of temperature, thereby broadening the phase transition. Temperature variations would otherwise alter the thickness of the membrane dramatically.

2.1.5 Extramembraneous structures

Bacteria usually possess a rigid cell wall outside the cell membrane, counterbalancing the turgor pressure and protecting the cell from osmotic lysis. Cell membrane plus cell wall are referred to as the cell envelope. The cell wall consists of peptidoglycan, a heteropolymere, in

which linear chains of alternating N-acetylglucosamine and N-actylmureic acid are cross-linked by group- and strainspecific, often unusual, amino acids (Madigan 2001; Voet 2002).
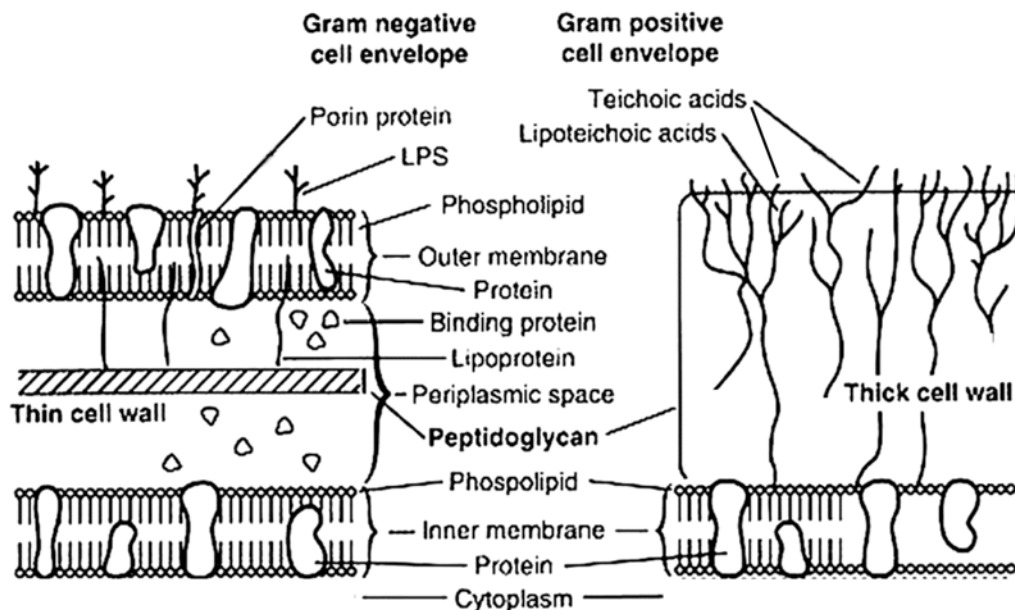
Figure 2.4 The cell envelope of Gram-negative (left) and Gram- positive bacteria (right).
(Modified from Baron 1991)

In Gram-positive bacteria the cell wall consists of multiple layers together making up about 25 nm in thickness. Characteristic for Gram-positive bacteria is the occurrence of extracellular anionic polymers (Neuhaus 2003; Sutcliffe 1991; Kennedy 1974). Typically these are teichoic acids (TA), contributing to the cell wall mass with up to 10 %. They are phosphorus-containing polymers with 16 to 40 units of ribitol or glycerol and can be D-adenylated and/or glycosylated. TAs are usually covalently bound to the peptidoglycan (wall teichoic acids – WTA) or are associated with the membrane, anchored to a glycolipid (lipoteichoic acids – LTA). They possess cation-binding capabilities and are involved in maintaining metal cation homeostasis, thus may play a key role in the osmotic stability of the cell. They assist in the trafficking of ions, nutrients, proteins, and antibiotics. They can also direct enzymes which function on the cell periphery to the sites of cell wall biosynthesis, like autolytic enzymes. Occurring in the fimbriae on the outside of the cell they can be involved in adhesion, for instance to epithelial cells allowing colonization of the throat, e.g. by the group A *Streptococcus*.

Not all Gram-positive bacteria possess conventional LTA and WTA. Those that lack these polymers generally have functionally analog polyanions. The first Gram-positive bacterium found to lack TA was *Micrococcus luteus* (formerly *M. lysodeikticus*) (Sutcliffe

1991; Owen 1975). *M. luteus* possesses lipomannan, a polymer of mannosyl residues being esterified with succinyl groups to approximately 25 %.

Succinic acid
|
$(mannose)_n$—O—CH_2
|
CH—O—C(=O)—R^1
|
CH_2—O—C(=O)—R^2
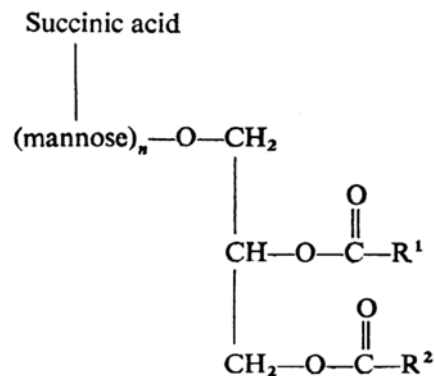
Figure 2.5 Structure of lipomannan of *M. luteus*. Mannose units (n=52-70) are succinicated to approximately 25 % (Powell 1975)

In Gram-negative bacteria the thickness of the cell wall is about 3 nm. The cell wall is located in the extended periplasmatic space between the cell membrane (inner membrane) and an additional complex outer membrane. The outer leaflet of the outer membrane contains mostly lipopolysacccharides (LPS). LPS consist of the Lipid A and an oligosaccharide component, which is highly specific for individual bacterial groups. LPS appear to render bacteria resistant to an attack of leucocytes in a host, as long as antibodies are not involved. Of biological relevance is the endotoxic activity of LPS in animals upon bacterial lysis (Voet 2002; Schlegel 1992).

Contrary to other *Eukarya*, animal cells lack cell walls. However, animal cell membranes possess further structures extrinsic to the lipid bilayer of the cytoplasmic membrane. Virtually all cells possess a highly developed glycocalyx (Voet 2002). This is a densely packed, highly mobile diffuse layer of heterogeneous composition, consisting of oligosaccharides bound to lipids in the outer layer of the membrane and to the extracellular site of integral proteins. The layer can be up to 140 nm in thickness. The glycocalyx is, in general, involved in intercellular communication and recognition processes.

The boundary of a cell usually goes beyond the plain structure of a lipid bilayer with embedded proteins. These extracellular structures provide initial sites of interaction or themselves are potential targets for antimicrobial peptides (Papo 2003).

2.1.6 The cell membrane of human erythrocytes

Erythrocytes (Figure 2.6) are probably the best-established cell system and the common model for eukaryotic cell membranes. First, they are of clinical interest. Second, their membranes are comparatively easy to isolate. They occur as separate, highly differentiated cells and when they are released into the blood stream, they no longer contain any organelles nor nucleic acids. They are highly specialized for the transport of O_2 and CO_2, being filled almost entirely with hemoglobin (90 % of their dry weight) (Begemann 1993).
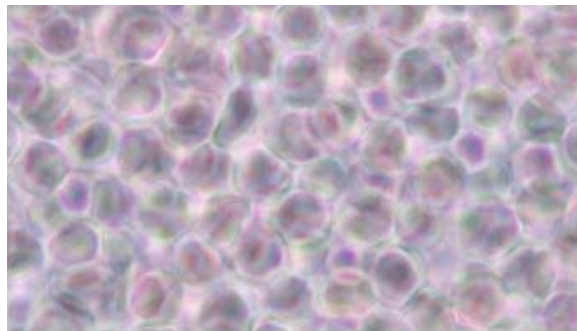
Figure 2.6 Intact human erythrocytes. Undiluted suspension from a blood bag.

The protein to lipid ratio of their membrane is about equal (Table 2.1). 60 to 80 % of their membrane lipids are phospholipids, up to 25 % cholesterol and up to 10 % glycolipids (Table 2.2) (Graham 1998; Evans 1991).

The erythrocyte membrane is transversally asymmetric (2.1.3), containing the zwitterionic net neutral SM and PC predominantly in the outer membrane leaflet of the bilayer. Zwitterionic PE and the net negatively charged PS are present predominantly in the inner bilayer leaflet. Glycolipids are almost entirely (95 %) located in the outer leaflet. Phosphatidylinositol (PI) is only present in low amounts and entirely located in the inner leaflet (Begemann 1993; Voet 2002; Graham 1998).

The erythrocyte membrane contains a wide variety of proteins. The number of protein molecules at the membrane interior outnumbers that of the exterior (Zwaal 1976). Glycoproteins are arranged such, that their hydrocarbon chains point outwards (2.1.5).

For the preparation of erythrocyte membranes (*ghosts*), the cells can be exposed to the hypotonic medium directly. Water molecules follow the gradient of solutes (hemoglobin) inside the cell and cause it to swell. In NaCl solution, lysis begins below 0,5 % (Baake 1994; Begemann1993). Increasing its volume by a factor of 1,5, the cell becomes leaky and solutes equilibrate across the cytoplasmic membrane (Schwoch 1973). The membrane reseals for

larger molecules like hemoglobin, but stays permeable for smaller compounds like ions (Baake 1994; Begemann1993; Schwoch 1973). Serveral types of *ghosts* have been described, depending on their purity with regard to their residual hemoglobin and their permeability (Dodge 1963; Ting-Beall 1981). Factors like osmolarity, pH and temperature of lysis solution and ratio of the lysis solution to erythrocyte volume influence properies of *ghosts* and have been systematically investigated (Dodge 1963).

2.1.7 The cell membrane of *Micrococcus luteus*

Micrococcus luteus (Figure 2.7) is a spherical Gram-positive bacterium. It forms yellow pigmented colonies on agar plates, is strictly aerobic, non-sporulating and arranged in small clusters (tetrades). It can be isolated from soil, water and dust particles, is a regular inhabitant of the human skin and various mucosae and is involved in food rotting (Madigan 2001; Schlegel 1992). *M. luteus* is generally considered to be non-pathogenic, however, it may cause skin infections in immunocompromised persons and even rare cases of prosthetic valve endocarditis are described for this bacterium (Seifert 1995; Durst 1991). Therefore, *M. luteus* must be considered a nosocomial pathogen or opportunist.

Figure 2.7 *Micrococcus luteus* ATCC 4698. Cells arranged as a tetrade.

The ratio of protein to lipid in the cell membrane of *M. luteus* is about 7 to 3 (Table 2.1). The lipids comprise up to 70 % negatively charged PG predominantly located in the outer layer and about 30 % dimannosyldiacylglycerol (DMDG) symmetrically distributed between both leaflets (de Bony 1989; Graham 1998).

However, cell cycle-dependent changes in the transbilayer distribution of the two major lipids PG and DMDG in cell membranes of *M. luteus* could be observed by application of synchronized cultures (Welby 1996). The distribution shows least heterogenity during cell growth and maximum heterogeneity during cell division. It is proposed, that DMDG together with other mannolipids, is involved in the transportation of mannose from the cytoplasm to

the external surface of the cytoplasmic membrane and the assembly of lipomannan there (Pakkiri 2004).

M. luteus belongs to the constantly growing group of bacteria known to lack TA. Most of them still possess phosphate-containing anionic cell wall components (Neuhaus 2003; Sutcliffe 1991). Micrococcal lipomannan (Figure 2.5), however, even lacks phosphate. Analytical studies on a highly purified preparation of the lipomannan revealed that it was composed of mannose, succinate, fatty acid, and glycerol in a ratio of 50/5/2/1 (Pless 1975).

To prepare cell membranes from *M. luteus* by osmotic lysis in a similar manner as described for erythrocytes, the thick cell wall first needs to be removed by lysozyme. Lysozyme hydrolyzes $\beta(1-4)$-linkages between N-acetylmuraic acid and N-acetylglucosamine residues in peptidoglycans. The activity of lysozyme is a function of pH and ionic strength, being active over a broad range of pH from approximately 5,0 to 9,0 (Banerjee 1973; Banerjee 1975). *M. luteus* shows a high sensitivity to lysozyme if grown under appropriate conditions (Prasad 1965). Since the sensitivity of bacteria towards lysozyme depends on numerous factors (Atrih 1999; Hayashi 1973; Araki 1972), careful conditioning of *M. luteus* is essential for the success of cell wall removal. Resistance to lysozyme increases, for instance, with the degree of peptidoglycan cross-linking. This in turn, is influenced by the growth phase, for instance, and is markedly increased in the stationary phase. However, in a non-synchronized culture, within each growth phase cells at various states of the cell cycle are present, resulting in a significant amount of lysozyme-resistant cells. Furthermore, modifications at various sites of peptidoglycan are known to reduce the sensitivity to lysozyme, e.g. de-N-acetylation or O-acetylation. These, in turn, may depend on the composition of the growth medium.

2.2 Antimicrobial peptides (AMPs)

2.2.1 General properties

Small cationic amphipathic peptides exhibiting antimicrobial activity are found in virtually all organisms throughout the whole phylogenetic tree (Hancock 1999; Epand 1999; Wu 1999). These antimicrobial peptides (AMPs) are typically 10 to 50 amino acids in length and possess positive charge mainly due to Lys, Arg and His residues clustered on one face of the molecule, with hydrophobic residues on the opposing face. Apart from those common features, AMPs vary significantly in length, sequences and secondary folds (Huang 2000; Matsuzaki 1999; Toke 2005; Papo 2003). Various approachs exist to classify them, one grouping them as (a) peptides that form α-helical structures, (b) peptides rich in cysteine residues forming intramolecular disulfide bonds, (c) peptides that form β-sheets, (d) peptides rich in a particular regular amino acid such as His, Arg and Pro and (e) peptides composed of rare and modified amino acids (Kamysz 2003; Reddy 2004).

To date more than 800 have been identified in nature (Bechinger 2006; Hancock 2006). They are listed in the Antimicrobial Sequences Database at the University of Triest http://www.bbcm.univ.trieste.it/~tossi/antimic.html. Representative AMPs with their proposed structures in membraneous or membrane-mimicking environments are listed in Table 2.4.

Table 2.4 Brief selection of AMPs with their primary sequence, supposed secondary structure and origin.

Peptide	Sequence	Structure	Origin	References
Gramicidin A	fV^{d}GA^{d}LA^{d}VV^{d}VW^{d}LW^{d}LW^{d}LWEt	β-helix	*Aneurinibacillus migulanus*	Wallace 2000 Berditsch 2007
Gramicidin S	cyclo-(VOL^{d}FP)$_2$	β-sheet	*Aneurinibacillus migulanus*	Prenner 2005 Berditsch 2007
Cecropin A	KWKLFKKIEKVGQNIRDGIIKAGPAVAVVGQ ATQIAK-CONH$_2$	α-helix	*Hyalophora cecropia*	Sato 2006
Melittin	GIGAVLKVLTTAGLPLISWIKRKRQQ-CONH$_2$	α-helix	*Apis melifera*	Sato 2006
Magainin 2	GIGKWLHSAKKFGKAFVGEIMNS	α-helix	*Xenopus laevis*	Hara 2001
Buforin 2	TRSSRAGLQWPVGRVHRLLRK	α-helix	*Bufo bufo gargarizans*	Park 2000
Histatin 5	DSHAKRHHGYKRKFHEKHHSHRGY	α-helix	*Homo sapiens*	Helmerhorst 1997

^{d} – D-enantiomer
f – Formyl
Et – Ethanolamine
O – Ornithine

In *Eukarya* AMPs are typically derived from genetically coded precursors and may undergo common post-translational modification. In *Bacteria*, AMPs may be drastically modified, as they may be produced or processed non-ribosomally by multifunctional enzymes. They may contain unusual or non-proteinogenic amino acids like Ornithin and D-enantiomers of amino acids, or moieties derived from amino acids (Hancock 2006; Hancock 1999; Toke 2005).

In animals AMPs appear to be key components of the innate immunity and constitute a primary defense system against invading microorganisms. They are produced, stored and secreted in exposed tissues or synthesized upon stimulation (Matsuzaki 1999; Wu 1999). However, the antimicrobial activity of AMPs from mammals is rather weak, and the modulation of the immune response by these peptides may be an important factor (Hancock 2006).

2.2.2 Targets

In general, the mechanism of antimicrobial action of AMPs is not very well established and remains a matter of controversy. There is, however, a consensus that most AMPs interact with the lipid bilayer of cell membranes and possess membrane perturbing and even disrupting potential (Reddy 2004; Epand 1999; Wu 1999). The amphipathic structural arrangement of AMPs plays an important role in this mechanism as modification of structural parameters like peptide helicity, hydrophobicity, hydrophobic moment, peptide charge and the ratio of the hydrophobic/hydrophilic domain modulate interaction with and the degree of perturbance of membranes (Dathe 1999; Dathe 1996).

High amounts of anionic polymers on the cell surface and of anionic phospholipids in the cell membranes of bacteria provide a ready explanation for the peptide specificity, as cationic AMPs will be preferentially accumulated in the cell wall and bind to negatively charged bacterial membranes, in contrast to predominantly zwitterionic amphiphiles in mammalian cell membranes (Epand 1999; Hancock 2006; Reddy 2004). Modification of the net negative charge of the bacterial cell surface by addition of positively charged residues, helps bacteria to avoid being killed by antimicrobial peptides. This can be done for instance by esterification of teichoic and lipoteichoic acids with D-Ala, by incorporation of PE into the cell membrane or by addition of the cationic amino acid lysine to the negatively charged PG as in *S. aureus* (Pietiainen 2005; Cao 2004; Ganz 2001).

However, there is uncertainty as to how the membrane perturbation itself is related to the antimicrobial activity (Epand 1999). There is not always a simple correlation between the charge of a peptide and its antimicrobial activity, nor between its ability to permeabilize membranes and its antimicrobial activity (Dathe 1999; Wu 1999). Effects on membranes may

simply be the manner by which these peptides enter the cell to reach an alternative target (Epand 1999). For instance, buforin 2 (Table 2.4) was demonstrated to kill bacteria by binding to nucleic acids (Otvos 2005). It penetrates the membrane, but does not permeabilize it. It was found to accumulate in the cytoplasm. In contrast, magainin 2 (Table 2.4 and 2.2.4.2) remains associated with the inner leaflet of the lipid bilayer of artificial membranes after translocation (Park 2000).

For an increasing number of AMPs, complex activities are shown. On the one hand, they appear to have other mechanisms than membrane perturbance to kill bacteria (Reddy 2004). For instance, it has been hypothesized, that bovine seminalplasmin activates the autolysis cascade in bacteria. Another example is PP-39, that has been shown to inhibit protein synthesis and to induce degradation of proteins required for DNA synthesis. On the other hand, apart from their direct cytotoxic activity, AMPs appear to regulate the innate immunity of the host (Mookherjee 2007; Kamysz 2003), selectively enhancing or altering the host defence mechanism without targeting the pathogen directly. The above mentioned PP-39, for example, acts as a chemoattractant for phagocytes. Defensins influence the production of cytokines.

Even in cases when the bacterial cell membrane itself may be the primary target of AMPs, secondary effects apart from leakage as the direct cause for cell death, may be difficult to evaluate (Pietiainen 2005). The natural membrane-active cationic α-helical human AMP LL-37 from the cathelicidin family is assumed to disrupt membranes by a toroidal pore (2.2.3). For *Bacillus subtilis*, however, a rather complex stress response to LL-37 could be shown, including the activation of several signal transduction pathways at a subinhibitory concentration. It was hypothized that gene activation was stimulated by the interaction with the cell membrane surface and the cell wall, rather than deeper effects inside the membrane. The applied amount of an AMPs needs to be considered, as effects at low concentration may differ from effects at high concentration, where cell lysis becomes dominant (Kamysz 2003).

Toxicity against eukaryotic cells can be significant for some AMPs and may pose severe difficulties when thinking about a clinical application of AMPs. Hemolytic activity, being a direct result of membrane perturbance, seems to be primarily related to hydrophobic interactions between AMPs and lipids (Dathe 1999; Toke 2005).

2.2.3 Modes of interaction with lipid membranes

The model explaining the membrane-perturbing activity of most AMPs is the Shai-Matsuzaki-Huang (SMH) model (Zasloff 2002; Huang 2000; Matsuzaki 1999; Shai 1999).

This model was initially proposed for magainin 2 describing the formation of transmembrane (toroidal) pores. The described stepwise membrane perturbance, however, is applicable on most AMPs.

In an initial step, AMPs bind to a membrane in the lipid head group region according to their amphipatic properties (Figure 2.8 upper). Hydrophilic cationic residues are directed towards the surrounding medium, hydrophobic residues are inserted into the core of the membrane. This surfacial alignment is supposedly functionally inactive (Matsuzaki 1999; Huang 2000). After reaching a threshold concentration, peptide perturbation of the membrane occurs. Several complex and controversial mechanisms describe the permeabilizing and disrupting effects. Three cooperative mechanisms are illustrated in Figure 2.8 and described below.
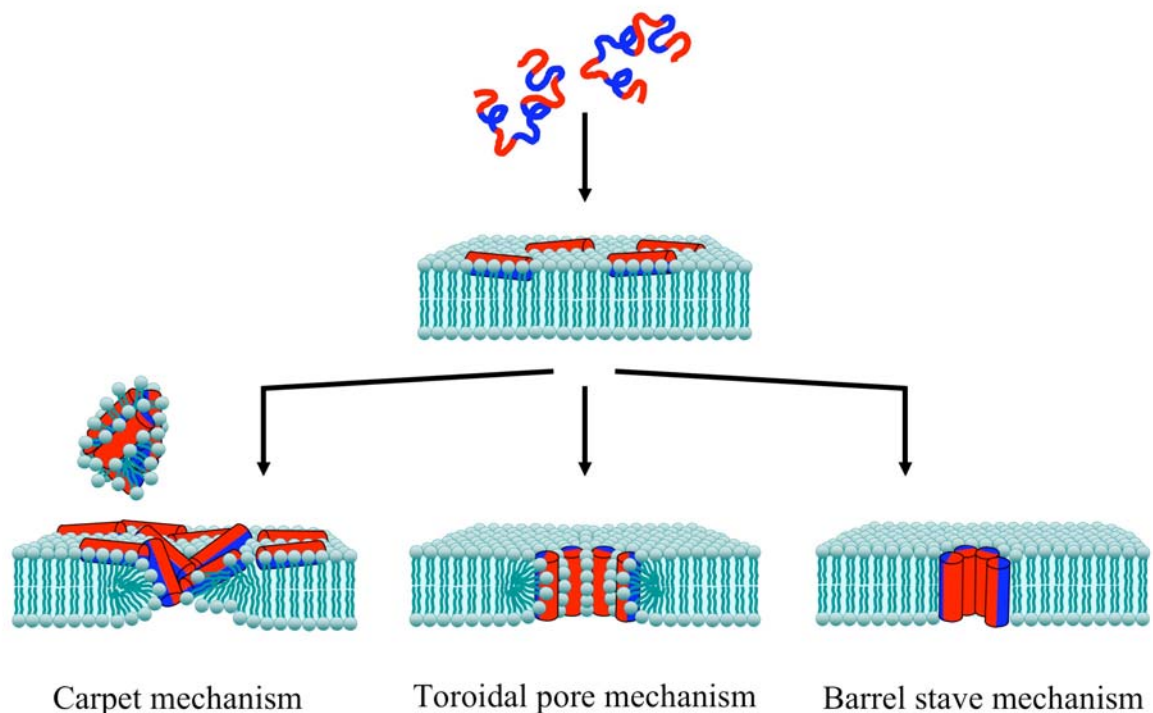
Figure 2.8 The Shai-Matsuzaki-Huang (SMH) model describes the activity of AMPs as a stepwise event. First, the AMP binds to the membrane surface. When a threshold concentration is reached, membrane perturbance occurs. Three cooperative permeabilization mechanisms are illustrated (see text below). In this figure α-helical AMPs are depicted as cylinders with their hydrophilic (charged) and hydrophobic faces coloured in red and blue, respectively.

1.) The *carpet mechanism* describes the disruption of the membrane at high local peptide concentrations (Shai 1999). The presence of negatively charged lipids is important for a peptide carpet to form, as they help to reduce the repulsive electrostatic forces between positively charged peptides. High local peptide concentrations can be achieved, when cationic

peptides phase-separate into domains rich in acidic phospholipids (Bechinger 1999). This mechanism is used to describe the mode of action of dermaseptins.

2.) The *barrel stave* or *transmembrane helical bundle* is the classical picture to explain the formation of pores. Above a threshold concentration peptides aggregate and align to an inserted state (Shai 2000; Matsuzaki 1999). Discrete openings are proposed to form, with the hydrophobic face of the peptide interacting with the non-polar lipid acyl chains and the hydrophilic face of the peptide forming the interior of the pore (Toke 2005). This mechanism is observed predominantly for peptides where not too many cationic residues will accumulate in the highly restricted volume of the pore interior (Bechinger 2006; Bechinger 1999). Alamethicin is assumed to form this type of pore (Yang 2001).

3.) The *wormhole-* or *toroidal pore mechanism* is an extension of the transmembrane helical bundle. To relieve the bilayer from unfavourable stress induced by the accumulation of peptide molecules in the outer leaflet, the layers bend continuously from one membrane leaflet to the other like the inside of a doughnut (Toke 2005). Peptides translocate stochastically to the inner leaflet (Matsuzaki 1995b; Matsuzaki 1999). Negatively charged phospholipid head groups together with positively charged peptide chains line the wall of the pore to reduce repulsive interactions due to the high positive charge-density of the peptides (Matsuzaki 1996; Bechinger 2006). Such a pore structure was first proposed for melittin and magainin (Yang 2001; Tamm 2005) upon the observation that magainin induces rapid lipid flip-flop coupled with pore formation (Matsuzaki 1996). Formation of transmembrane pores is a transient event. Translocation of peptide from the outer leaflet to the less populated inner leaflet reduces membrane stress, slowing down channel formation and leading to a deactivation of the pore (Matsuzaki 1995b). The lifetime of a pore is reduced with increasing positive charge of the involved peptide (Matsuzaki 1999).

2.2.4 Antimicrobial peptides used in this study

Amphibian tissues are an abundant source of bioactive peptides and amines. Many of them are strikingly similar or identical to mammalian hormones and neurotransmitters. Several such peptides exhibit a broad spectrum of antimicrobial and membrane perturbing activites (Dockray 1975; Andreu 1985; Sures 1984; Gibson 1986; Moore 1991; Soravia 1988).

Two of these peptides are Peptidyl-glycine-leucine-carboxyamide (PGLa) and magainin 2 of the South African clawed frog *Xenopus laevis*, which were employed in this study.

2.2.4.1 Peptidyl-glycine-leucine-carboxyamide (PGLa)

Peptidyl-glycine-leucine-carboxyamide (PGLa) is a linear peptide of 21 amino acid residues (GMASKAGAIAGKIAKVALKAL-NH$_2$). It is basic, carrys five positive charges (four lysines and one charge at the N-terminus) and has a high amount of hydrophobic residues, especially alanines. In aqueous solutions it has no well-defined secondary structure, but adopts an amphipathic α-helical structure, demonstrates for the residues 6 to 21, upon binding to lipid bilayers (Bechinger 1998; Wieprecht 2000). A helical wheel representation is shown in Figure 2.9.

GMASKAGAIAGKIAKVALKAL-NH$_2$ GIGKFLHSAKKFGKAFVGEIMNS
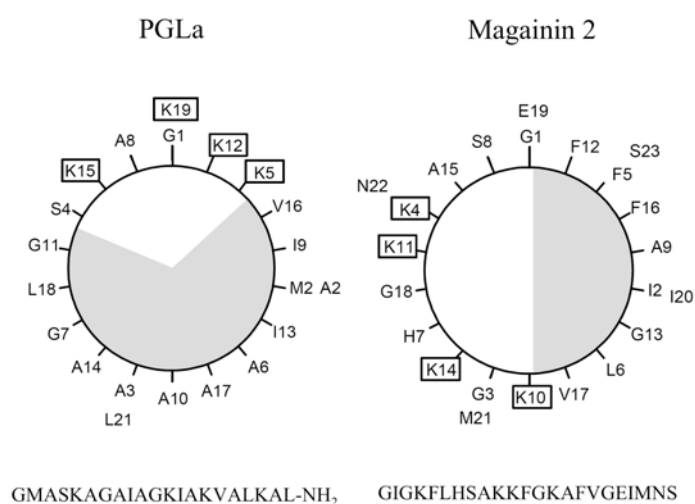
Figure 2.9 Helical wheel representations and sequences of PGLa and magainin 2. Hydrophobic faces of the helices are shown in grey, cationic residues are boxed. PGLa has an amidated C-terminus (modified from Tremouilhac 2006a).

PGLa was originally found in the skin secretion of the South African clawed frog *Xenopus laevis* (Hoffmann 1983; Andreu 1985), subsequently also in its gastrointestinal system (Moore 1991). Its direct precursor, from which it is produced by proteolytic cleavage, is the 24 amino acid intermediate PYLa, which originates from a 64 amino acid long parent polypeptide. Together with a number of other peptides produced from the xenopsin-, caerulein- and PGLa-precursor families, PGLa is stored in the secretory vesicles in the granular glands (Gibson 1986; Giovannini 1987). Xenopsin, caerulein and PGLa are assumed to derive from genes representing different members of the same gene family (Sures 1984). Xenopsin shows similarity to mammalian neurotensin. In the skin, these peptides are secreted especially upon stress, suggesting a defensive function (Giovannini 1987), presumably against predators, as PGLa was proposed to serve as a permeability factor, that could facilitate the uptake of highly active hormones through mucuous membranes and thereby

make the skin secretion of *X. laevis* very effective (Andreu 1985). In the stomach, active control over bacterial growth was proposed, as *X. laevis* swallows its prey intact and stores it for some time before digestion begins (Moore 1991).

PGLa exhibits significant broad spectrum antibacterial activity and was shown to induce osmotic lysis on several protozoa, but possesses negligible hemolytic activity. It was proposed that its mechanism of action could involve the formation of transmembrane channels (Soravia 1988).

PGLa was shown by solid state NMR to undergo a concentration-dependent realignment at ambient temperature in fluid phase synthetic lipid bilayers consisting of dimyristoylphosphatidylcholine (DMPC) and dimyristoylphosphatidylglycerol (DMPG) at the lipid molar ratio of 3 to 1 (Glaser 2004; Glaser 2005; Strandberg 2006) (Figure 2.10). PGLa was shown to reside in a peripherally-bound surface alignment (S-state) at the low peptide to lipid ratio (P/L) of 1/200 and to adopt a tilted alignment (T-state) at a high P/L ratio of 1/50. Upon realignment the C-terminus of the helix immerges into the hydrophobic core of the lipid bilayer. PGLa in the T-state was suggested to form antiparallel dimers.
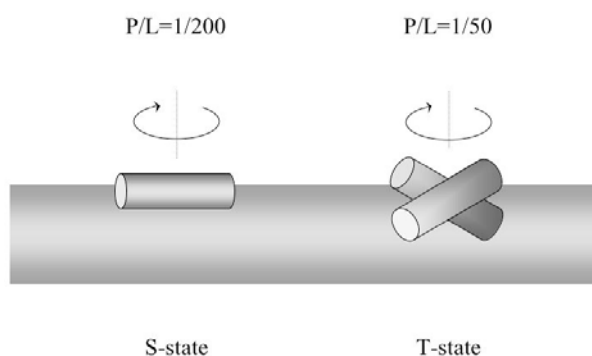
Figure 2.10 Concentration-dependent realignment of PGLa in oriented lipid bilayers (see text). Peptide helices are shown as cylinders. Arrows above indicate rotational mobility of the peptide around the membrane normal.

Factors like lipid head group charge and hydration of a sample were shown to influence the process of realignment with regard to the threshold concentration for the S-T transition, but not the orientations themselves (Tremouilhac 2006b).

A transmembrane alignment of PGLa, which is postulated by the toroidal pore model as the mechanism of antimicrobial function could not be detected so far.

2.2.4.2 Magainin 2

Magainin 2 is a linear peptide of 23 amino acid residues (GIGKFLHSAKKFGKAFVGEIMNS). It is basic, carries five positive charges (four lysines and one charge at the N-terminus) and two negative charges (glutamate and the C-terminus). Like PGLa it adopts an amphipathic α-helical structure upon binding to lipid bilayers. A helical wheel representation is shown in Figure 2.9.

Magainin 2 was originally extracted from the ventral skin of the South African clawed frog *X. laevis* following the intriguing observation that despite non-sterile surgical removal of ovaries, wounds extremely rarely developed infections (Zasloff 1987). Subsequently it could also be found in the secretions of the skin (Giovannini 1987) and like PGLa in the gastrointestinal system. The precursor protein of 160 amino acids is cleaved inti one molecule of magainin 1 and two molecules of magainin 2.

Like PGLa, magainin 2 exhibits significant broad spectrum antimicrobial activity, including bactericidal activity and lytic activity on protozoa, but almost no hemolytic activity (Soravia 1988; Zasloff 1987).

Magainin 2 was demonstrated to form weak voltage-dependent anion-selective channels (Zasloff 1988; Sitaram 1999). Coupling of lipid flip-flop and peptide translocation to the formation and deactivation of these pores was shown. The concept of the toroidal pore was proposed for magainin 2 (Ludtke 1996; Matsuzaki 1999; Matsuzaki 1996; Matsuzaki 1995b). In addition to an orientation of the peptide helix parallel to the membrane surface (Bechinger 1993), the formation of water-filled cavities, resembling pores, could be detected in aligned membranes at high magainin 2 concentrations (Matsuzaki 1999; Bechinger 2006). The activity of magainin 2 was shown to be sensitive to the lipid composition of the bilayer (Matsuzaki 1998) preferentially interacting with anionic phospholipids and exhibiting weak activity in the presence of sterols (Matsuzaki 1995). Both is in full accordance with selective action on bacteria but not on erythrocytes.

2.2.4.3 Synergistic effects of PGLa and magainin 2

PGLa and magainin 2 exhibit marked functional synergism in antibacterial activity and leakage of synthetic membrane vesicles (Westerhoff 1995), as well as in hemolytic activity. Synergism is explained to arise as a result of the formation of parallel heterodimers in membrane bilayers (Hara 2001), allowing the formation of pores at a faster rate as either peptide, being moderately more stable than pores formed by PGLa alone (Matsuzaki 1998b).

By solid state ^{2}H-NMR spectroscopy, PGLa could indeed be shown to adopt an upright alignment (I-state) in the presence of magainin 2 in the 1/1/75/25 molar ratio of PGLa/magainin/DMPC/DMPG (Tremhouilhac 2006a) (Figure 2.11). That finding is compatible with the above mentioned postulated toroidal pore structure and higher stability of the pores could explain the synergistic enhancement in activity.
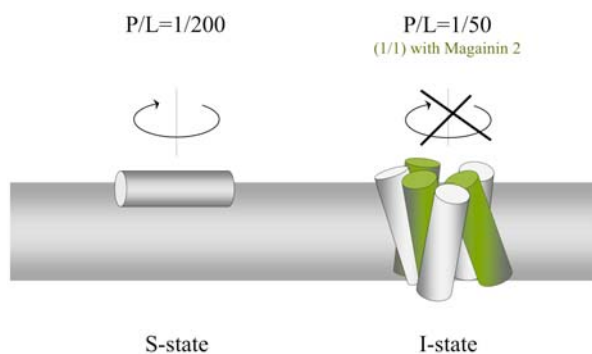
Figure 2.11 The recently found insertion of PGLa in presence of magainin 2 (in a molar ratio of 1/1) (see text). Peptide helices are shown as cylinders, PGLa coloured in grey, magainin 2 in green. Arrow above PGLa at low P/L ratio indicates rotational mobility of peptide along the membrane normal. This is absent in the I-state in presence of magainin 2.

2.3 Solid state nuclear magnetic resonance (NMR) spectroscopy

This chapter deals with the fundamentals of nuclear magnetic resonance (NMR) spectroscopy in general, the principal concept of solid state NMR and the employment of the CF₃-group to study peptides in lipid environment (Strandberg 2004b; Ulrich 2004; Bechmann 2000; Dürr 2005; Duerr 2002; Hoffmann 2000; James 1998; Afonin 2003a).

2.3.1 Fundamentals of NMR spectroscopy

NMR employs an intrinsic property of atomic nuclei, their *nuclear spin*. Only nuclei with spin $I > 0$ are suited for this method. Placing the nuclei in an external *magnetic field* gives rise to different energy for different spin states. Application of electromagnetic radiation in the radio frequency (RF) range, enables transitions between different energy states (*resonance*) to be measured, resulting in the NMR *spectrum*.

In *solid state* NMR spectroscopy the orientational dependence of internal interactions, i.e. interactions between nuclear spins of a sample, can be detected. In solution these interactions are averaged out due to fast isotropic motions of the molecules and cannot be observed directly.

The spin of an atomic nucleus is composed of the spins of its protons and neutrons, each having a spin $I = 1/2$. The resulting nuclear spin is described by its spin quantum number I, being an integer multiple of 1/2. A selection of nuclear isotopes along with their properties is shown in Table 2.5.

Table 2.5 A selection of nuclear isotopes and their properties (compiled from references above).

Isotope	Spin quantum number I	Gyromagnetic ratio γ [$T^{-1}s^{-1}$]	Natural abundance [%]	Sensitivity (relative to ^{1}H)
^{1}H	½	$2{,}675 \cdot 10^8$	99,98	1,0
^{2}H	1	$4{,}11 \cdot 10^7$	0,015	0,0096
^{12}C	0	–	98,9	–
^{13}C	½	$6{,}73 \cdot 10^7$	1,1	0,0159
^{14}N	1	$1{,}93 \cdot 10^7$	99,6	0,00101
^{15}N	½	$-2{,}71 \cdot 10^7$	0,36	0,00104
^{19}F	½	$2{,}517 \cdot 10^8$	100,0	0,833
^{31}P	½	$1{,}083 \cdot 10^8$	100,0	0,0663
^{32}S	0	–	99,26	–

Due to its nuclear spin the nucleus has a magnetic moment $\bar{\mu}$. This is proportional to the spin vector $\bar{I}$ and to the gyromagnetic ratio γ, a constant for each nucleus, according to $\bar{\mu} = \gamma \bar{I}$. When no magnetic field is present, the magnetic moments of nuclei can be aligned randomly in any direction. The energies of all nuclei are identical, i.e. they exhibit Zeeman degeneracy. When these nuclei are placed in a magnetic field B_0, they exhibit Zeeman splitting, i.e. they adopt different discrete energy states proportional to their magnetic moment µ and the applied magnetic field (Figure 2.12). The number of possible energy states they can adopt, depends on their spin quantum number I.
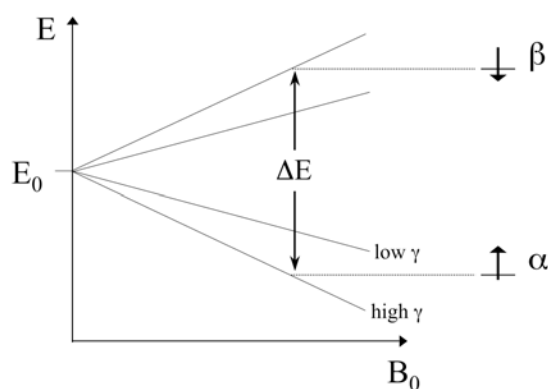
Figure 2.12 Zeeman splitting for nuclei with I=1/2 results in the two different spin states β (higher) and α (lower). ΔE between the energy levels of both spin states is linearly dependent on the external magnetic field B_0 and on the gyromagnetic ratio γ of a particular type of nucleus.

Nuclei ^{31}P and ^{19}F with $I = 1/2$ were used in this study. They exhibit two energy states, lower α and higher β. The projection of a nuclear spin magnetic moment along the direction of the magnetic field, is either parallel or antiparallel, with the parallel orientation being the lower energy state. The extent to which nuclear spins favour the low-energy state over the high-energy state at equilibrium is described by the Boltzmann equation.

The slight excess of nuclear spins in the lower energy state at equilibrium results in a net magnetic field (vector) of a sample along the direction of the applied magnetic field, i.e. the z-axis. That is called the bulk equilibrium magnetization.

The different energy levels give rise to the NMR spectrum, as the nuclear spins can undergo a transition between both energy states upon absorption of electromagnetic radiation matching these energy difference (resonance). At magnetic field strengths used in NMR experiments, the frequencies necessary to fulfill that condition are in the RF range, i.e. in the range of tens to hundreds of MHz.

2.3.2 Single-pulse experiment

In a single-pulse experiment (Figure 2.13) an RF pulse of appropiate frequency and duration is applied from the (sample/receiver) coil along the x-axis. That $90°_x$-pulse rotates the magnetization vector M_0 away from its equilibrium position along the z-axis around the x-axis onto the -y-axis. The magnetization vector rotates around the external magnetic field vector in the xy-plane at its Lamor frequency $\omega = -\gamma B_0$. The Lamor frequency corresponds to the difference between the two energy states and for a given external static magnetic field is proportional to the gyromagnetic ratio γ of a nucleus, hence it is a characteristic for each isotope. The rotation of the magnetization vector around the z-axis induces an oscillating current in the (sample/receiver) coil along the x-axis, the free induction signal. This is the NMR-signal. Relaxation processes cause this x-magnetization to decay away to zero over time, returning to equilibrium. The signal is also called free induction decay (FID). Fourier transformation converts the time domain signal, the FID, into a frequency domain signal, the NMR spectrum.
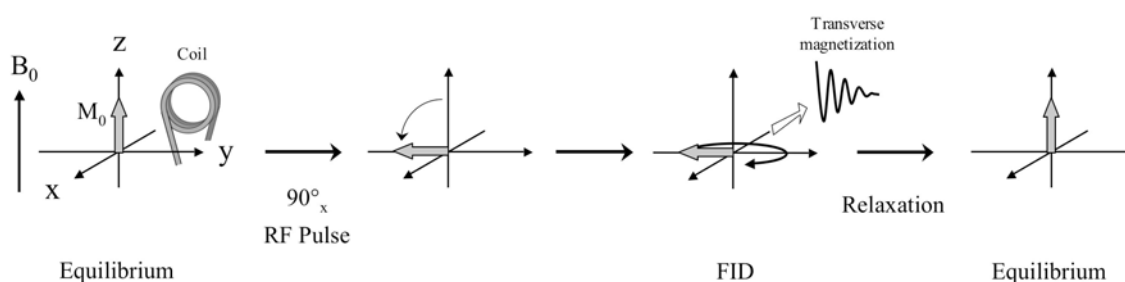
Figure 2.13 Basic principle of a single-pulse experiment as described in the text.

2.3.3 Spin interactions

Spin interactions can be grouped into external and internal interactions. External interactions are the above described Zeeman interaction with the external static magnetic field B_0 and the interaction with the applied B_1-field (RF). From the above description one should expect the same frequency signal for identical isotopes in a particular NMR experiment. However, the exact resonance frequency is slightly changed due to several internal interactions of the nuclear spins, i.e. due to their environment in the sample. These internal interactions modulate the energy states and the transitions between them. That is the main source of the information NMR spectroscopy can give, including the local structural information. Internal interactions are chemical shielding, J-coupling, dipolar coupling and quadrupolar coupling. They depend on the chemical environment of a nucleus.

Only two of these essential internal interactions will be used in this work and will be described in brief below, i.e. the chemical shielding and the dipolar coupling, resulting in shifts and splittings of signals in the spectrum, respectively.

2.3.3.1 Chemical shielding

The effective magnetic field that a nucleus encounters depends on its electronic environment, as the surrounding electrons may enhance or reduce the applied external magnetic field, by generating a secondary magnetic field. Depending on the chemical surrounding, the resonance frequency of a nucleus is slightly shifted. Values for the chemical shift are very small compared to the Lamor frequency and are given in parts per million (ppm). The chemical shift has a time-averaged (isotropic) value in solutions, where molecular tumbling is in the range of up to 10^3 GHz. That results in a particular resonance shift for nuclei in a particular type of chemical surrounding, e.g. for a certain chemical group.

However, the electron distribution around a nucleus is not spherically symmetric, but depends on the shape of its molecular orbital. In solids, where the motion of molecules is restricted, the chemical shift hence depends on the orientation of a molecule within the applied external magnetic field. This effect is called chemical shift anisotropy (CSA). Every orientation of a molecule with regard to the magnetic field contributes to the overall spectrum by a single line of a particular frequence.

In a single crystal, all molecules have the same orientation and a single signal is obtained, varying with the orientation of the crystal. In a powder, where all orientations of molecules are present, the resulting spectrum is called a "powder spectrum".

The orientational dependence (anisotropy) of the chemical shift can be mathematically described by a CSA tensor (3 x 3 matrix) and can be visualized as an asymmetric ellipsoid, in the most general case with three different main tensor components. Transformed into its own principal axes system (PAS) by diagonalization, the three main tensor elements coincide with the three coordinate axes of the PAS. The PAS is characteristic for each nucleus in its specific chemical environment and the applied external magnetic field is not necessarily aligned along the z-axis anymore. A general tensor with three different principal axes is shown in Figure 2.14. The order of shielding magnitude of the tensor elements is defined as $\sigma_{11} \leq \sigma_{22} \leq \sigma_{33}$ with σ_{11} representing the least shielded element, resulting in the highest field resonance, and σ_{33} the most shielded element, resulting in the lowest field resonance (Figure 2.15, upper three pictures). The orientation of the external magnetic field B_0 vector in the PAS system is described by the angles θ and Φ between B_0 and the PAS z-axis, i.e. σ_{33} (Figure 2.14).
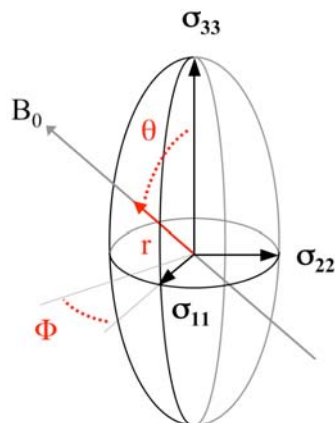
Figure 2.14 Graphical presentation of a CSA tensor with three different principle axes. The tensor represents the orientation-dependence of the chemical shielding. The lenght of a vector along B_0 from center to surface (r) of the ellipsoid defines the frequency in the NMR spectrum.

In an unoriented powder, all orientations of a molecule are present with equal probability. However, except for the outermost tensor values, several combinations of the polar angles deliver the same values for r, resulting in a characteristic powder pattern or tensor line shape (Figure 2.15, lower).
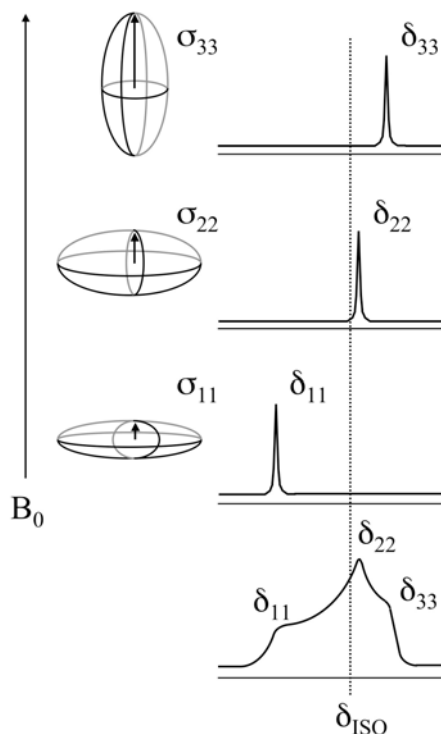
Figure 2.15 CSA anisotropy for a tensor with three different principle axes. The tensor ellipsoid (left) is depicted aligned with its principal axes along the magnetic field, resulting in the characteristic frequencies right upper) of the powder spectrum (right lower), which is the sum of single frequencies of multiple randomly aligned tensors in a sample, i.e. molecules with different orientations.

In solutions of low viscosity, where the molecules move rapidly along all three axes, the electronic environment is averaged out to a spherical distribution, giving an isotropic value for the CSA tensor and hence for the chemical shift, as mentioned above, according to $\sigma_{ISO} = (\sigma_{11} + \sigma_{22} + \sigma_{33})/3$.

2.3.3.2 Dipolar coupling

The magnetic behaviour of a nucleus may be influenced by the dipolar moment of another nuclei in the vicinity and vice versa. The NMR transition splits up into two or more lines. This interaction through space is called dipolar coupling. The NMR spectrum shows respective dipolar splitting of signals. Dipolar couplings can be hetero- and homonuclear.

The value of the dipolar splitting depends on the distance r between the nuclei and on the angle θ between the internuclear connection vector and the applied magnetic field (Figure 2.16). The dipolar tensor is intrinsically axially symmetric. The secular part of the dipolar coupling is described by $\Delta_{SS} = \Delta_{SS}^0 (3\cos^2\theta - 1)/2$ and is expressed in kHz. The absolute value of the dipolar coupling is measured. The coupling constant Δ_{SS}^0 is proportional to $1/r^3$ and to the magnetic moments of the two nuclei, i.e. it depends on the types of nuclei.
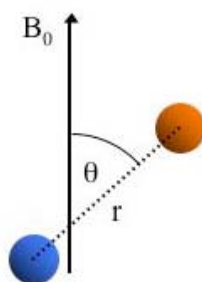
Figure 2.16 The dipolar coupling between two nuclear spins depends on their distance r and the angle θ between the internuclear vector and the applied magnetic field.

Like the chemical shift, the dipolar coupling of an unoriented powder sample shows a broad distribution of lines in the spectrum, according to all orientations being present. In solution, the dipolar coupling is averaged to zero as it does not possess an isotropic component.

2.3.4 ^{31}P-NMR as a tool to study phospholipids

Phospholipids in a membrane environment under physiological conditions can rotate freely along their longitudinal axis, but are restricted in their tilt. Hence, the three-component ^{31}P

CSA tensor of the phospholipid head group is averaged to an axially symmetric CSA tensor, with two of three axes being identical. In the fluid lamellar bilayer phase the axis of rotation of a phospholipid is aligned parallel to the local membrane normal, so is the least shielded element σ_{II} (0° edge) of the averaged ^{31}P CSA tensor, resulting in the highest chemical shift. The most shielded perpendicular CSA element $\sigma_{\perp}$ (90° edge) results in the lowest chemical shift.

Therefore, when lipid bilayers are macroscopically aligned, i.e. the molecular orientation is fixed with regard to the magnetic field, the resulting spectrum shows one narrow line. The exact position under a particular alignment is characteristic for a particular lipid. Oriented DMPC lipid bilayers, for example, at 0° alignment of their membrane normal with regard to the magnetic field, show a signal at about +30 ppm corresponding to σ_{II}. Badly oriented lipid bilayers give rise to additional signals along the whole CSA range, in case of DMPC bilayers from approximately +30 up to about -15 ppm ($\sigma_{\perp}$). Upon integration and comparison of signals at the 0° edge with the whole CSA range, the degree of the orientation of a sample can be determined.

Multilamellar vesicles are concentric spheres of about 1 µm in diameter. Suspensions of phospholipid vesicles due to spherical distribution of lipids, result in a characteristic shape of the spectrum with more lipids contributing to $\sigma_{\perp}$ than to σ_{II} (Figure 2.17).
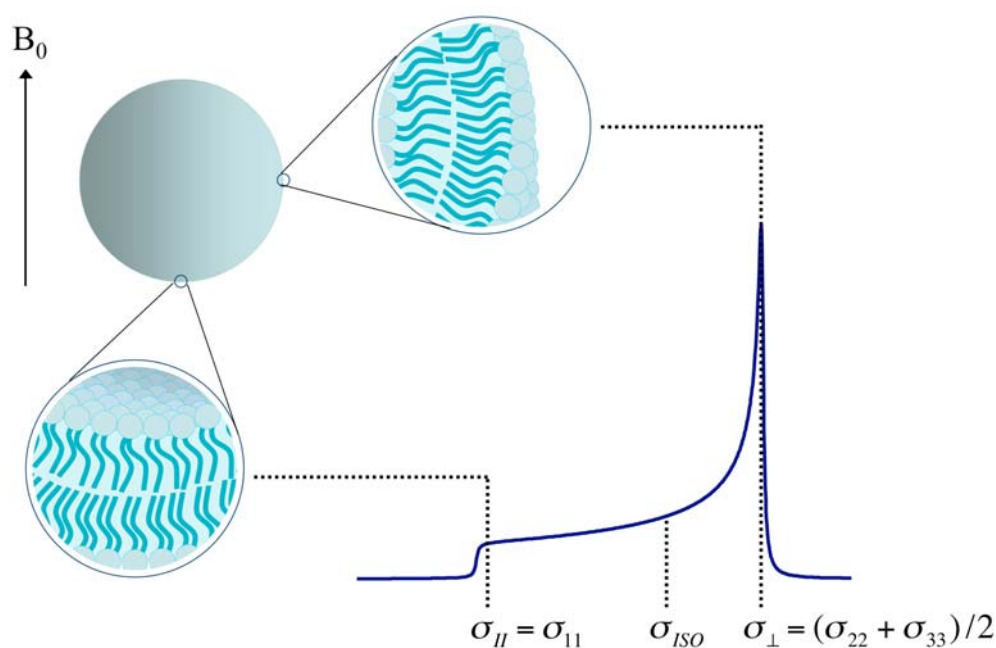
Figure 2.17 Simulated solid state ^{31}P-NMR spectrum of phospholipids in fluid lamellar bilayers in vesicles. The CSA tensor is axially symmetric due to rotation of lipids around the membrane normal.

2.3.5 ^{19}F-NMR as a tool to study antimicrobial peptides in lipid membranes

In macroscopically aligned samples, when each type of molecule is oriented identically with regard to the magnetic field, above mentioned spin interactions and their orientational dependence may be employed to determine the orientation of a molecule.

In this study the CF$_3$-group with its characteristic chemical shift and dipolar splitting for a particular orientation with regard to the magnetic field serves as a reporter group for the helical antimicrobial peptide PGLa (Glaser 2004). Single CF$_3$-groups are rigidly attached to the helix backbone of PGLa via the non-natural amino acid L-4-trifluoromethyl-phenylglycine (CF$_3$-Phg) (Figure 2.18) as substitutes for hydrophobic leucine or alanine residues.
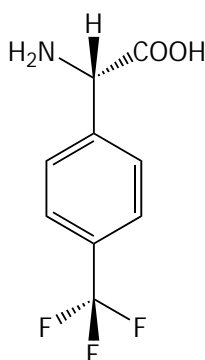
Figure 2.18 Chemical structure of CF$_3$-Phg (L-4-trifluoromethyl-phenylglycine)

The dipolar coupling between the three identical ^{19}F nuclei of the CF$_3$-group results in a triplett in the spectrum (Figure 2.19). The CF$_3$-group undergoes fast rotation around its axis (being equivalent to the C$_\alpha$-C$_\beta$ bond vector of CF$_3$-Phg), leading to an averaged dipolar coupling with a reduced coupling constant $\Delta_{FF}^0 = 15,8\,kHz$. The fast rotation will furthermore project all the three pair-wise dipolar couplings along the C$_\alpha$-C$_\beta$ bond vector. The angle θ between the C$_\alpha$-C$_\beta$ bond vector and the magnetic field can then be experimentally determined from the dipolar splitting $\Delta_{FF} = 15,8\,kHz\,(3\cos^2\theta - 1)/2$ (Figure 2.20) and the sign of the coupling can be determined when the CSA is taken into account.
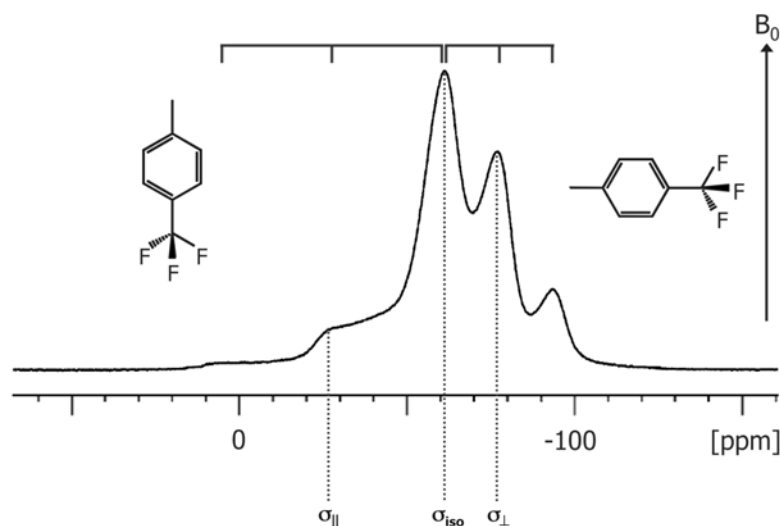
Figure 2.19 Orientational dependence of chemical shift and homonuclear dipolar splitting of the CF_3-group. The experimental powder spectrum is of randomly distributed polycrystalline CF_3-phenylglycine. The 0° and 90° edge of the axially symmetric CSA tensor and the positions of the corresponding tripletts are indicated.
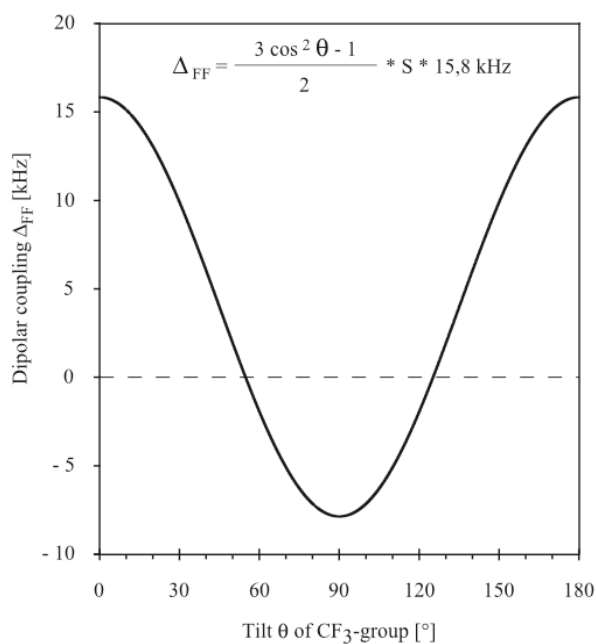
Figure 2.20 Dependence of the homonuclear dipolar splitting Δ_{FF} of the CF_3-group on its orientation with regard to the magnetic field. θ is the angle between the C_α-C_β bond vector and B_0.

The parameters which describe the orientation of the peptide helix in the membrane are shown in Figure 2.21. The tilt angle τ is the angle between the helix axis and the membrane normal. The azimuthal rotation ρ is defined as the right-handed rotation around the helix axis, with the axis directed from the N- to the C-terminus. At $\tau = 90°$, $\rho = 0°$ is defined as the

orientation, when the vector projecting radially from the helix axis to the C_α atom of Lys-12 is aligned parallel to the membrane plane (compare to PGLa helical wheel in Figure 2.9). The molecular order parameter S_{mol} describes the mobility of the molecule in the lipid bilayer (wobbling) as a factor between 0,0 (fully averaged system) and 1,0 (absence of wobble), reducing all NMR parameters by a constant factor.
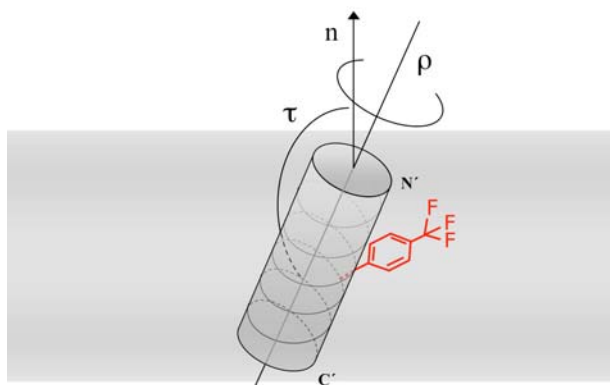
Figure 2.21 Parameters describing the orientation of a peptide helix in a lipid membrane (see text). The position of a CF_3-group is scetched in red.

The structure of a helix is generally reflected in the periodicity of an NMR parameter along its axis. Plotting an NMR parameter against the residue number, for instance the dipolar splitting, results in a wave-like curve with a repetition after 3,6 residues for an α-helix. The orientation of the helix with regard to the magnetic field can be extracted from the shape and the frequency (relative and absolute) of the wave (Figure 2.22).
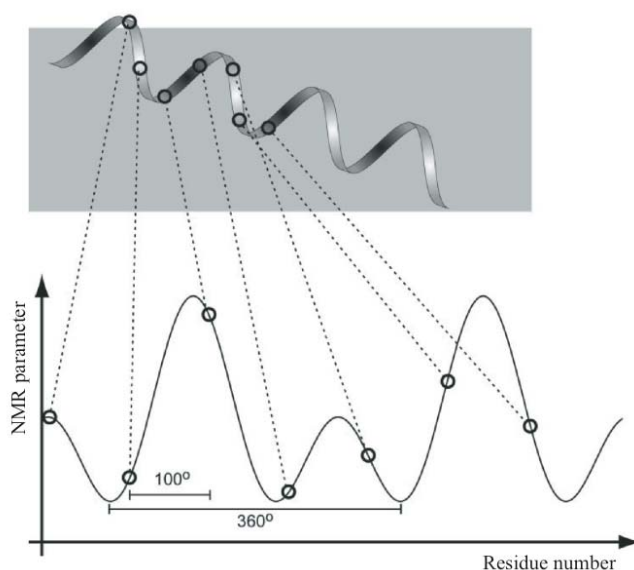
Figure 2.22 Wave-like dependence of an NMR parameter on the reporter position along the α-helix axis (from Strandberg 2004b).

2.4 A note about membrane models

NMR investigations of AMPs in synthetic lipid bilayers with a few well-defined components are employed to study the influence of individual parameters on the peptide-lipid interaction. The lipid environment may be adjusted to any desired condition by modification of, for instance, charge and size of the lipid head group, length and degree of unsaturation of the acyl chain, the ratio of the cross-sectional areas of both, the amount of water or the degree of membrane fluidity.

Macroscopically aligned lipid bilayers are the most often used membrane model to determine structure, orientation and dynamics of a peptide in lipid environment. Fully hydrated, these lipid membranes do not contain excess bulk water, thus the affinity of peptides does not play a significant role in binding to the membrane, e.g. anionic lipids are not necessary.

Multilamellar vesicle suspensions are employed to mimic more physiological conditions, i.e. with quasi unlimited supply of water. The advantage over aligned lipid systems is easier handling and that hydration and the bulk water content can be adjusted to any desired value. However, to reach the same effective peptide amount in the lipid membrane compared to oriented samples, dependent on charge of the membrane lipids, a higher P/L ratio may be necessary in this kind of sample, as peptides may escape into the water bulk.

However, natural membranes are far more complex systems and contain various types of lipid and protein components. The direct determination of structural parameters for a peptide under this situation is difficult, if not impossible, and straightforward investigations on these systems may fail. It may be speculated that any results found for any uniform synthetic lipid model under certain conditions can be found in cytoplasmic membranes, perhaps simultaneously. For the understanding of the mode of action of AMPs in real biomembranes, spectra of peptide in synthetic lipid membranes representing different states under various defined conditions have to be used as reference for spectra of peptide in cytoplasmic membranes.

3   Aims and strategies

The principle aim of this study was to determine the structure and orientation of PGLa in cytoplasmic membranes. Of particular interest was the question whether the different orientations observed for PGLa in synthetic lipid bilayers can also be identified in cell membranes of *Bacteria* and *Eukarya*, and if any principal differences can be found that may be rationalized in terms of the selective activity of the peptide.

Solid state NMR spectroscopy was used to observe the membrane orientations of PGLa. The highly sensitive and in biological samples background-free ^{19}F nucleus was used as an NMR label. Hydrophobic amino acids Ile-9, Ala-10, Ile-13 or Ala-14 of PGLa were singly substituted by the non-natural amino acid 4-CF$_3$-phenylglycine. These labeled PGLa analoga were synthesized in our group and were previously shown to be structurally and functionally intact, i.e. neither severe disturbance of the helical structure nor alteration of antimicrobial activity occured (Strandberg 2006; Ulrich 2004; Glaser 2004). The orientational dependence of dipolar coupling and chemical shift of the CF$_3$-group rigidly attached to the helix backbone was employed as a reporter for the orientation and dynamics of the peptide in membranes.

One main challenge in this study was the preparation of cell membranes in sufficient yield and purity to be employed as vesicle suspensions and macroscopically aligned membranes in solid state NMR spectroscopy. Two common systems representing cells of *Eukarya* and *Bacteria* were finally chosen: human erythrocytes and *Micrococcus luteus*. Human erythrocyte membranes are the most often used model for eukaryotic membranes in biophysical and biochemical studies. Their clinical relevance is obvious. Since cells are osmotically sensitive, membranes could be accessed directly. Among Gram-positive bacteria, *Bacillus subtilis* and *Micrococcus luteus* are excellent models for studying pathogenic bacteria and are themselves responsible for nosocomial infections. Furthermore, in contrast to Gram-negative bacteria, their membrane preparations do not involve time-consuming and yield-reducing separation steps. After initial attempts on *Bacillus subtilis*, however, a decision was made in favour of *M. luteus*. It is usually highly sensitive to lysozyme, making its cell membrane easily accessible. Its envelope, furthermore, lacks phosphorus-containing teichoic acids, which were assumed in *B. subtilis* to be responsible for disturbance of solid state ^{31}P-NMR spectra.

Heterogenity and complex phase behaviour of real biomembranes, prior to application of ^{19}F-labeled PGLa to cell membrane preparations, required characterization of structure and orientation of peptide in simple model systems. Two such model systems of different

hydration levels were employed. Macroscopically aligned bilayers are adequate for the determination of structural NMR parameters. Multilamellar vesicles of high water bulk content resemble the native situation in biomembrane vesicles more closely. DMPC and DMPG at a 3/1 ratio provide an experimentally accessible gel as well as fluid bilayer phase and supply sufficient amounts of negative charge to bind cationic PGLa even at high water bulk content. For all four ^{19}F-labeled PGLa analoga at high P/L ratio of 1/50, a detailed investigation of temperature-dependence of dipolar splittings was performed, followed by the determination of orientational parameters of PGLa, thus giving a set of spectra for all alignment states of PGLa (S, T and I). From ^{2}H-NMR experiments, magainin 2 is known to stabilize an inserted alignment state of PGLa. Therefore, the same temperature-dependent experimental procedure was undertaken in presence of unlabeled magainin 2 at equimolar ratio to obtain ^{19}F-NMR spectra for PGLa in the I-state.

The most appropiate labeled PGLa analogue (13CF$_3$-Phg PGLa) was selected thereafter as a reporter reference to identify the respective states of PGLa in cell membranes of human erythrocytes and *Micrococcus luteus* both in vesicle suspensions and as oriented membranes.

4 Solid state NMR studies of PGLa in synthetic lipid bilayers in the presence or absence of magainin 2

4.1 Materials and methods

4.1.1 Instruments

Balance M2P Sartorius (acc. 0,0001 mg)	Mettler Toledo (Greifensee, Switzerland)
Centrifuge Biofuge Pico	Heraeus (Hanau, Germany)
Diaphragm vacuum pump	Vacuubrand (Wertheim, Germany)
Microsyringes	Hamilton (Bonaduz, Switzerland)
(10 µl; 25 µl; 1000 µl)	
NMR spectrometer Avance 500	Bruker Biospin (Karlsruhe, Germany)
Probehead for ^{31}P H/X/Y	Bruker Biospin (Karlsruhe, Germany)
Probehead for ^{19}F Doty	Doty Scientific (Columbia, SC, USA)
Oven B5042	Heraeus (Hanau, Germany)
Pipettes Reference	Eppendorf (Hamburg, Germany)
(0,5-10 µl; 10-100 µl; 100-1000 µl)	
Sonifier Bandelin Sonorex Super RK510	Schalltec (Berlin, Germany)
Vortex mixer Genie K-550-GE	Bender & Hobein (Zurich, Switzerland)

4.1.2 Consumables

Centrifuge tubes	Sarstedt (Nuembrecht, Germany)
(15 ml; 50 ml)	
Glass plates (18 x 7,5 x 0,08 mm)	Marienfeld Laboratory Glassware (Lauda-Königshofen, Germany)
Parafilm	American National Can (Chicago, IL, USA)
Pipette tips	Sarstedt (Nümbrecht, Germany)
Reaction tubes	Sarstedt (Nuembrecht, Germany)
(0,5 ml; 1,5 ml; 2,0 ml)	

4.1.3 Chemicals

$CHCl_3$	Merck (Darmstadt, Germany)
K_2SO_4	Roth (Karlsruhe, Germany)

Methanol	Fischer Scientific (Leicestershire, UK)
Silica gel	Merck (Darmstadt, Germany)

4.1.4 Lipids

Dimyristoylphosphatidylcholine (DMPC)	Avanti Polar Lipids (Alabaster, AL, USA)
Dimyristoylphosphatidylglycerol (DMPG)	Avanti Polar Lipids (Alabaster, AL, USA)

4.1.5 Peptides

4-CF$_3$-Phg-labeled analogues of Peptidyl-glycine-leucine-carboxyamide (PGLa) (Table 4.1) and unlabeled magainin 2 were synthesized in our group by standard Fmoc (9-fluorenylmethoxycarbonyl) solid phase peptide synthesis (Fields 1990). Peptides were purified to more than 95 % purity by RP-HPLC and characterized by MALDI-TOF and Marey assay.

Table 4.1 Amino acid sequences of peptides used in this study. For comparison with labeled analoga the sequence of unlabeled PGLa is given.

Peptide	Labeled position	Sequence
PGLa wt	-	GMASKAGAIAGKIAKVALKAL-NH$_2$
9CF$_3$-Phg PGLa	Ile-9	GMASKAGA-**4-CF$_3$-Phg-**AGKIAKVALKAL-NH$_2$
10CF$_3$-Phg PGLa	Ala-10	GMASKAGAI-**4-CF$_3$-Phg-**GKIAKVALKAL-NH$_2$
13CF$_3$-Phg PGLa	Ile-13	GMASKAGAIAGK-**4-CF$_3$-Phg-**AKVALKAL-NH$_2$
14CF$_3$-Phg PGLa	Ala-14	GMASKAGAIAGKI-**4-CF$_3$-Phg-**KVALKAL-NH$_2$
Magainin 2	-	GIGKFLHSAKKFGKAFVGEIMNS

4.1.6 Software

TopSpin 2.0 (Bruker)

XWinNMR (Bruker)

FITPS program (written by Dr. Erik Strandberg of our group)

dmfit (Massiot 2002)

Illustrator 10 (Adobe)

Excel 2004 for Mac Version 11 (Microsoft)

Photoshop 7 (Adobe)

Power Point 2004 for Mac Version 11 (Microsoft)

Word 2004 for Mac Version 11 (Microsoft)

4.1.7 Preparation of oriented lipid bilayers

Macroscopically aligned lipid bilayers were prepared according to common protocols with some modifications (Strandberg 2006; Strandberg 2004b).

Thin glass plates (18 mm x 7,5 mm x 0,08 mm) were washed with methanol and dried under vacuum for 2 h. Appropiate amounts of DMPC, DMPG and peptide(s) to obtain the desired molar ratios were codissolved in 400 to 600 µl methanol/$CHCl_3$ (1/1 (v/v)), resulting in about 1 mg of total material per glass plate (dissolved in 20-30 µl) for up to 20 glass plates in total. Aliquots were deposited onto the glass plates, dried in air for about 1 h, followed by drying under vacuum overnight (about 12 h). The glass plates were stacked, covered with an additional clean glass plate and hydrated at 96 % relative humidity (over a saturated solution of K_2SO_4) at 46 °C for 24-48 h. The stacks were wrapped in parafilm and a polyethylene foil. Samples were stored at -20 °C when not used.

4.1.8 Preparation of multilamellar vesicle samples

Multilamellar vesicles were prepared according to common protocols with some modifications (Strandberg 2006; Strandberg 2004b).

Appropiate amounts of DMPC, DMPG and peptide(s) (typically 1-4 mg) to obtain desired molar ratios were codissolved in up to 500 µl methanol/$CHCl_3$ (2/1 (v/v)). The solution was dried under a gentle stream of N_2, followed by drying under vacuum over night (about 12 h). Double-destilled water was added to the dry lipid-peptide mixture to obtain 60 % water (v/w). The sample was thoroughly mixed by vortexing and freeze-thawed about eight times. The material was then transferred with a spatula into a small polyethylene bag which was heat sealed and packed into a second bag. The samples were stored at -80 °C when not used.

4.1.9 Solid state NMR spectroscopy

All measurements were carried out on a widebore Bruker Avance 500 MHz NMR spectrometer (Bruker Biospin, Karlsruhe, Germany) at a transmitter frequency of 470,6 MHz (^{19}F) and 202,5 MHz (^{31}P).

For solid state ^{19}F-NMR a ^{19}F/^{1}H double-tuned flat-coil probehead (Doty Scientific, Columbia, SC) equipped with a goniometer was used. Oriented samples were aligned with the lipid membrane normal either parallel or perpendicular to B_0. Between 2000 and 12000 scans were aquired for single-pulse ^{19}F-NMR spectra with [1]H-decoupling. Spectra were referenced against externally measured 100 mM NaF solution aquired at 308 K which was set to -119,5 ppm (Glaser 2003).

For solid state ^{31}P-NMR a ^{1}H/X/Y probehead with interchangeable flat-coils for horizontal or vertical alignment of samples was used. Oriented samples were aligned with the membrane normal parallel or perpendicular to B_0. ^{31}P-NMR spectra were usually aquired at 308 K. ^{1}H-decoupled Hahn-echo spectra were recorded with a typical 90° pulse duration of 6 µs, relaxation delay of 2 s and inter-pulse echo delay of 30 µs. The number of scans was typically 512 for oriented samples and 1024 for multilamellar vesicles. Spectra were referenced against externally measured 85% H_3PO_4 solution aquired at 308 K which was set to 0 ppm.

4.1.10 Calculation of the helix orientation

To describe the orientation of PGLa in synthetic lipid bilayers, a molecular frame was defined, where the z-axis is the helix axis of the peptide and the C_α atom of Lys-12 lies in the bilayer plane (y-axis). For an explanation of the angles describing the orientation of the helix in the laboratory frame, i.e. in the oriented lipid bilayer, see Figure 2.21.

The angles α, β and ω describe the orientation of an amino acid side chain in the α-helix. α is the angle between the projection of the C_α-C_β bond vector of a particular amino acid in the xy-plane and the vector pointing radially from the the helix axis to the C_α atom. β is the angle between the helix axis and the C_α-C_β bond vector. ω describes the pitch angle between the C_α atom and the C_α atom of the subsequent residue. For a "standard" α-helix (poly-Ala) the characteristic values for α, β and ω are 53,2°, 121,1° and 99,8°, respectively. As CF$_3$-Phg induces some structural distortions, an energy-minimized model of PGLa was employed, with angles 47,0°, 110° and 100,0° respectively (Glaser 2004; Strandberg 2004a; Dürr 2005).

The signed dipolar splittings for the individual labels were calculated for different peptide orientation with regard to the magnetic field, and a grid search of τ, ρ and S_{mol} was performed to find the smallest root mean square deviation (RMSD) between the calculated values and the experimental data (Glaser 2004; Strandberg 2004b; Ulrich 2004). The RMSD are visualized in a ρ/τ-diagram, giving the difference between the calculated values and the experimental data for each orientation of the peptide. Calculations were performed with a program written by Dr. Erik Strandberg from our group.

4.2 Results

4.2.1 ^{31}P-NMR

^{31}P-NMR spectra of DMPC/DMPG (3/1) prepared as multilamellar vesicles, in the presence of peptide, show broad spectra with a CSA range of about 45 ppm in the gel phase as well as in the fluid phase. This is characteristic for lamellar lipid bilayers and furthermore corresponds to the respective spectra of pure lipids. Typical ^{31}P-NMR spectra at 308 K are shown in Figure 4.1. In oriented bilayers from the same lipids with the membrane normal parallel to the magnetic field, signals with high chemical shift (0° edge) correspond to the oriented fraction of phospholipids. Other signals along the spectrum up to the 90° edge derive from nonoriented lipids. Upon integration of signal at the 0° edge and comparison with the whole CSA range, the fraction of oriented phospholipid can be determined. Synthetic bilayers were oriented between 60 % and far above 90 %. Separated peaks of the lipid components DMPC and DMPG are observed only rarely and irregularly. The ratio of signal intensities in these cases is approximately 3 to 1, as determined by integration if the peaks, corresponding to the applied molar ratio of DMPC and DMPG. No indications for isotropic or nonlamellar phases can be detected in either type of sample.
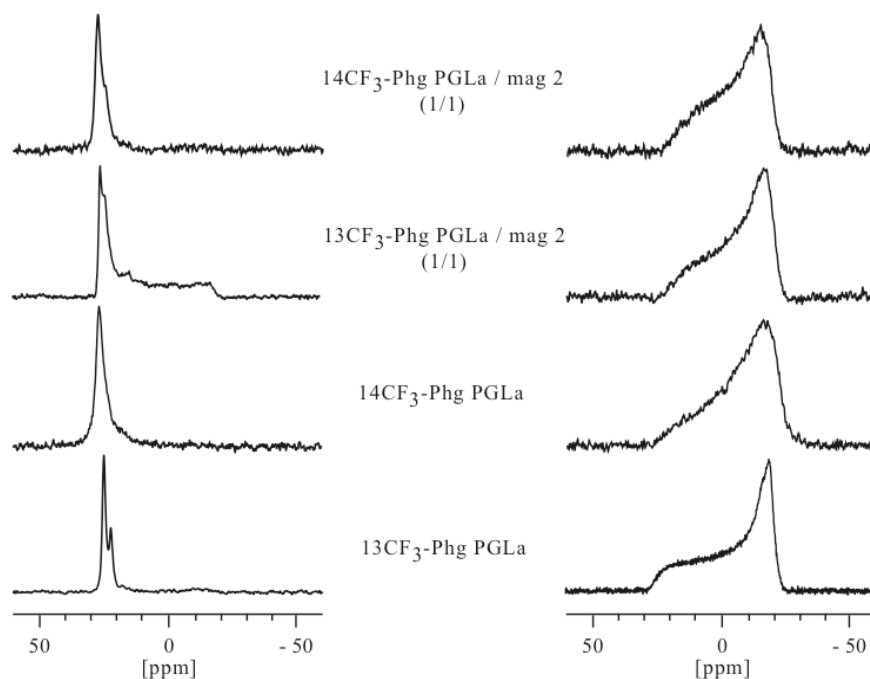
Figure 4.1 Representative solid state ^{31}P-NMR spectra from DMPC/DMPG (3/1), measured at 308 K. All samples at high P/L ratio (1/50), either PGLa alone (lower two rows) or at 1/1 ratio with magainin 2 (upper two rows). Phospholipids in oriented bilayers at 0° tilt (left column) show orientation to an extent of well over 90 % in the presence of 14CF$_3$-Phg PGLa. In the presence of 13CF$_3$-Phg PGLa together with magainin 2, phospholipids are oriented to about 60 %. In this sample the whole CSA range up to the 90° edge can be identified. Individual peaks can be identified for DMPC and DMPG with 13CF$_3$-Phg PGLa. Intensities correspond to the lipid ratio of 3/1 as determined by integration. All multilamellar vesicles (right column) show lipids being in the lamellar phase. No signs for isotropic or nonlamellar lipids can be found.

4.2.2 Concentration-dependent realignment and mobility of 13CF$_3$-Phg PGLa in fluid oriented bilayers

^{19}F-NMR spectra of 13CF$_3$-Phg PGLa at low (1/200) and high (1/50) P/L ratio in oriented DMPC/DMPG (3/1) bilayers are shown in Figure 4.2. It was already demonstrated by a set of four singly ^{19}F-labeled PGLa analogues in oriented bilayers of pure DMPC (Glaser 2005), that PGLa undergoes a concentration-dependent realignment from a surface-bound state (S-state) to a tilted state (T-state) (2.2.4.1), reflected in a characteristic change of dipolar splitting of 13CF$_3$-Phg PGLa from +5,6 kHz to -3,3 kHz. It was further shown on 13CF$_3$-Phg PGLa that the qualitative change of the spectrum is not influenced by the introduction of negative charges into the lipid bilayer, namely in DMPC/DMPG bilayers, but that the orientational behaviour of PGLa is the same in both lipid systems.

As a starting point for the upcoming investigations, ^{19}F-NMR spectra were recorded from 13CF$_3$-Phg PGLa in oriented DMPC/DMPG (3/1) bilayers (Figure 4.2, upper row), showing dipolar splittings of +6,0 kHz at low (1/200) P/L ratio and of -2,5 kHz at high (1/50) P/L ratio, being characteristic for S-state and T-state, respectively.

In addition, upon tilting the samples to 90°, dipolar splittings scaled around the isotropic position by about -1/2 (Figure 4.2, lower row). This is indicative for fast rotation of 13CF$_3$-Phg PGLa around the normal of fluid DMPC/DMPG (3/1) bilayers, and is consistent with previous data for pure DMPC bilayers.
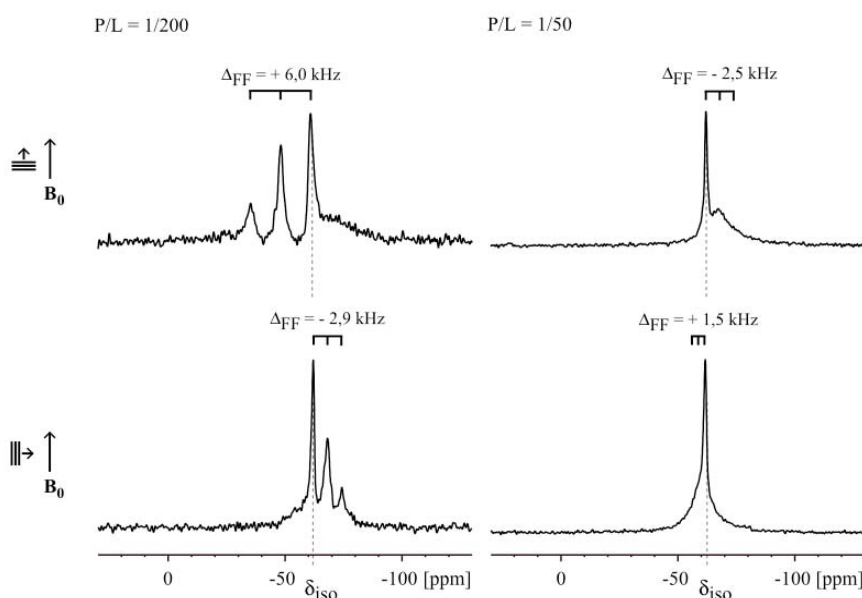
Figure 4.2 Solid state ^{19}F-NMR spectra of 13CF$_3$-Phg PGLa in oriented DMPC/DMPG (3/1) bilayers at low (1/200) (left column) and high (1/50) (right colomn) P/L ratio at 0° (upper row) and 90° (lower row) tilt of sample membrane normal with regard to the magnetic field. Dipolar splittings are given as averages above each spectrum. Positions of peaks are indicate above. The dipolar splittings in spectra at P/L of 1/50 at 0° and 90° tilt are estimated with an accuracy of 0,5 kHz.

4.2.3 Temperature-dependent behaviour of 13CF$_3$-Phg PGLa at low P/L ratio (1/200) in oriented bilayers

At low P/L ratio (1/200) in oriented DMPC/DMPG (3/1) bilayers, 13CF$_3$-Phg PGLa shows a temperature-dependent change of the dipolar splitting at 0° as well as at 90° tilt (Figure 4.3). At all temperatures spectra show orientation of peptide. Spectral lines are broader and dipolar splittings larger at lower temperatures, showing an abrupt change of features upon elevation of temperature to 298 K and above, i.e. upon transition of the membrane to the fluid phase (Lewis 2005). Upon further increase in temperature lines sharpen and splittings decrease. Below T$_m$ PGLa is surface-aligned, but motionally restricted, as spectra at 90° tilt show broad distributions of signals comparable to unoriented immobilized peptides. From 298 K upwards, scaling of dipolar splitting around the isotropic position by a factor of -1/2 upon tilt of sample (Table 4.2) shows fast rotational mobility around the membrane normal of 13CF$_3$-Phg PGLa in the S-state.
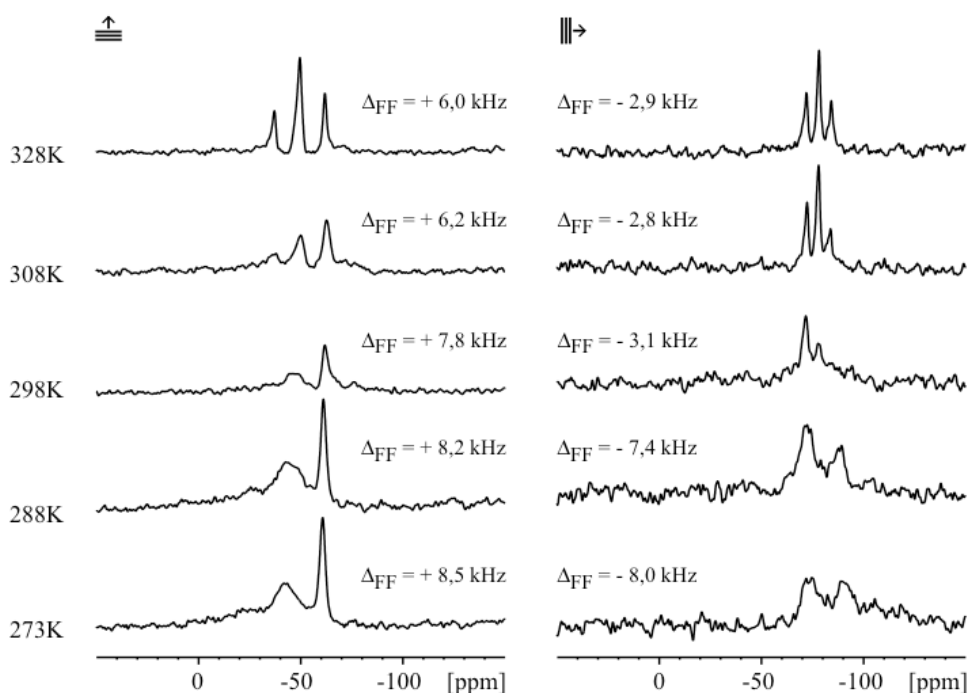
Figure 4.3 Solid state ^{19}F-NMR spectra of 13CF$_3$-Phg PGLa in oriented DMPC/DMPG (3/1) bilayers at low P/L ratio (1/200) at different temperatures. The sample is aligned with its membrane normal at 0° (left column) and 90° (right column) to the magnetic field. Values of the corresponding dipolar splittings are given next to each spectrum.

Table 4.2 Dipolar splittings for 13CF₃-Phg PGLa in oriented DMPC/DMPG (3/1) bilayers at low P/L ratio (1/200) at 0° and 90° tilt. Last column shows dipolar splitting at 90° tilt multiplied by (-2). Scaling around the isotropic position by -1/2 indicating peptide mobility can be observed from 298 K upwards (see text).

T [K]	Δ_{FF} [kHz]		Δ_{FF} (90°) * (- 2)
	0°	90°	
328	+ 6,0	- 2,9	+ 5,8
308	+ 6,2	- 2,8	+ 5,6
298	+ 7,8	- 3,1	+ 6,2
288	+ 8,2	- 7,4	+ 14,8
273	+ 8,5	- 8,0	+ 16,0

4.2.4 Temperature-dependent behaviour of 13CF₃-Phg PGLa at low P/L ratio (1/200) in multilamellar vesicles

Spectra of 13CF₃-Phg PGLa at low P/L ratio (1/200) in multilamellar vesicles of DMPC/DMPG (3/1) at a hydration of 60 % (v/w) exhibit a temperature-dependent change of the line shape. Below T_m spectra have dipolar splittings of approximately -7 kHz. Spectra show an abrupt change around T_m and a continuous development of splitting upon further increase in temperature (Figure 4.4).
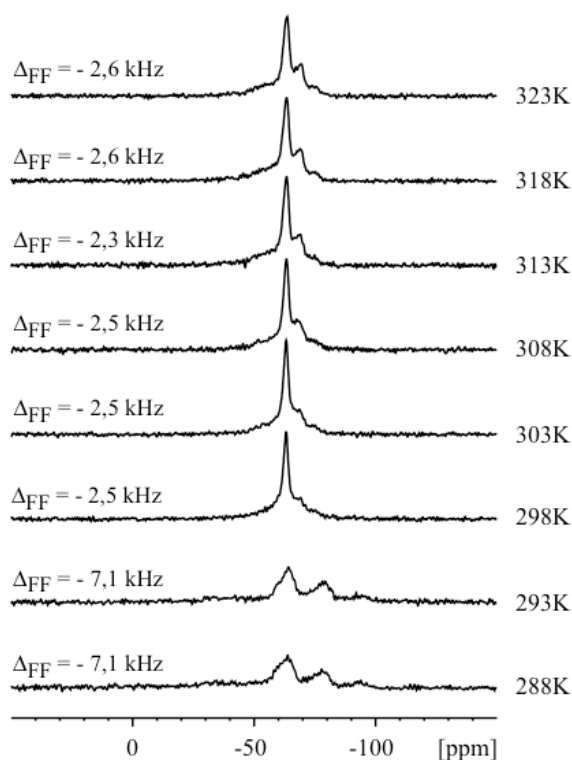
Figure 4.4 Solid state ¹⁹F-NMR spectra of 13CF₃-Phg PGLa in multilamellar vesicles of DMPC/DMPG (3/1) at low P/L ratio (1/200) at different temperatures. Values if the corresponding dipolar splittings are given next to each spectrum.

Above T_m spectra suggest a surface alignment of rotationally mobile 13CF$_3$-Phg PGLa. Peptide molecules at the equator of the vesicles exhibit a dipolar splitting corresponding to oriented samples at 90° tilt (Figure 4.3), contributing most to the signal intensity of the spectrum on the high field side (compare to ^{31}P-NMR spectra of phospholipids (2.3.4)). Reflecting the decrease in number of peptide molecules closer to the poles, the signal intensity drops to the low field side.

4.2.5 Temperature-dependent realignment of PGLa at high P/L ratio (1/50) in oriented bilayers

PGLa is known to adopt a T-state at high P/L ratio (1/50) in oriented DMPC and DMPC/DMPG bilayers at ambient temperature (2.2.4.1). A temperature series performed at high P/L ratio (1/50) of 13CF$_3$-Phg PGLa in oriented DMPC/DMPG (3/1) bilayers as for low P/L ratio (1/200) above (Figure 4.3), revealed a significant change in the line shape of spectra, indicating a temperature-dependence of PGLa alignment. Therefore, the whole set of CF$_3$-Phg-labeled PGLa analogues was tested at different temperatures.

In the temperature range from 273 to 328 K, the line shape of ^{19}F-NMR spectra of CF$_3$-Phg-labeled PGLa shows three major situations, changing discretely with increase in temperature. Spectra are shown in Figure 4.5. Dipolar splittings are summarized in Table 4.3. All spectra exhibit the expected triplet signals, having distinct splittings over the three different temperature ranges 273-288 K, 298-308 K and 318-328 K. Splittings of 9CF$_3$-Phg and 10CF$_3$-Phg PGLa at elevated temperature do not reflect a rapidly tumbling peptide, but happen to be zero for geometric reasons, as becoming apparent from 2.3.5 and from the fact that splittings of other labeled peptides in Figure 4.5 have values different from zero. The line shape of spectra of 14CF$_3$-Phg PGLa shows the transition between these distinct states, as the middle peaks of the respective triplets can be identified side by side around 288 and 298 K. A similar transient overlap of signals can be found for 13CF$_3$-Phg PGLa at 318 K. For further analysis only the most predominant situation among the whole set of spectra at each temperature was taken into account.
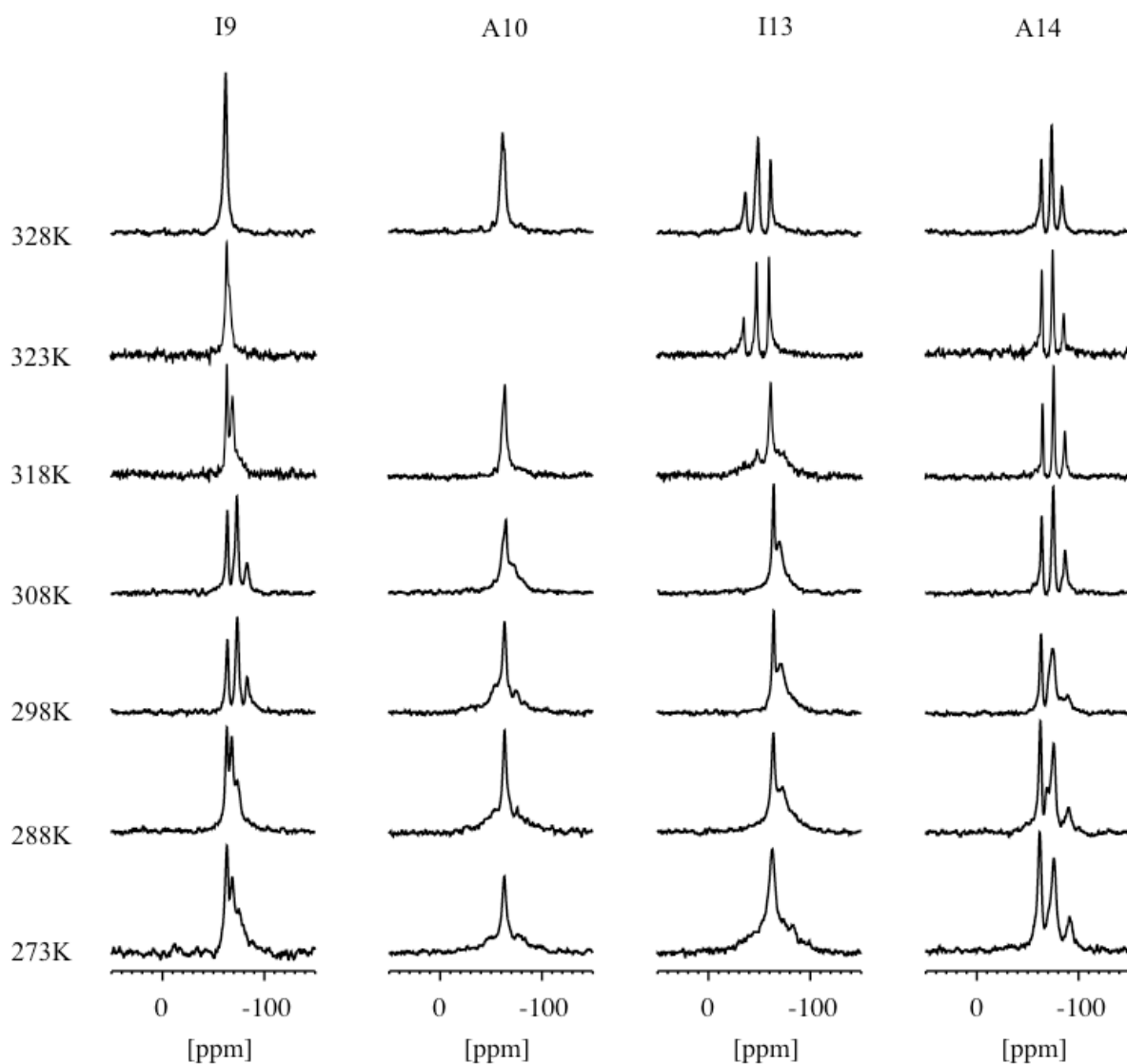
Figure 4.5 Solid state ^{19}F-NMR spectra of CF$_3$-Phg-labeled PGLa analogues (labeled position given on top of each column) in oriented DMPC/DMPG (3/1) bilayers at high P/L ratio (1/50) at different temperatures at 0° tilt. Due to experimental difficulties, one spectrum is lacking.

Table 4.3 Dipolar splittings for different CF$_3$-Phg-labeled PGLa analogues in oriented DMPC/DMPG (3/1) bilayers at high P/L ratio (1/50).

T [K]	Δ_{FF} [kHz]			
	I9	A10	I13	A14
328	0	0	+ 5,9	- 4,6
323	- 1,0	n/a	+ 6,3	- 5,1
318	- 2,5	0	+ 6,0	- 5,1
308	- 4,5	- 3,4	- 2,3	- 5,3
298	- 4,6	- 5,0	- 2,8	- 5,5
288	- 2,6	- 5,8	- 3,8	- 6,5
273	- 2,7	- 6,0	- 4,0	- 6,5

To describe the alignment of PGLa in the lipid bilayer, the helix tilt angle τ, the azimuthal rotation angle ρ and the molecular order parameter S_{mol} quantifying the motional averaging (2.3.5) were determined as described in section 4.1.10.

A full list of calculated best fit parameters is presented in Table 4.4. For data collected at 288, 308 and 328 K, being representative for the three major situations, in Figure 4.6 the best fit curves and the ρ/τ-diagrams are displayed in the left and right column, respectively. A T/τ-diagram is shown in Figure 4.7.
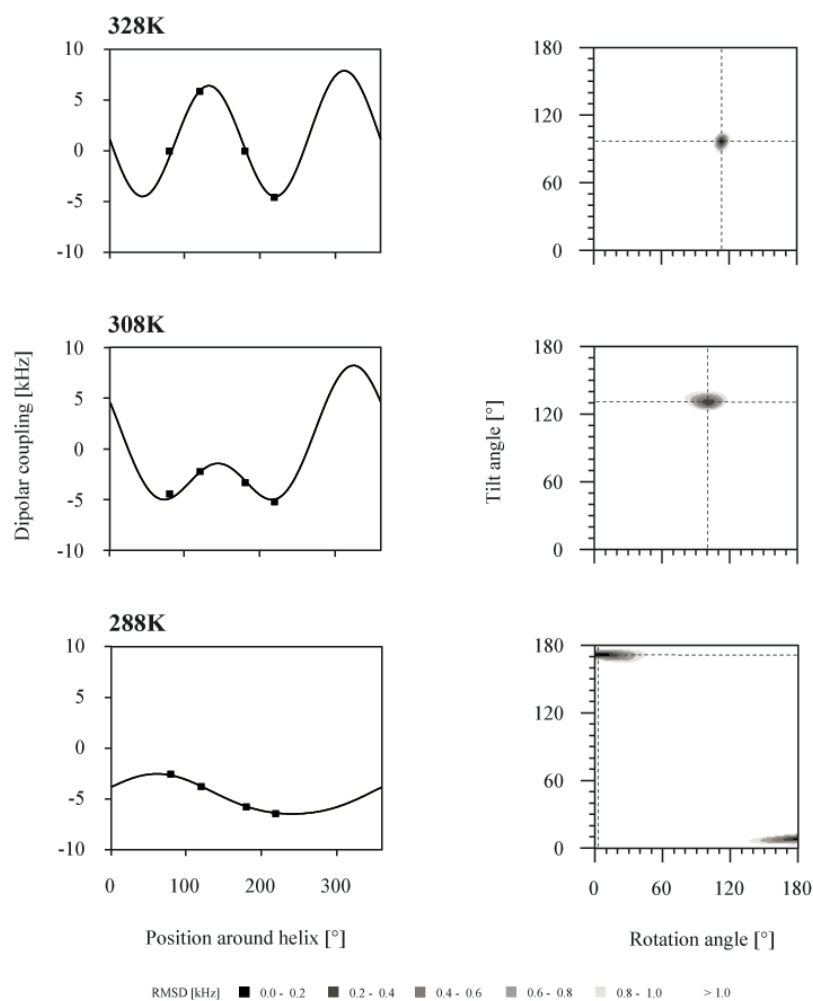
Figure 4.6 Best fit curve (left) and ρ/τ-diagram (right) for CF$_3$-Phg-labeled PGLa analogues in DMPC/DMPG (3/1) at high P/L ratio (1/50) showing the characteristic situation for each of the three temperature ranges. Dashed lines indicate the angles ρ and τ corresponding to the global minima.

Table 4.4 Full list of best-fit orientational parameters from data in Table 4.3.

T [K]	S_{mol}	Tilt [°]	Rotation [°]	RMSD [kHz]
328	0,6	96	113	0,2
323	0,7	98	111	0,0
318	0,7	102	108	0,4
308	0,6	131	101	0,3
298	0,7	134	110	0,4
288	1,0	172	3	0,1
273	0,9	172	11	0,0

For each set of triplets one unique well-defined minimum can be found. PGLa adopts a tilted alignment (T-state) at 298 and 308 K as previously found in DMPC and DMPC/DMPG lipid bilayers at ambient temperature (2.2.4.1). However, temperatures beyond that range show a clearly different situation. An inserted and almost upright orientation (I-state) is found at 273 and 288 K, a surface alignment (S-state) is found at elevated temperatures above 308 K. The order parameter S, describing the peptide wobble, adopts its maximum value of close to 1,0 below T_m, reflecting much lower mobility in the lipid bilayer gel phase as compared to the fluid phase. A diagram showing all tilt angles as a function of temperature is displayed in Figure 4.7. For each alignment state, a plateau can be found in the diagram. For the T- and the S-state, a slight decline in τ within each state is observed.
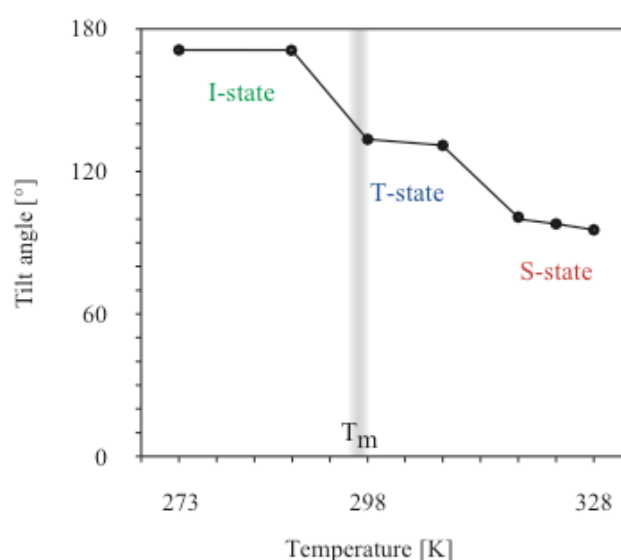
Figure 4.7 Temperature-dependence of PGLa tilt angle in oriented DMPC/DMPG (3/1) bilayers at high P/L ratio (1/50). Data points are connected for an easier identification. Grey bar indicates main phase transition temperature (T_m) of the pure lipid mixture (according to Lewis 2005).

At temperatures of about 298 K and higher, upon tilt of samples by 90°, spectra can be found to scale around the isotropic position by a factor of -1/2 (Figure 4.8 and Table 4.5), indicating rotational mobility of PGLa around the membrane normal. From about 298 K downwards, the spectral line shape indicates that this motion is significantly slowed down or stopped. At temperatures close to T_m the transition can be observed as the coexistence of two states as also seen at 0° tilt (compare to Figure 4.5).

Figure 4.8 Solid state ^{19}F-NMR spectra of CF$_3$-Phg-labeled PGLa analogues (labeled position given on top of each column) in oriented DMPC/DMPG (3/1) bilayers at high P/L ratio (1/50), at different temperatures at 90° tilt. Values of the corresponding dipolar splittings [kHz] are given next to each spectrum. The dipolar splitting of I9 up to 298 K are estimated with an accuracy of 0,5 kHz. Corresponding spectra at 0° tilt are shown in Figure 4.5.

Table 4.5 Dipolar splittings for different CF$_3$-Phg-labeled PGLa analogues in oriented DMPC/DMPG (3/1) bilayers at high P/L ratio (1/50) at 0° and 90° tilt, as read from spectra in Figure 4.8. The last two columns show dipolar splittings at 90° tilt multiplied by (-2). Scaling of splittings due to rotation of peptide around the bilayer normal can be observed from 298 K upwards (see text).

T [K]	Δ_{FF} [kHz]				Δ_{FF} (90°) * (-2)	
	I9		A14		I9	A14
	0°	90°	0°	90°		
328	0	0	- 4,6	+ 2,2	0	- 4,4
308	- 4,5	+ 2,2	- 5,3	+ 2,7	- 4,4	- 5,4
298	- 4,6	+ 2,5	- 5,5	- 8,4	- 5,0	+ 16,8
288	- 2,6	- 2,5	- 6,5	- 7,4	+ 5,0	+ 14,8
273	- 2,7	- 5,0	- 6,5	- 7,5	+ 10,0	+ 15,0

4.2.6   Temperature-dependent realignment of PGLa at high P/L ratio (1/50) in multilamellar vesicles

All four PGLa analogues as above were used to check if temperature-dependent realignment takes place in multilamellar vesicles likewise in oriented samples above. Thereby fingerprint spectra of 13CF$_3$-Phg with regard to dipolar splitting and chemical shift for the different states observed in oriented samples were obtained, for later comparison with spectra of 13CF$_3$-Phg PGLa in native membrane vesicles from erythrocytes and *M. luteus*. Fitting of the dipolar splittings as in oriented samples was not performed, as splittings were comparatively small and poorly resolved throughout and would not have delivered more and sufficiently accurate information compared to oriented lipid bilayers.

Spectra of PGLa at high P/L ratio (1/50) in multilamellar vesicles of DMPC/DMPG (3/1) at a hydration of 60 % (v/w) show a temperature-dependent change of line shapes in the range of 288 K to 323 K. Spectra are shown in Figure 4.9. Dipolar splittings are summarized in Table 4.6.
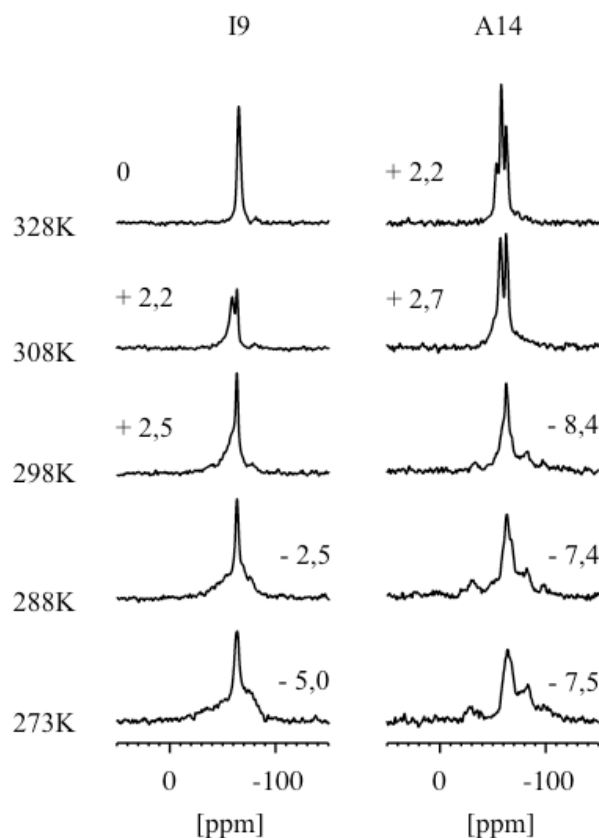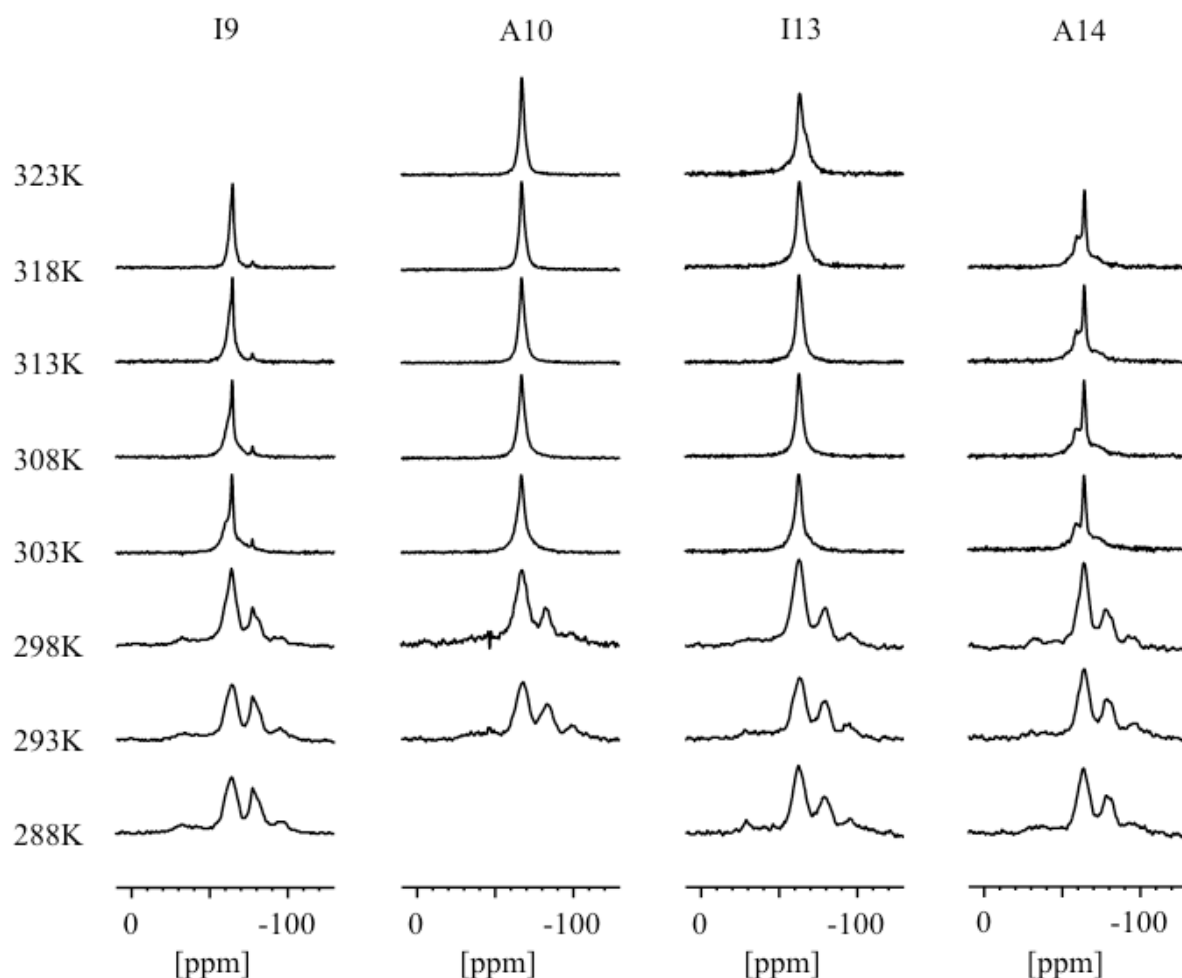
Figure 4.9 Solid state ^{19}F-NMR spectra of CF$_3$-Phg-labeled PGLa analogues (labeled position given on top of each column) in multilamellar vesicles of DMPC/DMPG (3/1) at high P/L ratio (1/50) at different temperatures. Due to experimental difficulties, a few spectra are lacking.

Up to 298 K, all labeled PGLa analogues exhibit dipolar splittings close to -7 kHz. At higher temperatures, i.e. in the fluid phase, spectra are significantly different, exhibiting further continuous changes in line shape and splittings upon an increase in temperature. 14CF$_3$-Phg PGLa exhibits positive dipolar splittings of slightly above +2 kHz throughout. The isotropic-like signal from 10CF3-Phg PGLa does not allow dipolar splittings to be determined. 9CF$_3$-Phg PGLa exhibits splitting of +2 kHz at 303 K and a transition to an apparently isotropic signal at elevated temperature. 13CF$_3$-Phg PGLa shows no obvious splitting at 303 K, but evolves a splitting of about -2 kHz upon increase in temperature.

Table 4.6 Dipolar splittings for different CF$_3$-Phg-labeled PGLa analogues in multilamellar vesicles of DMPC/DMPG (3/1) at high P/L ratio (1/50). Dipolar splitting of I9 between 303 K and 318 K and of I13 between 313 K and 323 K are estimated with an accuracy of 0,5 kHz.

T [K]	Δ_{FF} [kHz]			
	I9	A10	I13	A14
323	n/a	0	- 2,0	n/a
318	+ 0,5	0	- 1,5	+ 2,1
313	+ 1,0	0	- 1,0	+ 2,2
308	+ 1,5	0	0	+ 2,3
303	+ 2,0	0	0	+ 2,5
298	- 6,9	- 7,3	- 7,3	- 7,2
293	- 7,4	- 7,5	- 7,1	- 7,4
288	- 7,6	n/a	- 7,3	- 7,4

A comparison of dipolar splittings from multilamellar vesicles with those of oriented samples reveals a corresponding temperature-dependent realignment of PGLa in the fluid lamellar lipid phase. Contrary to oriented samples, in multilamellar vesicles this change appears to be gradual. Line shapes of 14CF$_3$-Phg PGLa in multilamellar vesicles throughout the whole temperature range above 298 K may correspond to the T-state as well as the S-state (Figure 4.5, Table 4.3). The maximum signal for both states in vesicles is expected to be found at the low field side with a dipolar splitting of approximately +2,5 kHz (Table 4.5, Figure 4.8). In Figure 4.10 spectra of 9CF$_3$-Phg PGLa at 303 K and 13CF$_3$-Phg PGLa at 323 K are expanded from Figure 4.9. At 303 K, a positive dipolar splitting of 9CF$_3$-Phg PGLa indicates a tilted alignment. 13CF$_3$-Phg PGLa excludes a surface alignment and the isotropic-looking signal indicates that PGLa is tilted. With increasing temperature up to 323 K, 13CF$_3$-Phg PGLa exhibits negative dipolar splitting as expected for the S-state. Correspondingly, 9CF$_3$-Phg PGLa shows a continuous decrease of dipolar splitting. Measurements of 9CF$_3$-Phg PGLa and 14CF$_3$-Phg PGLa at the highest temperature are lacking for experimental difficulties, but the tendency of both is obvious. Poor resolution of the isotropic-looking signal from 10CF$_3$-Phg PGLa does not allow for a differentiation between surface and tilted alignment for the whole temperature range on this label.

$\Delta_{FF} = + 2,0$ kHz

I9
303K

$\Delta_{FF} = - 2,0$ kHz

I13
323K

0   - 50   - 100   [ppm]
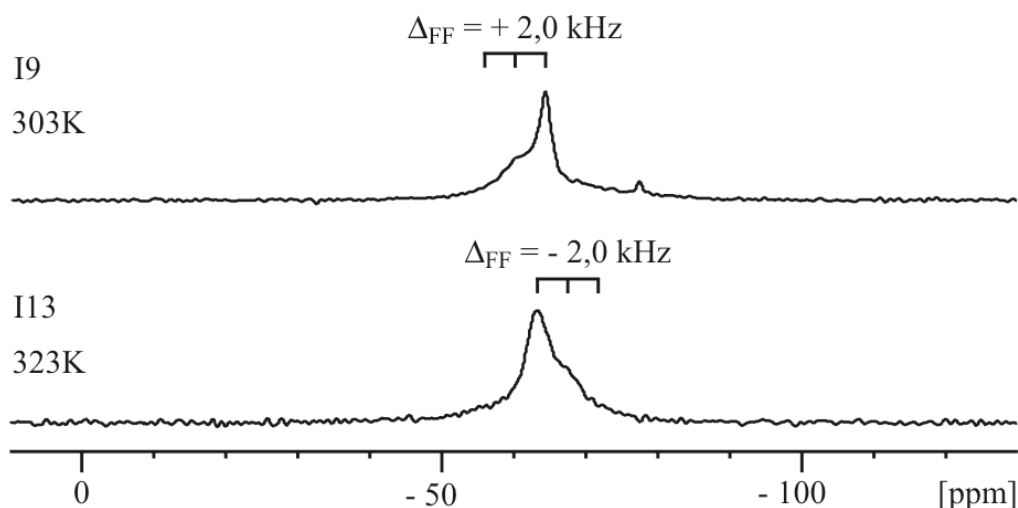
Figure 4.10 Spectra of 9CF$_3$-Phg PGLa at 303 K (upper) and 13CF$_3$-Phg PGLa at 323 K (lower) in multilamellar vesicles of DMPC/DMPG (3/1) at high P/L ratio (1/50). Dipolar splittings are estimated with an accuracy of 0,5 kHz.

4.2.7 Temperature-dependent realignment of PGLa in the presence of magainin 2 (1/1) at high P/L ratio (1/50) in oriented bilayers

By ^{2}H-NMR spectroscopy, PGLa was previously shown to adopt an upright inserted alignment (I-state) in the presence of magainin 2 at a high P/L ratio (1/50) in oriented DMPC/DMPG bilayers at ambient temperature (2.2.4.3). In order to obtain ^{19}F-NMR spectra of 13CF$_3$-Phg PGLa in this inserted state, later to be used as reference for cytoplasmic membranes, spectra of all four CF$_3$-Phg-labeled PGLa analogues were recorded in a temperature series, as results above (4.2.5) revealed the alignment of PGLa to be temperature-dependent.

In the 1/1/75/25 molar ratio of PGLa/magainin/DMPC/DMPG, ^{19}F-NMR spectra of CF$_3$-Phg-labeled PGLa show a temperature-dependent change of line shape upon increase in temperature from 288 K to 328 K (Figure 4.11). Under all conditions, spectra indicate a specific orientation of peptide and exhibit the expected triplet signals. Isotropic signals in spectra of 9CF$_3$-Phg and 10CF$_3$-Phg PGLa at elevated temperatures do not reflect a rapidly tumbling peptide, as already explained in 4.2.5.
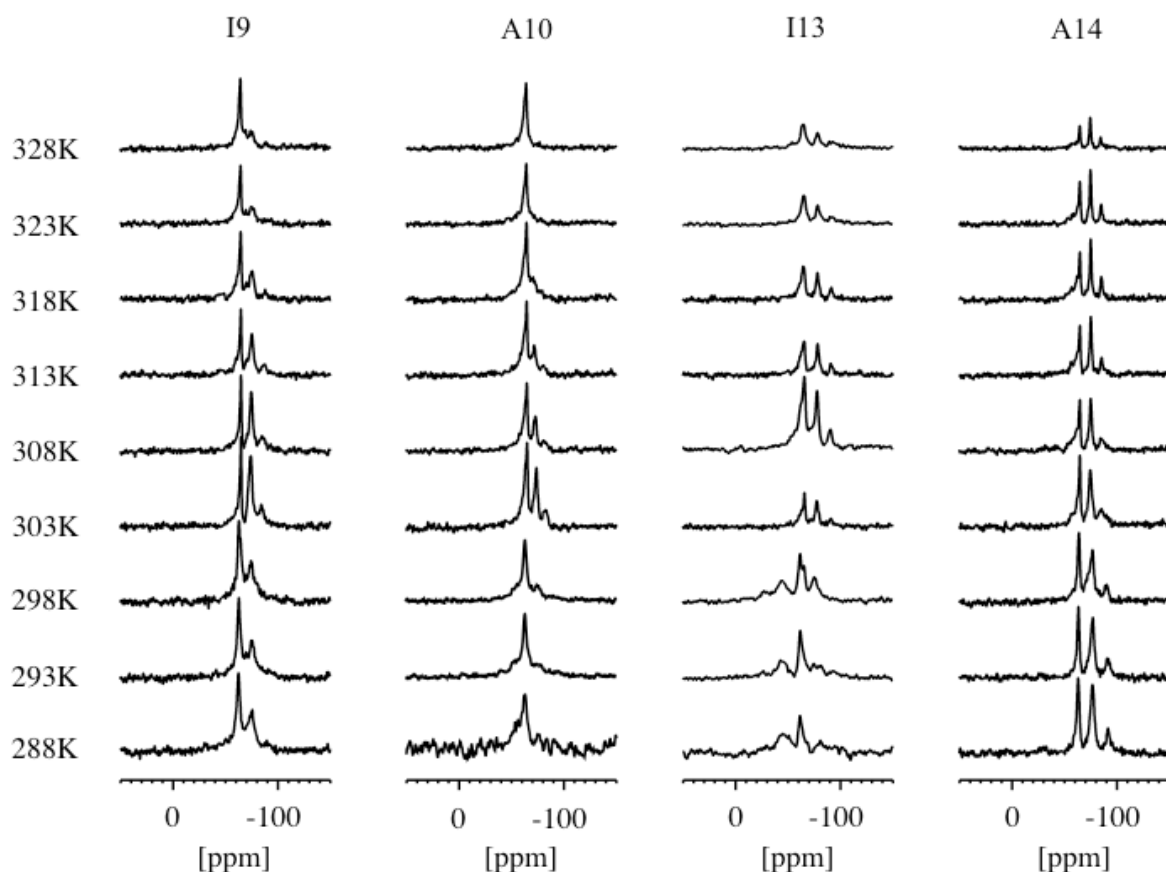
Figure 4.11 Solid state ^{19}F-NMR spectra of CF$_3$-Phg-labeled PGLa analogues (labeled position given on top of each column) with magainin 2 (1/1) in oriented DMPC/DMPG (3/1) bilayers at high P/L ratio (1/50) at different temperatures at 0° tilt.

Up to 298 K, spectra of 13CF$_3$-Phg PGLa in fact exhibit two triplet signals, indicating the coexistence of two discrete states. The spectrum of 13CF$_3$-Phg PGLa at 298 K, showing both triplets most pronounced, is expanded in Figure 4.12. However, no additional triplet can unambiguously be identified among the spectra of the other labeled peptides.
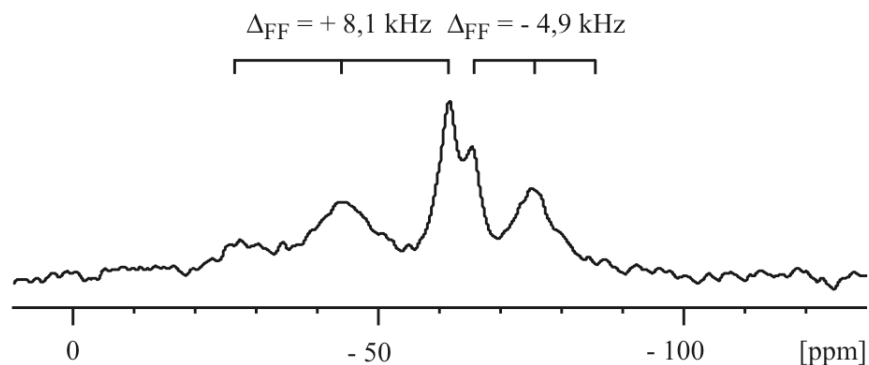
Figure 4.12 Spectrum of 13CF$_3$-Phg PGLa with magainin 2 (1/1) in oriented DMPC/DMPG (3/1) bilayers at high P/L ratio (1/50) at 298K.

Between 298 and 303 K, spectra of all labeled peptides exhibit an abrupt change of line shape. This is especially pronounced in the spectrum of 13CF$_3$-Phg PGLa, where one of the two triplets vanishes. In the spectra of 14CF$_3$-Phg PGLa, a significant drop in the value of the dipolar splitting can be observed. Upon further increase in temperature, all spectral line shapes gradually change. On the one hand, dipolar splittings alter slightly. On the other hand, among 9CF$_3$-Phg and 10CF$_3$-Phg PGLa, the intensities of a part of their triplets can be observed to drop. For instance, for 10CF$_3$-Phg PGLa only one signal with a broadened basis remains around the isotropic position. Dipolar splittings read from spectra in Figure 4.11 are summarized in Table 4.7.

Table 4.7 Dipolar splittings of CF$_3$-labeled PGLa analogues in the presence of magainin 2 (1/1) at high P/L ratio (1/50) in oriented DMPC/DMPG (3/1) bilayers. Up to 298 K two triplets can be identified in the spectra of 13CF$_3$-Phg PGLa.

T [K]	Δ_{FF} [kHz]			
	I9	A10	I13	A14
328	- 5,8	0,0	- 6,4	- 4,7
323	- 5,7	0,0	- 6,4	- 4,8
318	- 5,5	- 3,0	- 6,3	- 4,8
313	- 4,9	- 3,6	- 6,1	- 4,9
308	- 4,7	- 3,8	- 5,9	- 4,8
303	- 4,6	- 4,1	- 5,8	- 4,7
298	- 5,1	- 5,3	+ 8,1 / - 4,9	- 6,1
293	-5,7	- 5,5	+ 8,3 / - 7,1	- 6,5
288	- 6,2	?	+ 7,8 / - 6,0	- 6,7

To describe the alignment of PGLa in the lipid bilayer, orientational parameters were determined from the measured dipolar splittings, as described in sections 4.2.5 and 4.1.10.

Spectra of all CF$_3$-labeled PGLa analogues at temperatures just above 298 K show only one single well-defined set of triplets, representing one distinct alignment state for PGLa, and can thus be assigned to each other. At further elevated temperatures, a redistribution between two distinct states may be suggested. Contrary to spectra from 298 K downwards, however, no additional triplet of that evolving state can be identified clearly. Without an indication for that state, signals cannot unambiguously be assigned. Therefore, for further analysis only the most predominant situation among the whole set of spectra was

taken into account. The corresponding best fit curves and ρ/τ-diagrams for temperatures above 298 K are shown in Figure 4.15.

From 298 K downwards, one set of dipolar splittings can be assigned to each other corresponding to those at temperatures above 298 K. This procedure is supported by previous solid state ^{2}H-NMR studies, as explained above. PGLa was demonstrated to adopt an upright orientation in the presence of magainin 2 at ambient temperature. Hence, it is reasonable to assign negative dipolar splittings to another, as observed in 4.2.5. The resulting best fit curves and ρ/τ-diagrams for this first set of splittings are shown in Figure 4.13. After the assignment of that set of dipolar splittings, the only undoubtedly identifiable triplet remaining is that of 13CF$_3$-Phg PGLa. Considering the amphipathicity of the peptide, the positive dipolar splitting suggests a surface alignment of PGLa (compare to 4.2.2, 4.2.3 and 4.2.5). In fact, the positive component of the spectrum and the corresponding dipolar splitting of 13CF$_3$-Phg PGLa at 298 K displayed in Figure 4.12 show considerable similarity to Figure 4.3, representing an immobilized and surface-aligned 13CF$_3$-Phg PGLa. For the assumed surface alignment of the peptide, 9CF$_3$-Phg and 10CF$_3$-Phg PGLa are expected to exhibit an isotropic signal (Figure 4.5), which could not be identified underneath the present triplets. Structural analysis has been performed with differently assigned obvious negative dipolar splittings and supposed splittings of 0 kHz (also under omission of the broad and badly resolved 10CF$_3$-Phg PGLa). For 13CF$_3$-Phg PGLa, however, a positive splitting was always retained. All combinations delivered qualitatively similar results, namely a surfacially aligned PGLa, but of different quality of fits (data not shown). The best fits with the lowest RMSD throughout the gel phase represented the common S-state and are depicted in Figure 4.14.

The best fit orientational parameters are summarized in Table 4.8. A diagram with all tilt angles in dependence of the temperature is shown in Figure 4.16.

Figure 4.13 Best fit curves (left) and ρ/τ-diagrams (right) for PGLa alignments in the presence of magainin 2 (1/1) at high P/L ratio (1/50) in DMPC/DMPG (3/1) in the gel phase. Dashed lines indicate the angles ρ and τ corresponding to the global minima. As described in the text, data represent the inserted state of two alignments.
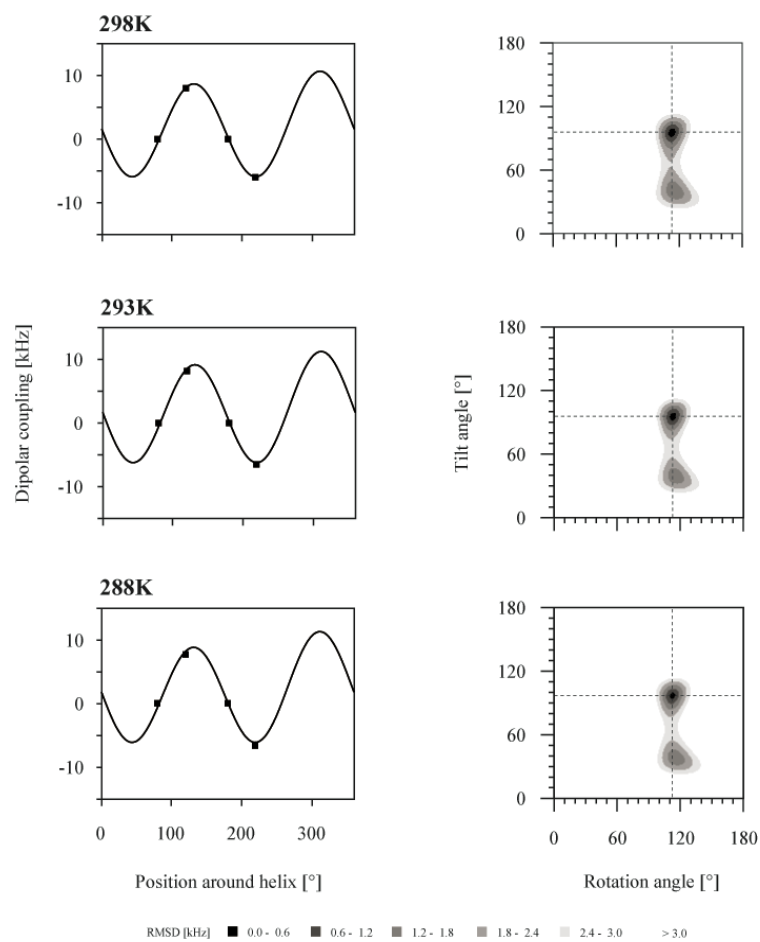
Figure 4.14 Best fit curves (left) and ρ/τ-diagrams (right) for PGLa alignments in the presence of magainin 2 (1/1) at high P/L ratio (1/50) in DMPC/DMPG (3/1) in the gel phase. Dashed lines indicate the angles ρ and τ corresponding to the global minima. As described in the text, data represent the surface state of two alignments.
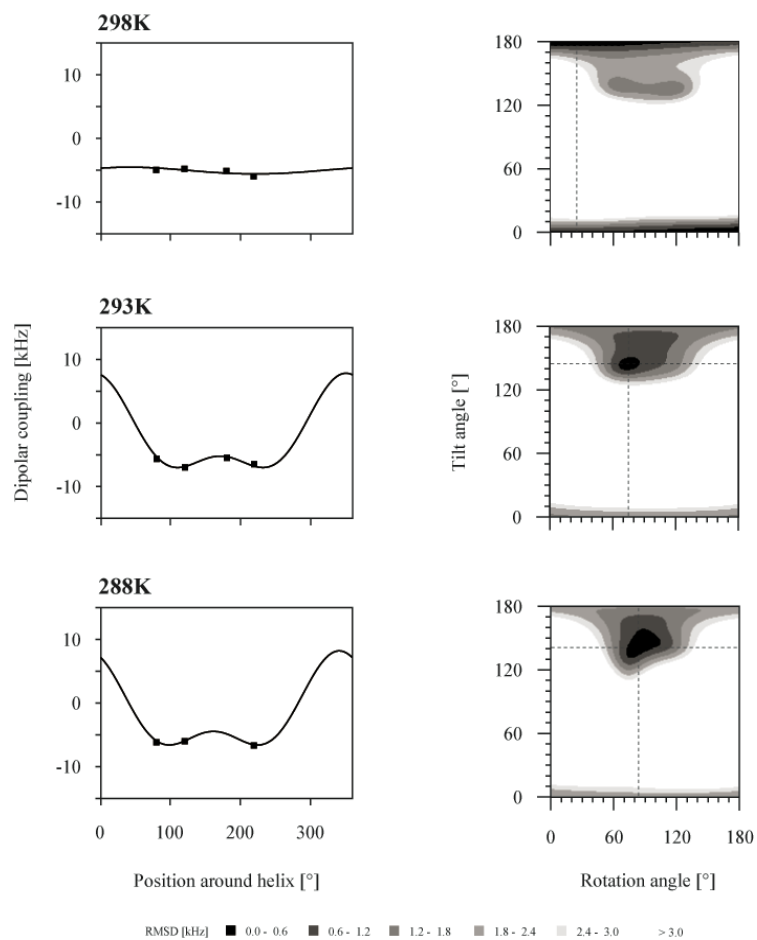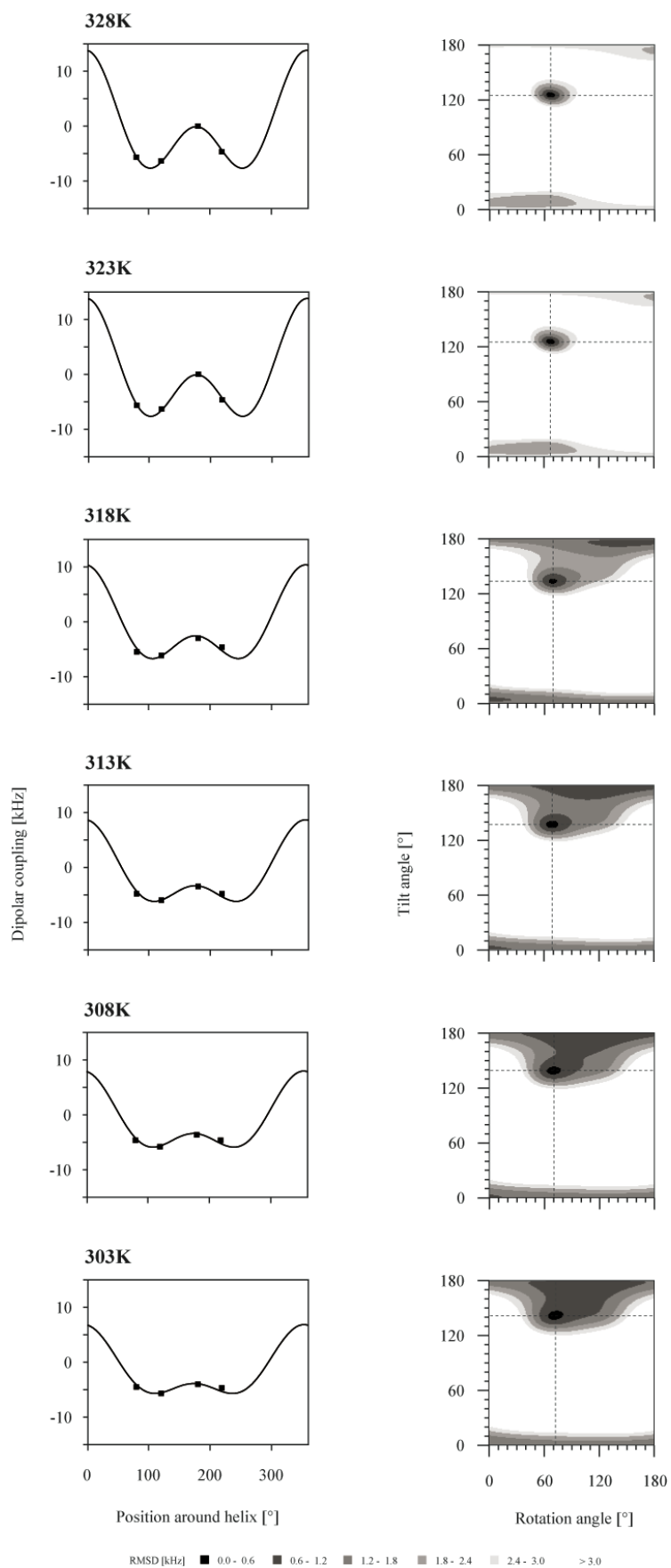
Figure 4.15 Best fit curves (left) and ρ/τ-diagrams (right) for PGLa alignments in the presence of magainin 2 (1/1) at high P/L ratio (1/50) in DMPC/DMPG (3/1) in the fluid phase. Dashed lines indicate the angles ρ and τ corresponding to the global minima.

Table 4.8 List of best-fit orientational parameters for PGLa in the presence of magainin 2 (1/1) at high P/L ratio (1/50) in oriented DMPC/DMPG (3/1) bilayers. Below 298 K two solutions correspond to the two sets of dipolar splittings found (Table 4.7).

T [K]	S_{mol}	Tilt [°]	Rotation [°]	RMSD [kHz]
328	1,0	125	67	0,1
323	1,0	125	67	0,1
318	0,9	133	69	0,5
313	0,8	137	69	0,4
308	0,8	139	70	0,4
303	0,7	141	71	0,4
298	1,0	178	23	0,3
	0,8	95	113	0,1
293	0,9	144	74	0,3
	0,8	96	113	0,2
288	0,9	141	84	0,0
	0,8	97	113	0,4

At all temperatures for each set of triplets, one unique well-defined minimum can be found. PGLa in the presence of magainin 2 adopts a strongly tilted alignment in the fluid phase. The tilt can be found to decrease upon increase in temperature. However, at no temperature the alignment resembles the T-state as observed for PGLa alone. In the gel phase bilayer, at temperatures close to the phase transition, an upright inserted alignment can be found, more inclined as observed previously by ^{2}H-NMR at ambient temperature (2.2.4.3). Corresponding populations of PGLa at lower temperatures exhibit smaller tilt angles. Surprisingly, in the gel phase a significant fraction of PGLa exhibits a surface alignment. For both alignment states below T_m, the order parameter S adopts values close to one, reflecting the restriction of peptide mobility in the gel phase of the lipid bilayer. The maximum value of 1,0 can be found for the inserted state with a tilt angle τ of close to 180° at T_m. Above 298 K, S reduces to 0,7, similar to PGLa alone in the T-state, indicating no large aggregates are being formed. Upon further elevation of temperature, an unexpected increase in S_{mol} takes place, accompanied by a gradual decrease in tilt as observed in Figure 4.7. A jump in the tilt angle τ can be observed from 318 to 323 K. S adopts the maximum value of 1,0. It is noticeable that the azimuthal rotation angle ρ retains a constantly small value throughout the whole fluid phase. A diagram showing all tilt angles as a function of temperature is displayed in Figure 4.16.
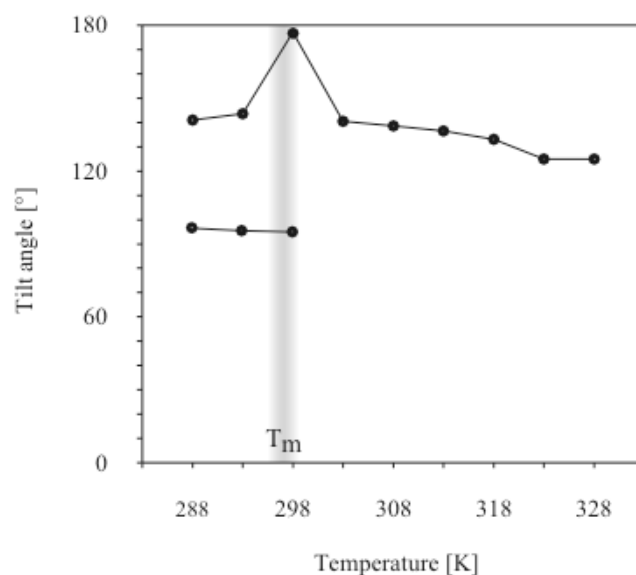
Figure 4.16 Temperature-dependence of PGLa tilt angle in presence of magainin 2 (1/1) in oriented DMPC/DMPG (3/1) bilayers at high P/L ratio (1/50). Data points are connected for an easier identification. Grey bar indicates main phase transition temperature (T_m) of the pure lipid mixture (according to Lewis 2005).

Upon tilt of the sample by 90°, ^{19}F-NMR spectra of 13CF$_3$-Phg PGLa up to 298 K exhibit broad signals with negative nonresolved dipolar splittings. This line shape is expected for a superposition of signals from a surface-aligned and a membrane-inserted fraction of the peptide, both being restricted in their mobility. Just above 298 K dipolar splittings can be found to scale around the isotropic position. The scaling factor can only be estimated roughly, as spectra are not sufficiently resolved. However, the principal behaviour suggests rotational mobility of PGLa, here. Upon further elevation of temperature, an extension of signal to the high field side, towards and across the isotropic position, can be observed. Apparently, the complex behaviour of PGLa under these conditions as indicated so far, as well as poor resolution of spectra, unfortunately do not allow a detailed analysis. Since no obvious corresponding change in the spectral line shape of 13CF$_3$-Phg PGLa at 0° tilt can be observed, the change may be attributed to the increase in S, i.e. the restricted mobility of the peptide. However, taking into account the evolution of the spectral line shapes of 9CF$_3$-Phg and 10CF$_3$-Phg PGLa at 0° tilt (Figure 4.11), this change may point towards a redistribution among two populations of peptide alignments.
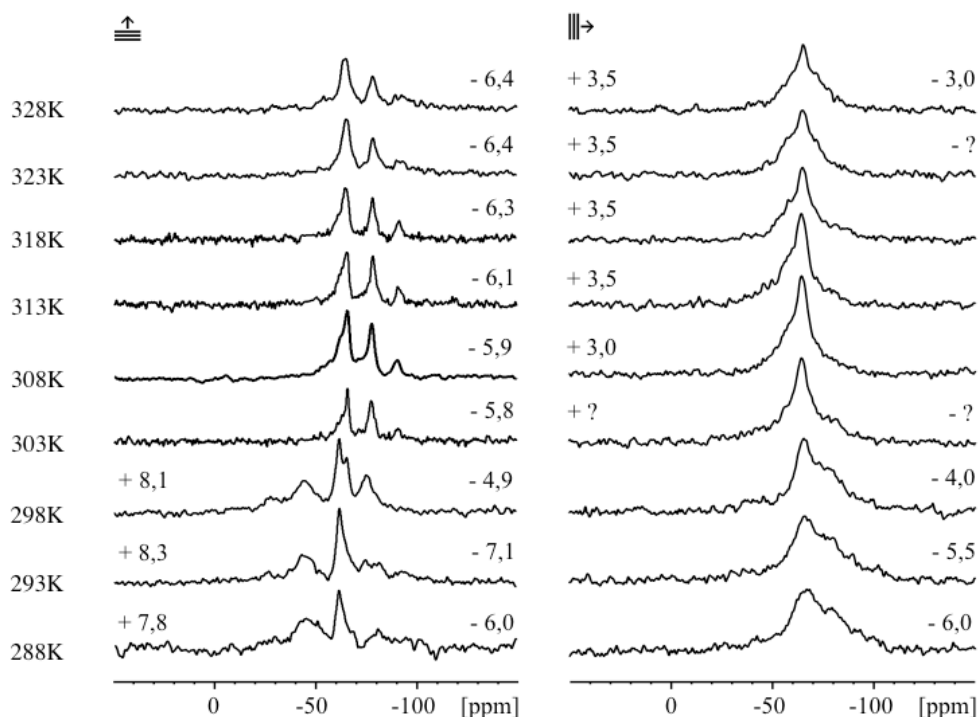
Figure 4.17 Solid state ^{19}F-NMR spectra of 13CF$_3$-Phg PGLa in the presence of magainin 2 in oriented DMPC/DMPG (3/1) bilayers at high P/L ratio (1/50) at different temperatures at 0° (left column) and 90° (right column) tilt. Dipolar splittings at 90° tilt are estimated with an accuracy of 0,5 kHz.

4.2.8 Temperature-dependent realignment of PGLa in the presence of magainin 2 (1/1) at high P/L ratio (1/50) in multilamellar vesicles

Solid state ^{19}F-NMR spectra of PGLa in the presence of magainin 2 (1/1) at high P/L ratio (1/50) in multilamellar vesicles of DMPC/DMPG (3/1) at hydration of 60 % (v/w) are displayed in Figure 4.18. Dipolar splittings are summarized in Table 4.9. Spectra exhibit a temperature-dependent change in the line shapes in the range of 288 K to 328 K.
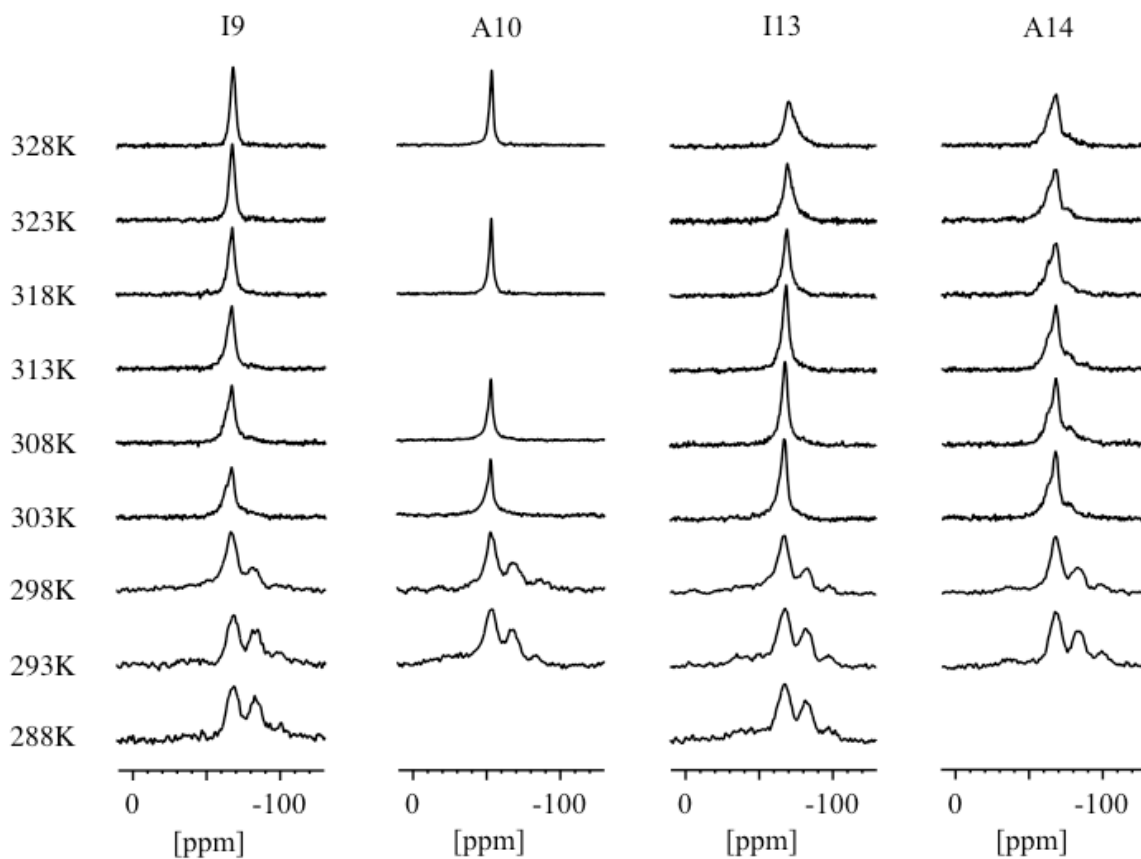
Figure 4.18 Solid state ^{19}F-NMR spectra of CF$_3$-Phg-labeled PGLa analogues (labeled position given on top of each column) in the presence of magainin 2 (1/1) in multilamellar vesicles of DMPC/DMPG (3/1) at high P/L ratio (1/50) at different temperatures. Due to experimental difficulties, some spectra are lacking.

Spectra are far less resolved, dipolar splittings are much smaller compared to multilamellar vesicles with PGLa alone (4.2.6). Again, due to unresolved dipolar splittings, no determination of the peptide orientational parameters was performed. Up to 298 K all labeled PGLa analogues exhibit dipolar splittings close to -7 kHz. Above 298 K, i.e. in the fluid lamellar bilayer phase, spectra are significantly different. All labeled peptides exhibit small positive dipolar splitting of approximately +2 kHz just above T$_m$. For illustration, 14CF$_3$-Phg PGLa as the most pronounced spectrum of that set at 303 K is expanded in Figure 4.19. Upon further elevation of temperature a slight change of spectral line shapes can be observed among all CF$_3$-labeled peptides, except for 14CF$_3$-Phg PGLa. Positive dipolar splitting persists in spectra of 14CF$_3$-Phg PGLa throughout the whole temperature range. Spectral line shapes of 9CF$_3$-Phg and 10CF$_3$-Phg PGLa shift to an isotropic-like signal upon elevation of temperature to 328 K. Simultaneously 13CF$_3$-Phg PGLa shows a gradual shift of line shape from positive to isotropic to negative dipolar splitting.

Table 4.9 Dipolar splittings for different CF$_3$-Phg-labeled PGLa analogues in the presence of magainin 2 (1/1) in DMPC/DMPG (3/1) multi-lamellar vesicles at high P/L ratio (1/50). Dipolar splittings from 303 K upwards are estimated with an accuracy of 0,5 kHz.

T [K]	Δ_{FF} [kHz]			
	I9	A10	I13	A14
328	0	0	- 2,0	+ 2,0
323	0	n/a	- 1,0	+ 2,5
318	+ 0,5	+ 1	0	+ 2,0
313	+ 1,0	n/a	0	+ 2,5
308	+ 1,5	+ 1,5	0	+ 2,5
303	+ 2,0	+ 1,5	+ 1,5	+ 2,5
298	- 7,4	- 7,5	- 7,2	- 7,2
293	- 7,2	- 6,9	- 6,9	- 7,3
288	- 7,2	n/a	- 7,0	n/a

Dipolar splittings in multilamellar vesicles indicate a gradual decrease in peptide tilt within the fluid lamellar lipid phase upon increase in temperature. Just above T_m, small positive dipolar splittings among all labeled analogues correspond to a tilted alignment of PGLa (4.2.5), corresponding to oriented samples in the presence of magainin 2 (4.2.7). The line shape of 14CF$_3$-Phg PGLa in multilamellar vesicles throughout the whole temperature range above 298 K may be attributed to a tilted as well as a surface alignment (compare to Figure 4.8 and 4.2.6). According to oriented samples with PGLa alone (4.2.5), changes of both the line shapes of 9CF$_3$ and 10CF$_3$-Phg PGLa to an isotropic and simultaneously of 13CF$_3$-Phg PGLa to an isotropic and beyond to a positive dipolar splitting, are expected for a realignment from a tilted to a surface orientation. However, due to bad resolution, the spectral line shapes in the fluid lamellar lipid phase towards 328 K do not provide an indication of a redistribution between two alignment states as it may be suggested in oriented samples in the presence of magainin 2.
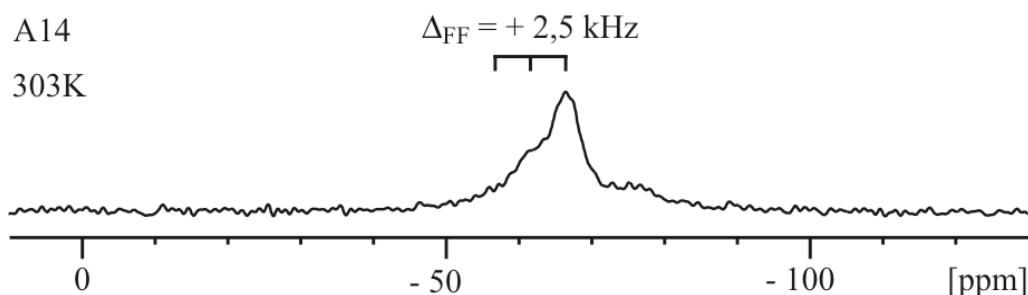
Figure 4.19 Spectrum of 14CF$_3$-Phg PGLa at 303 K in multilamellar vesicles of DMPC/DMPG (3/1) at high P/L ratio (1/50) expanded from Figure 4.18. Dipolar splitting is estimated with an accuracy of 0,5 kHz.

4.3 Discussion

In this part of the study, the structure and orientation of PGLa in synthetic lipid bilayers, alone and together with magainin 2 as a synergistic pair, was analyzed as a function of lipid phase and temperature.

To obtain orientational constraints, four differently labeled CF_3-Phg PGLa analoga were systematically analyzed in fully hydrated macroscopically aligned samples composed of DMPC/DMPG (3/1) at a high P/L ratio of 1/50 in absence or presence of equimolar amount of magainin 2. PGLa was modeled as a rigid regular α-helix (Glaser 2004) allowing the calculation of the orientational state and the overall mobility of the PGLa peptide. Results were subsequently compared to data from corresponding multilamellar vesicles at higher hydration.

In previous studies, PGLa alone in synthetic lipid bilayers (DMPC or DMPC/DMPG) at ambient temperature could be demonstrated to undergo a concentration-dependent realignment from a flat surface-bound state (S-state) at low (1/200) P/L ratio to a tilted alignment (T-state) at high (1/50) P/L ratio (Glaser 2005; Glaser 2004; Tremouilhac 2006b; Strandberg 2006). In both alignment states the peptide rotates fast around the membrane normal. In the S-state, the peptide was suggested to represent a monomeric state. At a tilt angle τ of approximately 100° and an azimuthal rotation angle ρ of approximately 115°, the hydrophobic lysine residues are arranged towards the aqueous surrounding. For the T-state, the formation of antiparallel homodimers was proposed, with the C-termini of both helices immersing into the hydrophobic core of the membrane at a τ of approximately 125° and a ρ of approximately 110°.

Only in the presence of magainin 2 at equimolar ratio at high P/L ratio (1/50), a motionally restricted, inserted peptide (I-state) with a tilt angle of approximately 160° could be observed at ambient temperature (Tremouilhac 2006a).

Overall, lipids in macroscopically aligned samples were well-oriented to an extent of usually above 80 % as determined upon integration of ^{31}P-NMR spectra. Spectra of multilamellar vesicles showed a typical spectrum for spherically distributed lipids in a lamellar bilayer phase. Both observations prove the compatibility of a lamellar bilayer with the presence of PGLa or PGLa/mag 2 even at a high P/L ratio of 1/50. No indication of significant curvature stress or disruption of the bilayer integrity was observed.

In the present study, PGLa was shown for the first time to adopt all three alignment states (S, T and I) on its own, depending on the temperature and the lipid phase. All three states could be determined very accurately, as assessed by the corresponding RMSD values.

In the lipid gel phase, PGLa adopts an upright inserted state (I-state) with a τ of approximately 170°. Due to this upright orientation, a broad range of values for ρ will give a good fit, as ρ will become undefinable in a perfectly upright orientation of the helix. In the fluid phase just above T_m, an oblique alignment (T-state) with a helix tilt angle τ of approximately 130° was found, changing discretely to approximately 100° (S-state) upon further elevation of temperature to 318 K and above. The azimuthal rotation angle retains a value of approximately 110° for both the S- and the T-state, and in accordance with the amphipathicity of the peptide helix places the positively charged lysine residues towards the aqueous surrounding.

In gel phase bilayers, the absence of rotational diffusion of PGLa, as determined by 90° tilt of samples, and an order parameter S_{mol} adopting high values of approximately 0,9 to 1,0, reflect the restricted mobility of PGLa in the I-state. In fluid bilayers, an order parameter S_{mol} of approximately 0,6 to 0,7 can be found for both the T- and the S-state. The high rotational mobility of PGLa excludes the formation of large peptide aggregates in this case.

The realignment of PGLa from the I- to the T-state appears to be related to the change of the lipid phase. A relatively rigid membrane in the gel phase, containing local defects, suggests to facilitate an insertion of PGLa. In the fluid phase above 318 K, during the transition from the T-state to the S-state, two distinct populations of peptide appear to exist. They rather represent a switch than a shift between both alignments, presumably effected by enhanced kinetic energy of the system breaking the supposed homodimers.

Assuming that the 21 residue-long PGLa forms an α-helix with 1,5 Å distance per residue (Tremhouilhac, 2007), upon adopting the I-state it will obtain an effective length across the membrane of approximately 31 Å according to $x = 21*1,5\,\text{Å}*\left|\cos\tau\right|$. Hence, the peptide should match the length of the hydrophobic region of the DMPC/DMPG bilayer. This can be estimated to be approximately 30 Å upon determination of the hydrocarbon length of gel phase DMPC bilayers (Tristam-Nagle, 2002).

High values of close to 1,0 for the order parameter in the I-state, indicate a rigid structure, supporting the presumption that the inserted PGLa helices might assemble into higher oligomers. Contact of the charged residues with the hydrophobic core of the membrane may be avoided by arranging the peptides into proposed transmembrane pores

with the hydrophobic residues facing the surrounding membrane core and the charged residues lining a water-filled interior of the channel (2.2.3).

The three different alignment states observed for PGLa in oriented samples in dependence of temperature and lipid phase, are schematically illustrated in Figure 4.20.
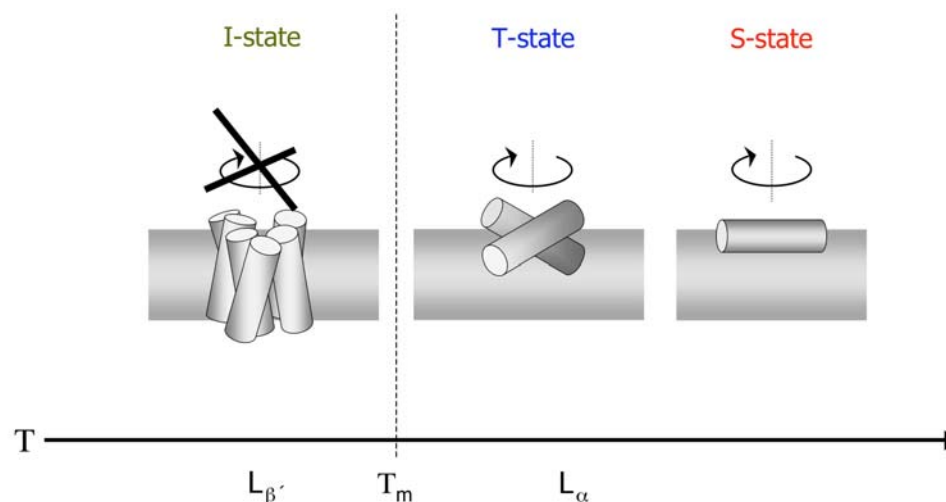
Figure 4.20 Illustration of the three different distinct alignment states identified for PGLa in oriented samples in dependence of temperature and lipid phase. In the lipid gel phase, PGLa is inserted almost upright (I-state), lacking rotational mobility. It is presumed, that homodimers arrange to form larger assemblies with an aqueous interior (pore structure). Just above the phase transition temperature, PGLa adopts a tilted alignment (T-state), supposedly as homodimers. Upon increase in temperature, these dimers are no longer stable and disassemble into monomers, which in accordance with their amphipathicity align on the surface of the membrane (S-state).

In multilamellar vesicles, no determination of orientational parameters comparable to macroscopically aligned bilayers was performed, due to poorly resolved dipolar splittings. Hence, data were interpreted qualitatively, and results will be discussed solely in comparison to the alignment states found for PGLa in macroscopically aligned bilayers and to findings reported previously.

For PGL at a high P/L ratio (1/50) in fluid phase multilamellar vesicles, in principle the same realignment as in oriented samples could be confirmed, from the T-state just above T_m to the S-state at elevated temperature. However, the realignment appeared to be a rather continuous event, instead of the expected distinct switch, as spectra showed a gradual change of line shapes and dipolar splittings with increasing temperature.

Previously, the hydration of a sample was shown to influence the realignment with regard to the threshold concentration for the S-T transition and the range for the full transition (Tremhouilhac 2006b). The influences due to hydration were interpreted in terms of bulk water providing a reservoir for free peptide molecules in equilibrium with membrane-bound peptide species. In detail, the amount of positively charged amphiphilic peptide molecules

that a membrane can accomodate before electrostatic repulsion between peptides molecules leads to an equilibrium with the bulk water, depends on the amount of negative charge in the lipid bilayer. In fully hydrated oriented samples with virtually no bulk water phase, the affinity of the peptide to the membrane does not play a significant role, but the peptide will be bound to the membrane completely (Afonin 2003b). For instance, in fully hydrated multilamellar vesicle samples purely of zwitterionic DMPC, more peptide molecules are needed in the sample, i.e. a higher P/L ratio, compared to oriented bilayers of DMPC or to corresponding samples composed of DMPC/DMPG, to accumulate sufficient peptide molecules in the membrane bilayer to trigger the switch from the S- to the T-state, as significant amount of peptide escapes into the bulk water. In particular, in multilamellar vesicles composed of the net uncharged lipid DMPC at a high P/L ratio expected to arrange PGLa in the T-state, by ^{2}H-NMR spectroscopy an atypical intermediate alignment between the S- and T-state was found (Tremhouilhac 2006b). It was rationalized as a fast exchange of peptides between the S-state and the T-state. In multilamellar vesicles composed of DMPC and the net negatively charged lipid DMPG, however, the decisive P/L ratios of 1/50 and 1/200 resulted in the expected T- and S-state, respectively.

Concerning the results of this study, it may thus reasonably be assumed that temperature, in addition to the previously determined factors (peptide concentration, lipid charge and hydration level), shifts the S-T equilibrium in multilamellar vesicles, and the observed spectra represent the averages of varying ratios of both alignment states.

In accordance with data from oriented samples, there is evidence that the peptide also adopts an I-state in multilamellar vesicles in the lipid gel phase. However, as a result of the above described properties of the I-state, this alignment state cannot be confirmed unambiguously in this type of model membrane. The spread of orientations adopted by PGLa in the I-state in vesicles and the associated restricted rotational mobility, result in a spectrum similar to unoriented peptide. In fact, any immobilized peptide spherically distributed as in vesicles will result in a spectrum similar to unoriented peptide.

As demonstrated above for PGLa alone, in oriented samples in the presence of magainin 2, the peptide was shown to realign in dependence of temperature and lipid phase. However, the situation is far more complex here.

In gel state bilayers, clear coexistence of two populations of PGLa at about equal amounts of peptide molecules could be identified. One population resides in a surface alignment, with the approximate angles τ and ρ being 95° and 115°, respectively. These

angles correspond to the S-state as observed for PGLa alone, however, restricted rotational diffusion and peptide wobble are indicated by broad unresolved lines upon 90° tilt of samples and high order parameter values close to 1,0. The second population of PGLa was shown to reside in an I-state, adopting the most pronounced upright orientation at τ being approximately 180° around the phase transition of the lipid bilayer. The corresponding populations at lower temperatures adopt tilt angles of aproximately 145°. Despite the fact that these tilt angles are slightly lower than even previously found for the I-state, all these alignments are termed I-state here, as they are all deeply immerged into the hydrophobic core of the membrane and are motionally restricted, thus suggesting the assembly of transmembrane pores. For the observed I-state of PGLa in the presence of magainin 2 around phase transition, the peptide will obtain an effective length across the membrane of approximately 32 Å, being in accordance with the hydrophobic length of the bilayer (as described above).

In the fluid phase upon increase in temperature up to 318 K, in the presence of magainin 2, PGLa was found to be strongly inclined at a continuously decreasing tilt angle from approximately 140° to 130°. Compared to the T-state adopted by PGLa alone, the peptide helix is rolled by about 40° in the membrane plane, obtaining an azimuthal rotation angle of approximately 70° throughout. As a result, the hydrophobic face of the helix is rather placed on one side to the aqueous surrounding, and three of four lysine residues may be expected to point straight out of the membrane plane. PGLa is rotationally mobile at lower temperatures, as it was demonstrated by measurements at 90° tilt. Hence, the formation of larger aggregates could be excluded there. However, a rapid increase upon elevation of temperature and decrease in tilt could be observed.

The highly tilted and rolled PGLa helix is consistent with previous studies, proposing the formation of parallel heterodimers of PGLa and magainin 2 (Matsuzaki 1998b; Hara 2001). These dimers were suggested to be stabilized by salt bridges between the charged residues Lys-19 of PGLa and Glu-19 of magainin 2 (Tremhouilhac 2006a). The azimuthal rotation angle actually observed here, may also suggests an interaction between the proximate Lys-15 of PGLa and Glu-19 of magainin 2. The presumed heterodimer would allow the peptides to immerge more deeply into the membrane as compared to the proposed PGLa homodimer.

A transition from this strongly inclined tilt to another distinct alignment state could be observed above 318 K, together with a surprising jump in the order parameter. This event suggests an involvement of a similar mechanism as the dimer-monomer transition described

above for PGLa alone. This second state in the fluid phase was determined as a tilted alignment with a lower inclination. However, due to the complexity of temperature-dependent behaviour of PGLa in the presence of magainin 2, an unambiguous determination of that alignment state (4.2.7) was not possible with the present data. It should therefore be noted, that apart from this tilted state, a different approach suggested a redistribution between above described strongly tilted and a surface-aligned population of PGLa. However, the indication of a peptide behaviour comparable to PGLa alone is identical in either interpretation.

The different alignment states observed for PGLa in oriented samples in dependence of temperature and lipid phase, are schematically illustrated in Figure 4.21.
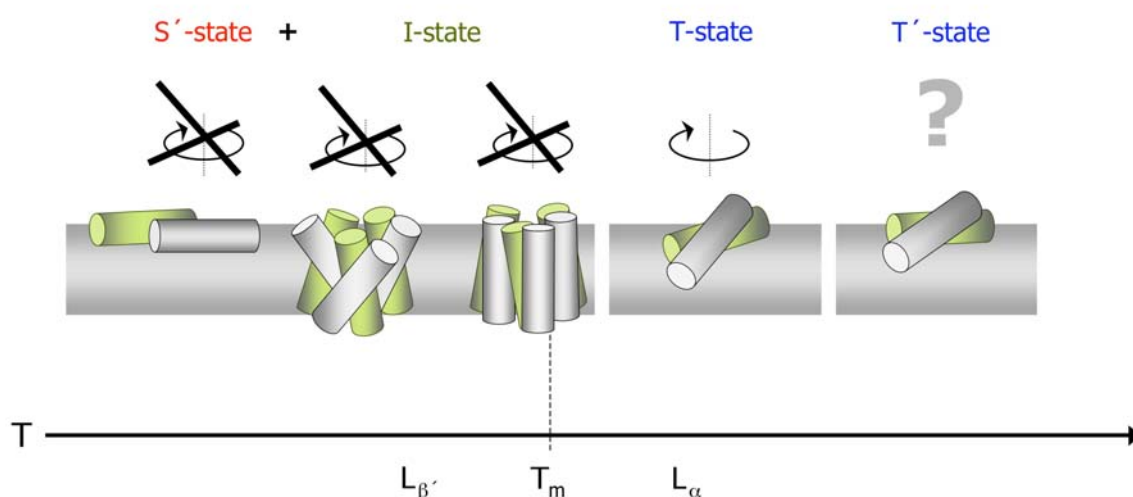
Figure 4.21 Illustration of the different alignment states identified for PGLa (grey) in the presence of magainin 2 (green) in a 1/1 molar ratio in oriented samples in dependence of temperature and lipid phase. The behaviour of magainin 2 is not confirmed. In the lipid gel phase, PGLa is inserted almost upright (I-state), lacking rotational mobility. The largest inclination is adopted around phase transition. It is presumed, that heterodimers of PGLa/magainin 2 arrange to form larger assemblies with an aqueous interior (pore structure). A coexisting immobilized surfacially aligned population is indicated aside (S´-state). Just above the phase transition, PGLa adopts a strongly tilted alignment, supposedly as heterodimers together with magainin 2 (termed T-state, as it is the corresponding alignment to PGLa alone). Upon increase in temperature, PGLa was observed to realign, presumably adopting a lower inclination (T`-state). However, the redistribution between the T-state and a surface alignment (comparable to PGLa alone) cannot be excluded.

For multilamellar vesicles with PGLa in the presence of magainin 2, the corresponding considerations as for PGLa alone are applicable. No determination of orientational parameters comparable to macroscopically aligned bilayers was performed, especially as spectra in this case additionally exhibited less resolved lines due to lower rotational mobility of the peptide. However, in fluid phase multilamellar vesicles as in the corresponding oriented samples, the signs of the broad spectral lines obviously display a comparable tilted alignment of PGL in the presence of magainin 2 just above T_m, and a subsequent realignment with decreasing tilt upon increase in temperature. A surface alignment is suggested at elevated temperature. As in

multilamellar vesicles with PGLa alone, the realignment appears to be a rather continuous event. As above in the gel phase, the inserted upright alignment cannot be confirmed unambiguously in this type of membrane model.

In summary, PGLa in macroscopically aligned synthetic lipid bilayers was demonstrated to exhibit a similar principle behaviour in the presence or absence of equimolar amounts of magainin 2, showing an upright inserted alignment in the gel phase, a tilted alignment in the fluid phase, and a further distinctly different alignment at elevated temperature. However, in the presence of magainin 2, a coexisting surface alignment was observed in the gel phase. Furthermore, in the fluid phase the PGLa helix inclination was shown to be markedly increased in the presence of magainin 2. Despite this complex behaviour, the presented results are well in accordance with previous studies. Previous NMR studies conducted at ambient temperature focused primarily on the variation of the parameters P/L ratio, lipid composition or hydration status (Glaser 2005; Tremouilhac 2006b), whereas the focus of this study was on temperature and lipid phase. The results of this study may structurally explain the different functional activities performed by PGLa alone and together with magainin 2 as a synergistic pair. They may as well exert considerable implications on the activity of AMPs in native cell membranes, in general.

Previous studies reported the functional synergism of PGLa/magainin 2 mixtures (Westerhoff 1995) and described the membrane lytic activity being maximal at an equimolar ratio of both peptides (Matsuzaki 1998b; Hara 2001; Nishida 2007). Synergism was attributed to the formation of parallel heterodimers, presumed to enable the synergetic pair to form pores at a faster rate as either peptide and being more stable than the transmembrane pores of PGLa (Ludtke 1996; Matsuzaki 1998b; Tremouilhac 2006a). This may at least partially be attributed to the observed larger inclination, presumably resulting in a deeper immersion in the membrane. However, neither for PGLa nor for PGLa/magainin 2 mixtures, such a pore structure has been observed, yet. PGLa in the presence of magainin 2 was only demonstrated to adopt an inserted alignment at ambient temperature (Tremouilhac 2006a).

Transient pore formation, however, is consistent with the SMH model. Leakage by magainin 2 was observed to be maximal in the early stage of the peptide-lipid interaction (Matsuzaki 1995b). Accumulation of peptide molecules in the outer membrane layer is assumed to induce curvature strain in the membrane, presenting one of the driving forces for the translocation of peptide molecules across the bilayer and for the potential membrane perturbance. Once the equilibrium is reached, only the most stable situation for this high

peptide concentration might be observed. That supposedly might be a shallow tilt for pure PGLa or a more deeply immersed peptide in equimolar PGLa/magainin 2 mixtures. Despite the fact, that a transient I-state therefore might only be trapped, identified and investigated under conditions of oriented membranes in gel phase lipid bilayers, the basic tendency of PGLa to insert into lipid bilayers is obvious, be it alone or to a larger extent in the presence of magainin 2.

5 Preparation of cytoplasmic membranes for solid state NMR spectroscopy

5.1 Materials and methods

5.1.1 Instruments

Autoclave Sanoclav	Wolf (Geislingen, Germany)
Autoclave Systec 2540 EL	Systec (Wettenberg, Germany)
Autoclave Varioklav 400	H+P Labortechnik (Oberschleissheim, Germany)
Balance PB 3001 (accuracy (acc.) 0,1 g)	Mettler Toledo (Greifensee, Switzerland)
Balance analytic Sartorius (acc. 0,0001 g)	Mettler Toledo (Greifensee, Switzerland)
Balance M2P Sartorius (acc. 0,0001 mg)	Mettler Toledo (Greifensee, Switzerland)
Camera PowerShot G5	Canon (Japan)
Centrifuge 3-18K	Sigma (Osterode am Harz, Germany)
with Rotor 19776-H	
Centrifuge Avanti J-25	Beckman Coulter (Fullerton, CA, USA)
with Rotors JA14 and JLA-9.1000	
Centrifuge Biofuge Pico	Heraeus (Hanau, Germany)
Centrifuge L8-60M Ultracentrifuge	Beckman (Palo Alto, CA, USA)
with Rotor VTi65	
Culture flasks (50 ml; 1 l; 2 l)	Schott Duran (Mainz, Germany)
Diaphragm vacuum pump	Vacuubrand (Wertheim, Germany)
Glass tubes	Schott Duran (Mainz, Germany)
Incubator shaker model G25	New Brunswick Scientific (Edison, NJ, USA)
Incubator shaker Innova 44	New Brunswick Scientific (Edison, NJ, USA)
Laminar flow box Hera safe	Heraeus Instruments (Stuttgart, Germany)
Microscope Axioskop 40	Zeiss (Heidelberg, Germany)
NMR spectrometer Avance 500	Bruker Biospin (Karlsruhe, Germany)
Probehead for ^{31}P H/X/Y	Bruker Biospin (Karlsruhe, Germany)
Oven B5042	Heraeus (Hanau, Germany)
Pipette Reference	Eppendorf (Hamburg, Germany)
(0,5-10 µl; 10-100 µl; 100-1000 µl)	

Pipettes Pipetus akku	Pipetus (Eberstadt, Germany)
Shaker	Biometra (Goettingen, Germany)
Shaker KS250 basic	IKA Labortechnik (Staufen, Germany)
Sonifier 250 Branson	Heinemann (Schwäbisch Gmünd, Germany)
Spectrophotometer Smart Spec Plus	Bio-Rad (Hercules, CA, USA)
Spectrophotometer Carey 1E	Varian (Palo Alto, CA, USA)
Tube sealer	Beckman (Palo Alto, CA, USA)
Vortex mixer Genie K-550-GE	Bender & Hobein (Zurich, Switzerland)
Water bath	GFL Migge Laborbedarf (Heidelberg, Germany)

5.1.2 Consumables

Centrifuge tubes (15 ml; 50 ml)	Sarstedt (Nuembrecht, Germany)
Centrifuge tubes Quick-seal Polyallomer	Beckman (Palo Alto, CA, USA)
Cover glasses (20 mm)	Roth (Karlsruhe, Germany)
Cryo tube vials (1,8 ml)	Nunc (Roskilde, Denmark)
Cuvettes	Sarstedt (Nümbrecht, Germany)
Glass plates (18 x 7,5 x 0,08 mm)	Marienfeld Laboratory Glassware (Lauda-Königshofen, Germany)
Glass slides	Roth (Karlsruhe, Germany)
Parafilm	American National Can (Chicago, IL, USA)
Pipette tips	Sarstedt (Nümbrecht, Germany)
Reaction tubes (0,5 ml; 1,5 ml; 2,0 ml)	Sarstedt (Nuembrecht, Germany)
Serological Pipettes (5 ml; 10 ml; 25 ml)	Roth (Karlsruhe, Germany)
Syringe needles Sterican	Braun (Melsungen, Germany)
Syringe (10 ml, 20 ml, 50 ml)	Braun (Melsungen, Germany)

5.1.3 Chemicals

Ascorbate	Merck (Darmstadt, Germany)
Bacto tryptone	Becton, Dickinson & Co (Sparks, MD, USA)
$CHCl_3$	Merck (Darmstadt, Germany)
EDTA	AppliChem (Darmstadt, Germany)
Ethanol	Roth (Karlsruhe, Germany)
Glycerol	Roth (Karlsruhe, Germany)

HCl 1 M	Roth (Karlsruhe, Germany)
H_2SO_4 98 %	Merck (Darmstadt, Germany)
K_2SO_4	Roth (Karlsruhe, Germany)
Methanol	Fischer Scientific (Leicestershire, UK)
$MgCl_2$ $6H_2O$	Roth (Karlsruhe, Germany)
$Mg(NO_3)_2$	Aldrich (Steinheim, Germany)
NaCl	Fischer Scientific (Leicestershire, UK)
Na_2HPO_4	AppliChem (Darmstadt, Germany)
NaN_3	Roth (Karlsruhe, Germany)
NaOH	Merck (Darmstadt, Germany)
$(NH_4)_6Mo_7O_{24}$ $4H_2O$	Sigma (Steinheim, Germany)
Silica gel	Merck (Darmstadt, Germany)
Tris	Roth (Karlsruhe, Germany)

5.1.4 Enzymes

Lysozyme	Fluka (Buchs, Switzerland)
DNase	AppliChem (Darmstadt, Germany)
RNase	AppliChem (Darmstadt, Germany)

5.1.5 Human erythrocytes

Citrate-phosphate-dextrose-stabilized blood bags (CPD) (erythrocyte suspensions) were obtained from the blood bank of the municipal hospital (Karlsruhe, Germany). Opened bags were used on the same day only.

5.1.6 Bacterial strains

Micrococcus luteus ATCC 4698 was obtained from Marina Berditch from our group. A set of glycerol stocks (20 %) was freshly prepared prior to this study and was stored at -20 °C throughout.

5.1.7 Software

TopSpin 2.0 (Bruker)

XWinNMR (Bruker)

dmfit (Massiot 2002)

Canon RemoteCapture 2.7.3.23 (2003)

Cary WinUV

Illustrator 10 (Adobe)

Excel 2004 for Mac Version 11 (Microsoft)

Photoshop 7 (Adobe)

Power Point 2004 for Mac Version 11 (Microsoft)

Word 2004 for Mac Version 11 (Microsoft)

5.1.8 Preparation of Erythrocyte *ghosts*

Preparation of cell membranes from erythrocytes was performed with modified and adapted protocols published previously (Dodge 1963; Hanahan 1974).

Human erythrocytes (35 ml) from CPD-stabilized blood bags were washed twice with 10-fold excess of ice-cold 172 mM Tris (pH 7,6) (600g, 10 min, 4 °C) and once more in 2-fold excess in a smaller tube (50 ml) to pack cells. To lyse erythrocytes, aliquots of packed cells (5 ml) were diluted 30-fold in ice-cold 9 mM Tris (pH 7,6) and agitated carefully (5 min, on ice). The cell membranes were collected (20000g, 70 min, 4 °C) and resuspended in the previous solution. After three further washings, membrane pellets of four erythrocyte aliquots were combined in 9 mM Tris (pH 7,6) containing 0,01 % NaN_3, to prevent bacterial growth later, and washed twice more. The final washing step was performed in a smaller tube (50 ml) to reduce the extent of the pellet, as it was rather soft and difficult to handle. The final membrane sediment was translucent and light pink in colour. It was resuspended thoroughly by pipetting in about 5 ml of the latter solution and stored on ice for forthcoming soon use.

5.1.9 Preparation of *Micrococcus luteus* membrane vesicles

Preparation of cell membranes from *Micrococcus luteus* ATCC 4698 was performed with previous protocols, modified and adapted concerning growth, lysozyme treatment and washing of membrane vesicles (Prasad 1965; Pakkiri 2004; Powell 1975; Hrafnsdottir 1997).

M. luteus was grown in 800 ml of basal medium (10 g Bacto peptone, 5 g NaCl in 1000 ml double-distilled water, pH 7,5) contained in 2000 ml flasks. Flasks were shaken at 220 rpm at 37 °C. Cells were harvested after the log phase in the late growth phase (20-24 h, A_{650} = 3-4) by centrifugation (6000g, 15 min, 4 °C). The cell pellets were washed twice in (ca. 600 ml) 0,9 % NaCl solution (0 °C) and then once in (ca. 50 ml) 50 mM Tris (pH 7,5, room temperature), containing 10 mM EDTA and 30 mM $MgCl_2$. Wet weight was determined, and the cells were resuspended thoroughly at 200 mg wet weight per 1 ml of the previous solution (ca. 35 ml). Lysozyme (1 mg/ml), DNase and RNase (10 µg/ml each) were added, and the cells suspension was incubated over night (12-14 h) at room temperature with careful agitation. During the incubation the viscosity markedly increased first, then the suspension became homogenous and fluid.

The suspension was diluted 20-fold with ice-cold 9 mM Tris (pH 7,6) and agitated carefully (5 min, on ice). The cell suspension was centrifuged (700g, 30 min, 4 °C) to remove unbroken and unlysed cells. The supernatant was removed and centrifuged (26000g, 150 min, 4 °C) to collect membrane vesicles. The previous sediment of unlysed cells was suspended, agitated and centrifuged again, and the supernatant was used to resuspend the previous membrane vesicles. The combined membrane vesicles were sedimented as above, the membrane pellets were resuspended (ca. 160 ml) and sedimented again. Membrane vesicles were washed twice more in 9 mM Tris (pH 7,6) containing 0,01 % NaN_3. The final membrane sediment was transparent and intense amber in colour. It was resuspended thoroughly by pipetting in about 6 ml of the latter solution for NMR experiments on vesicle suspensions or in double-distilled water for oriented membranes, and stored on ice for forthcoming use.

5.1.10 Extraction of lipids

Lipids were extracted according to previously published protocols with some modifications (Folch 1957; Bligh 1959)

An aliquot of the membrane suspension (typically 100 µl) was homogenized by repeated vortexing and sonication in 20-fold excess of $CHCl_3$/methanol (2/1). Four aliquots of 0,9 % NaCl solution were added, and the previous procedure was repeated. The mixture was left standing for about 20 min at room temperature and was then separated into two phases by centrifugation (9000 g, 10 min, 4 °C). The lower organic phase (typically about 1200 µl) is the total pure lipid extract. A phosphate assay was usually performed on the same day. Lipid extracts were stored at -80 °C when not immediately used.

5.1.11 Phosphate assay

The amount of phospholipids was determined from lipid extracts as inorganic phosphate content after ashing of organic material according to previously published protocols with some modifications (Ames 1966; Ames 1960).

Aliquots of the lipid extracts (typically 50, 100 and 200 µl) were mixed in Duran glass tubes with 50 µl of $Mg(NO_3)_2$ in ethanol. The mixture was evaporated to dryness over a strong flame with rapid shaking and further heating until the fumes had disappeared. That procedure resulted in the ashing of phospholipids to deliver inorganic phosphate. After the tube had cooled, 300 µl of 1 M HCl was added. The tube was capped with a marble and heated in a water bath (95 °C) for 20 minutes to hydrolyze to inorganic phosphate any pyrophosphate formed in the ashing procedure. 700 µl of freshly prepared 10 % ascorbic acid

plus molybdate in H_2SO_4 in a ratio of 6/1 was added to the tube. The mixture was incubated for 20 minutes at 45 °C to develop a blue colour complex. Absorbance was read at 820 nm against a blank containing water. Calibration was done with a series of Na_2HPO_4 dilutions in water, to which ascorbate/molybdate was added and incubation at 45 °C was performed.

5.1.12 Preparation of vesicle suspension samples

0,5 to 2,5 ml of pure membrane suspension was transferred to a polyallomer centrifuge tube, filled up with 9 mM Tris (pH 7,6) containing 0,01% NaN_3, heat-sealed and centrifuged in a vertical rotor (360000g, 19-21 h, 4 °C). The supernatant was carefully removed with a syringe and discarded. The membrane pellet was transferred with a spatula into a small polyethylene bag which was heat sealed and packed into a second bag. The sample was stored at 4 °C until impending use.

5.1.13 Preparation of oriented samples

Membrane suspensions were washed once more with 10-fold excess off double-distilled water, containing 0,005 % NaN_3 (18000g, 90 min, 4 °C) (typically) to remove salts, which delay drying of samples and thereby enhance microbial contamination. Thin glass plates (18 mm x 7,5 mm x 0,08 mm) were washed with methanol and dried under vacuum for 2 h. Aliquots of the membrane suspension (about 100 µl) were deposited onto the glass plates (up to 18 plates in total), dried over silica gel for 2-3 d, stacked, covered with an additional glass plate and hydrated at 96 % relative humidity (over a saturated solution of K_2SO_4) at 46 °C for about 36 h. The stacks were wrapped in parafilm and a polyethylene foil. Samples were stored at -20 °C until impending use.

5.1.14 Solid state ^{31}P-NMR spectroscopy of cytoplasmic membranes

^{31}P-NMR measurements were carried out on a widebore Bruker Avance 500 MHz NMR spectrometer (Bruker Biospin, Karlsruhe, Germany) at a transmitter frequency of 202,5 MHz. A ^{1}H/X/Y probehead with interchangeable flat-coils for horizontal or vertical alignment of samples was used. Oriented samples were aligned with the lipid membrane normal either parallel or perpendicular to B_0. ^{31}P-NMR spectra were aquired at 308 K. Typically ^{1}H-decoupled Hahn-echo spectra were recorded with 90° pulse durations of 6 µs, relaxation delays of 2 s and inter-pulse echo delays of 30 µs. Number of scans was typically 1024 for oriented cytoplasmic membranes and 2048 for vesicle suspensions. Spectra were referenced against externally measured 85% H_3PO_4 solution aquired at 308 K which was set to 0 ppm.

5.2 Results

5.2.1 Erythrocyte *ghosts*

Preparations of erythrocyte *ghosts* could be monitored by optical microscopy throughout the whole process (Figure 5.1).
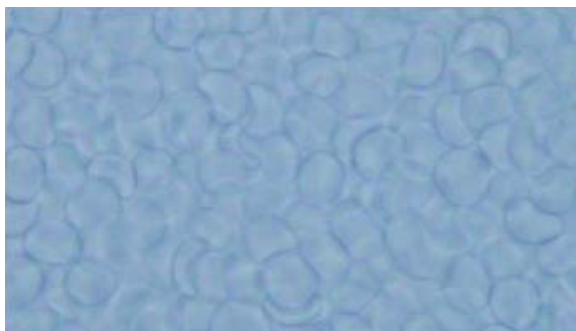

Figure 5.1 Representative photograph of erythrocyte *ghosts* after lysis of cells and repeated washings.

As the cytoplasm of erythrocytes comprises almost entirely of hemoglobin, the hemoglobin content (per cell dry weight) could be used as a measure for the purity of a preparation. Residual hemoglobin in erythrocyte *ghosts* was determined by KCN (Baake 1994) in preliminary experiments to adopt the method and later to control the consistency of the method. Cells contained well below 10 % of residual hemoglobin in both cases (data not shown).

Resulting membrane suspensions typically contained 4 to 8 mM of lipid phosphorus as determined by phosphate assay (data not shown). From each preparation process, typically a membrane suspension volume of 5 ml was available.

5.2.2 *Bacillus luteus* cytoplasmic membranes

Initially, for preparations of bacterial cytoplasmic membranes, *Bacillus subtilis* ATCC 6633 was employed. To access the membranes of *B. subtilis*, degradation of the cell wall by lysozyme and/or disruption of cells by French pressure cell or by sonification was performed. None of these methods delivered satisfying vesicle preparations in sufficient yield for solid state NMR spectroscopy. Membranes could be traced by the enzyme succinic acid dehydrogenase (SDH) of the respiratory chain, residing in the cell membrane of *B. subtilis* (results not shown). According to this, the largest amount of membrane material appeared to be lost during the first step of slow centrifugation. Optical microscopy observations showed

high numbers of unlysed cells in the sediment (pictures not shown). Apart from the low sensitivity of *B. subtilis* to lysozyme, the major difficulty became obvious in ^{31}P-NMR spectroscopy of membrane vesicle suspensions, employed to control the quality of the preparations. Membrane preparations were homogenous in microscopy (pictures not shown), but ^{31}P-NMR spectra suffered from a dominating signal component around the isotropic position (Figure 5.2). This component could not be removed upon further washing of membranes, hence was presumed to be membrane-related, and assigned to the phosphorus-containing teichoic acids (LTA), abundant in *B. subtilis*.
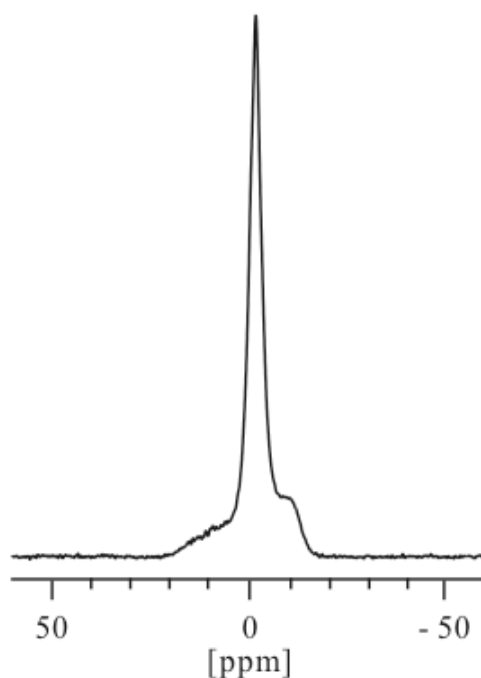
Figure 5.2 ^{31}P-NMR spectrum of unoriented membranes of *B. subtilis*. The spectrum is dominated by a large signal around the isotropic position. The signal of phospholipids in a lamellar lipid phase in vesicles can be identified underneath.

5.2.3 *Micrococcus luteus* cytoplasmic membranes

The enzyme SDH of the respiratory chain was employed as a marker enzyme in preparatory experiments to monitor small-sized cytoplasmic membrane vesicles of *Micrococcus luteus* ATCC 4698 (Figure 5.3). The largest amount of membrane material appeared to be lost during the first step of slow centrifugation (results not shown). Optical microscopy observations showed high numbers of unlysed cells in the sediment (pictures not shown). However, to achieve purer membrane preparations, these fractions were discarded. As

monitored by SDH, membrane vesicles from the supernatant could be recovered in each washing step.
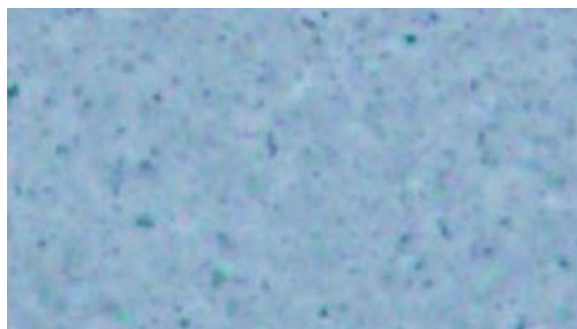
Figure 5.3 Representative photograph of *M. luteus* membrane vesicles after lysis of cells and repeated washings.

Since teichoic acids are absent in *M. luteus* envelopes, and the major membrane-related phosphorus-containing components are phospholipids, solid state ^{31}P-NMR spectroscopy was suited well to track the removal of residual cytoplasmic content in successive steps of a membrane preparation. In *M. luteus* membrane preparations, signals from phosphorous-containing components other than from phospholipids in the fluid lamellar lipid phase, disturbed the spectrum initially, but were possible to reduce upon additional lysis and sedimentation (Figure 5.4) and were apparently absent in the final membrane vesicles (Figure 5.5 upper right).
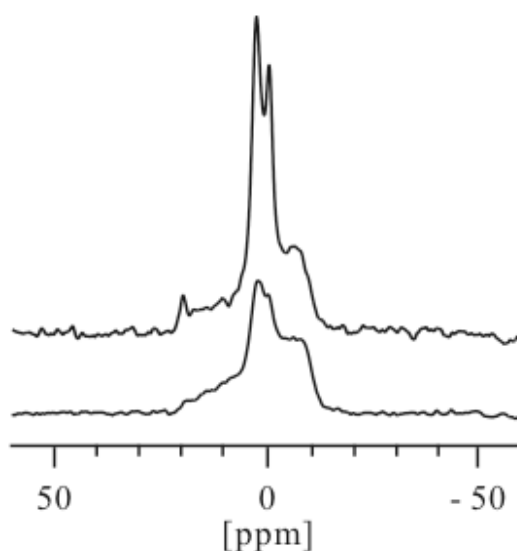
Figure 5.4 ^{31}P-NMR spectra of unoriented membranes of *M. luteus*. Upper spectrum obtained after initial hypotonic lysis of *M. luteus* cells and first sedimentation of membranes. Lower spectrum obtained after second lysis and sedimentation. The spectrum of the final membrane vesicles is shown in Figure 5.5.

Resulting membrane suspensions contained typically 1 to 2 mM of presumable lipid phosphorous as shown by phosphate assay (data not shown). From each preparation process, typically a membrane suspension volume of 6 ml was available.

5.2.4 Solid state ^{31}P-NMR spectroscopy of cytoplasmic membrane preparations

Representative solid state ^{31}P-NMR spectra of pure membranes of erythrocytes and *M. luteus* as vesicle suspensions as well as oriented samples at 308 K are shown in Figure 5.5. CSA parameters are listed in Table 5.1.

Figure 5.5 ^{31}P-NMR spectra of unoriented (upper) and oriented (middle and lower row) membranes of erythrocytes (left column) and *M. luteus* (right column) at 308 K. Spectra of oriented samples aquired at 0° (middle row) and 90° (lower row) tilt.

Table 5.1 Characteristic CSA parameters [ppm] extracted from spectra of unoriented and oriented membranes of erythrocytes and *M. luteus* in Figure 5.5.

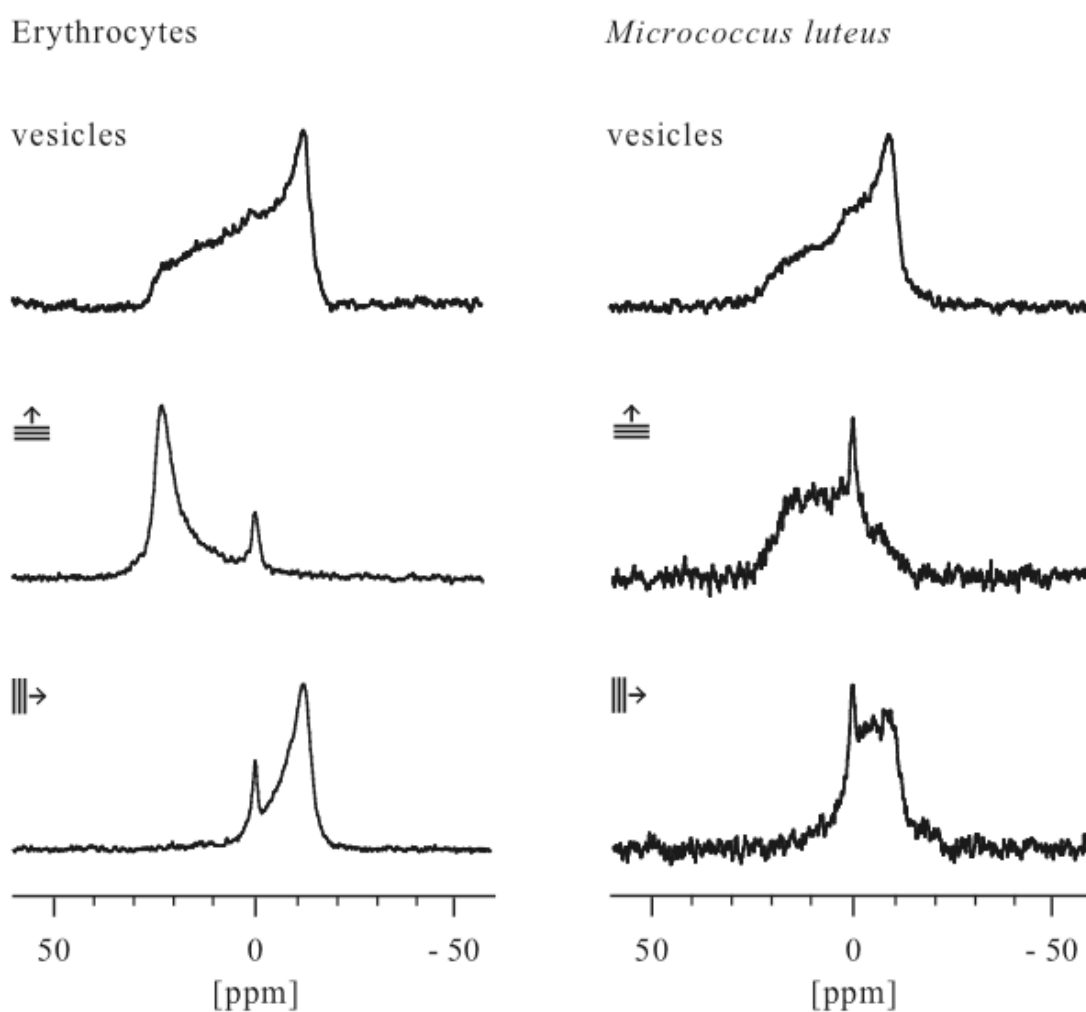|		Erythrocytes	*M. luteus*
Vesicle suspension	$\sigma_{\text{II}} - \sigma_{\perp}$	35	27
Oriented sample (0°)	σ_{II}	23	17
Oriented sample (90°)	$\sigma_{\perp}$	-12	-9
	$\sigma_{\text{II}}(0°) - \sigma_{\perp}(90°)$	35	26

Suspensions of cell membranes show broad powder spectra with shoulders at +23 ppm and -12 ppm for erythrocytes and +17 ppm and -9 ppm for *M. luteus*. The line shapes correspond to spherically distributed phospholipids rotating freely along their longitudinal axis, i.e. lipids within a fluid phase membrane (see section 2.3.4). A small isotropic-like component of varying intensity could be observed non-systematically among different freshly prepared samples.

Oriented samples of erythrocytes aligned at 0° and 90° tilt of their membrane normal with respect to the magnetic field give rise to signals with well-defined peaks around +23 ppm and -12 ppm with a width of 6 and 7 ppm, respectively, demonstrating good alignment of phospholipids. No separate signals of individual types of phospholipids in erythrocyte membranes are resolved. Oriented samples at 0° and 90° tilt exhibit isotropic signals, coinciding with isotropic signals observed in spectra of unoriented membranes.

Oriented samples of *M. luteus* give rise to signals at approximately +17 ppm as the 0° edge and at -9 ppm as the 90° edge of the spectrum, demonstrating alignment of phospholipids. No separate signals of individual types of phospholipids are resolved. Signal widths of 24 and 15 ppm are significantely larger as in oriented erythrocyte membranes. As in oriented erythrocyte membranes, isotropic signals with low intensity are present.

Both types of membranes show good match of CSA values from unoriented and oriented samples (Table 5.1).

^{31}P-NMR spectra of cytoplasmic membranes of erythrocytes and *Micrococcus luteus* together with peptide were comparable to spectra of pure membranes shown above (Figure 5.5).

5.3 Discussion

The preparation of erythrocyte ghosts is well-established. Some solid state NMR investigations have already been performed on erythrocyte membrane vesicles (McLaughlin 1975; Yeagle 1982) and even on erythrocyte membranes, aligned by an isopotential spin-dry ultracentrifugation technique (Gröbner 1997). Cytoplasmic membrane preparations of Bacteria, however, have apparently never been employed in solid state NMR spectroscopy. In this part of the present study, cell membranes of human erythrocytes and the Gram-positive bacterium *M. luteus* were prepared as vesicle suspension and oriented bilayers, for solid state NMR structural studies of an AMP in an environment closer to the in vivo situation than any previously used membrane systems.

Membranes were prepared by hypotonic lysis of cells, followed by extensive washing of vesicles. The quality of the membrane preparations was monitored directly by ^{31}P-NMR spectroscopy of vesicles. Membrane preparations exhibited the characteristic line shape for a lamellar phase in vesicle suspensions and showed orientation of phospholipids in macroscopically aligned bilayers, thus providing a situation utilizable to study PGLa. The rather high mosaic spread of the oriented lipids on glass slides was assigned largely to the complex lipid composition and high amount of protein in cell membranes. These effects have to be more pronounced in the *M. luteus* membranes, as they contain 70 to 80 % of proteins, compared to roughly 50 % in erythrocytes membranes. *M. luteus* membranes indeed exhibited spectra with significantly more inhomogenities and a far larger mosaic spread as in erythrocytes, whose spectra were smooth and peaked. Yet, it should also be considered that preparations of *M. luteus* membranes consist of much smaller vesicles, whereas erythrocyte preparations delivered ghosts as large as the original cells. An isotropic component observable in both types of oriented samples could be due to residual inorganic phosphorus after washing, or a fraction of non-bilayer lipid phase like micelles or a cubic phase. Since this was only a minor component in the spectra, it was not further investigated. However, these isotropic signals were empirically found to be useful as an internal reference and as an indicator on the hydration status of a sample. They are comperatively sharp in freshly prepared samples, but were found to broaden, decrease or vanish during long measurements upon heating. This was attributed to the drying of a sample, as the initial isotropic signal could be restored after rehydration of a sample.

Initial attempts on *B. subtilis* delivered unsuitable material, presumably not in view of the membranes themselves, but with regard to the ^{31}P-NMR spectrum employed for control, as spectra of phospholipids were dominated by some large isotropic compount. Since this

component was not removable by washing and therefore obviously membrane-bound, it presumably originates from teichoic acids, which are known to be abundant in the envelope of most Gram-positive bacteria including *B. subtilis*. *M. luteus*, in this respect, poses a lucky exception, as its envelope is not only devoid of teichoic acids, but also of other phosphorus-containing polymers. Instead, it contains the functionally analogous and phosphate-free lipomannan, which is also not removable even by extensive washing (Pless 1975).

6 Solid state NMR investigations of PGLa in cytoplasmic membranes

6.1 Materials and methods

Instruments, consumables, chemicals and other materials used below are described in 4.1 and 5.1. Samples were prepared with erythrocyte *ghosts* or *M. luteus* membrane vesicles as obtained in 5.1.8 and 5.1.9, respectively. 13CF$_3$-Phg PGLa was applied to cytoplasmic membrane preparations at the desired P/PL ratio (peptide to phospholipid ratio) on the basis of the amount of phospholipids determined in 5.1.11.

6.1.1 Preparation of vesicle suspension samples

The appropriate amount of peptide (about 0,2-0,6 mg) was dissolved in 9 mM Tris (pH 7,6) containing 0,01 % NaN$_3$ (typically 1-2 ml) by thorough vortexing and sonication. An appropiate volume of membrane vesicle suspension (about 0,5-2,5 ml) was added. The suspension was incubated overnight (14-16 h) at room temperature with careful agitation, then transferred to a polyallomer centrifuge tube, filled up with above Tris buffer, heat-sealed and centrifuged in a vertical rotor (360000g, 19-21 h, 4 °C). A sample of the supernatant was used for ^{19}F-NMR spectroscopy in solution to ensure that the peptide was in the membrane pellet. The membrane pellet was transferred with a spatula into a small polyethylene bag which was heat sealed and packed into a second bag. The sample was stored at 4 °C until impending use.

6.1.2 Preparation of oriented samples

Prior to the addition of peptide, membrane suspensions were washed once more with 10-fold excess of double-distilled water, containing 0,005 % NaN$_3$ (18000g, 90 min, 4 °C) (typically) to remove salts, which delay drying of samples and thereby enhance microbial contamination. The appropiate amount of peptide (typically 0,1-0,5 mg) was dissolved in double-distilled water (about 40 µl) by thorough vortexing and sonication. An appropiate volume of the membrane vesicle suspension (typically 0,9-1,8 ml) was added. The suspension was incubated overnight (about 14 h) at room temperature with careful agitation. Thin glass plates (18 mm x 7,5 mm x 0,08 mm) were washed with methanol and dried under vacuum for 2 h. Aliquots of the membrane suspension with peptide (about 100 µl) were deposited onto the glass plates (up to 18 plates in total), dried over silica gel for 2-3 d, stacked, covered with an additional glass plate and hydrated at 96 % relative humidity (over a saturated solution of

K_2SO_4) at 46 °C for about 36 h. The stacks were wrapped into parafilm and a polyethylene foil. Samples were stored at -20 °C until impending use.

6.1.3 Solid state NMR spectroscopy

^{31}P-NMR spectroscopy was carried out as described in 5.1.14. ^{19}F-NMR was performed as described in 4.1.9, except for the higher number of scans being 10000 to 60000 for samples at high P/PL ratios and 20000 to 100000 for samples at low P/PL ratios.

6.2 Results

The given ratio P/PL denotes the ratio of peptide (P) to phospholipid (PL) as determined by the assay for inorganic phosphate.

After incubation of membranes with 13CF$_3$-Phg PGLa and collection of material for unoriented samples by ultracentrifugation, a sample of the supernatant was used for ^{19}F-NMR spectroscopy in solution. No signal was observed (spectra not shown). Moreover, ^{19}F-NMR spectra of vesicle suspensions did not reveal line shapes characteristic for unoriented immobilized (aggregated) peptide. Thus, 13CF$_3$-Phg PGLa can be concluded to be bound to the membrane.

^{31}P-NMR spectra of the presented samples recorded before and after ^{19}F-NMR measurements, showed no signs of sample drying.

Since dipolar splittings obtained from a single PGLa analogue are not enough for a full determination of the peptide helix orientation in accordance with the peptide amphipathicity, the characteristic line shapes obtained for 13CF$_3$-Phg PGLa from synthetic lipid bilayers were used as a fingerprint for a particular alignment.

6.2.1 13CF$_3$-Phg PGLa in vesicle suspensions of erythrocyte membranes

As can be seen from Figure 6.1, the NMR line shape at 308 K corresponds to surface aligned 13CF$_3$-Phg PGLa in vesicles, irrespective of the P/PL ratio (compare line shape to Figure 4.4 at low P/L ratio from 298 K upwards and to Figure 4.10 at high P/L ratio at 323 K, both representing the S-state). Negative dipolar splittings, as extracted from the spectra, correspond to 13CF$_3$-Phg PGLa in the S-state, as determined for oriented samples (compare to 4.2.2, 4.2.3 and 4.2.5).

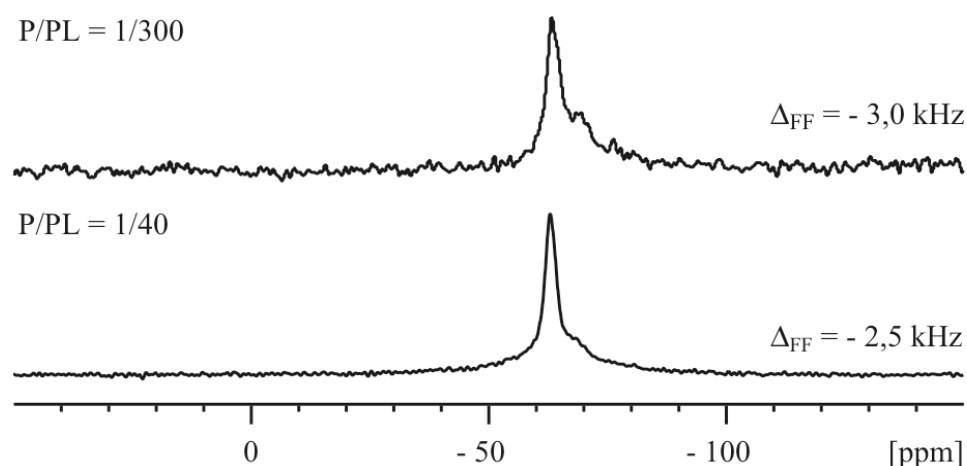**Figure 6.1 Solid state ^{19}F-NMR spectra of 13CF$_3$-Phg PGLa in suspensions of erythrocyte ghosts at low (1/300) (upper) and high (1/40) (lower) P/PL ratio at 308 K.** Dipolar splittings are estimated with an accuracy of 0,5 kHz.

Figure 6.2 shows the NMR spectra at high P/PL ratio (1/40) as a function of temperature. Upon increase in temperature from 278 to 318 K a gradual change in the line shape can be observed. Identical numbers of scans for each step in the temperature series allow the comparison of signal intensities. At 278 K a sharp isotropic signal dominates the spectrum. Its intensity decreases and base broadens gradually upon elevation of temperature, and the negative dipolar splitting corresponding to a surface alignment evolves. Due to the collection of less scans in the temperature series compared to the spectra recorded at single temperatures to avoid drying out of the sample, the signal intensity and the signal-to-noise ratio of spectra in Figure 6.2 is lower compared to Figure 6.1. Here, the surface alignment is only well-pronounced at 318 K.
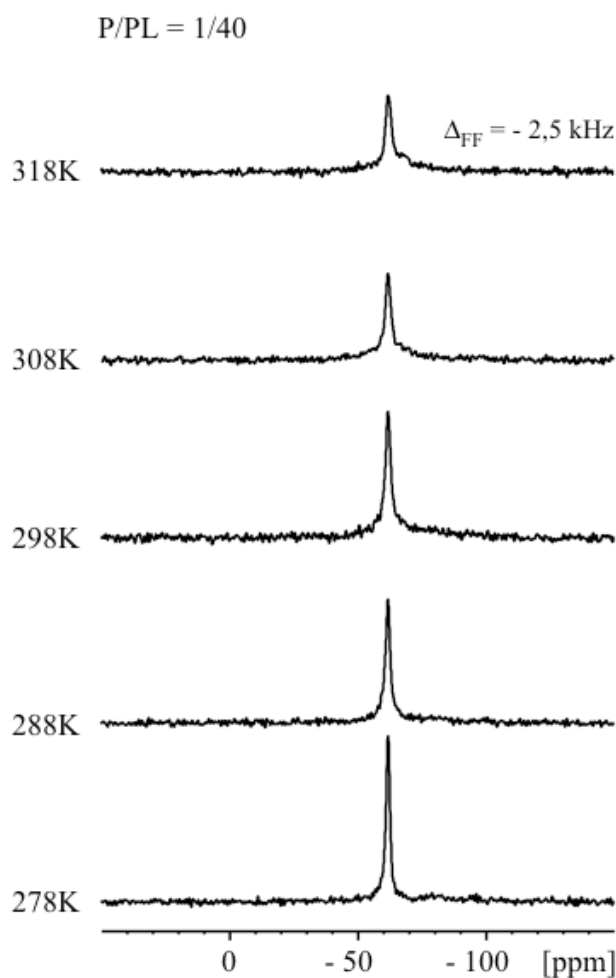

Figure 6.2 Solid state ^{19}F-NMR spectra of 13CF$_3$-Phg PGLa in suspensions of erythrocyte ghosts at high P/PL ratio (1/40) at different temperatures. Dipolar splitting at 318 K is estimated with an accuracy of 0,5 kHz.

6.2.2 13CF$_3$-Phg PGLa in vesicle suspensions of *Micrococcus luteus*

The ^{19}F-NMR spectrum at high P/PL ratio (1/20) at 308 K (Figure 6.3) does not show signals corresponding to aggregated and unoriented peptide. Similar to erythrocyte membranes at 308 K (Figure 6.1), it exhibits the line shape characteristic for 13CF$_3$-Phg PGLa in a surface alignment in vesicles. However, it is comparatively broad and with a slightly larger negative dipolar splitting. Compared to erythrocytes, the spectrum is better resolved.

P/PL = 1/20

$\Delta_{FF} = - 3,5$ kHz

0   - 50   - 100   [ppm]

Figure 6.3 Solid state ^{19}F-NMR spectrum of 13CF$_3$-Phg PGLa in suspensions of *M. luteus* membrane vesicles at high P/PL ratio (1/20) at 308 K. Dipolar splitting is estimated with an accuracy of 0,5 kHz.

With increase in temperature from 288 K to 323 K at high P/PL ratio (1/20), a gradual significant change of the line shape can be observed (Figure 6.4). At lower temperature the signal around the isotropic position is broad. An unresolved signal with a dipolar splitting estimated to be larger than -5 kHz at 288 K, distinctly differs from the maximal splitting of an unoriented immobilized peptide. Upon increase in temperature, the base of the isotropic signal becomes narrower. The size of the negative dipolar splitting decreases, while its triplet gradually becomes more pronounced. These might indicate a reorientation between an inclined to a surface alignment. At 308 K, the line shape as above can already be identified. Upon further elevation of temperature, the dipolar splitting becomes more pronounced and its value slightly decreases.
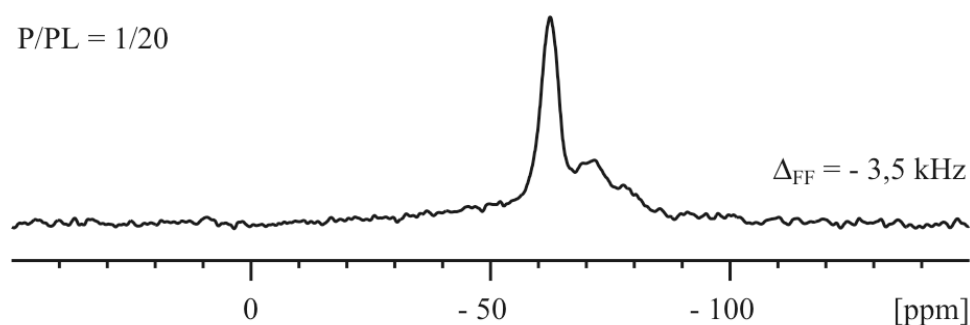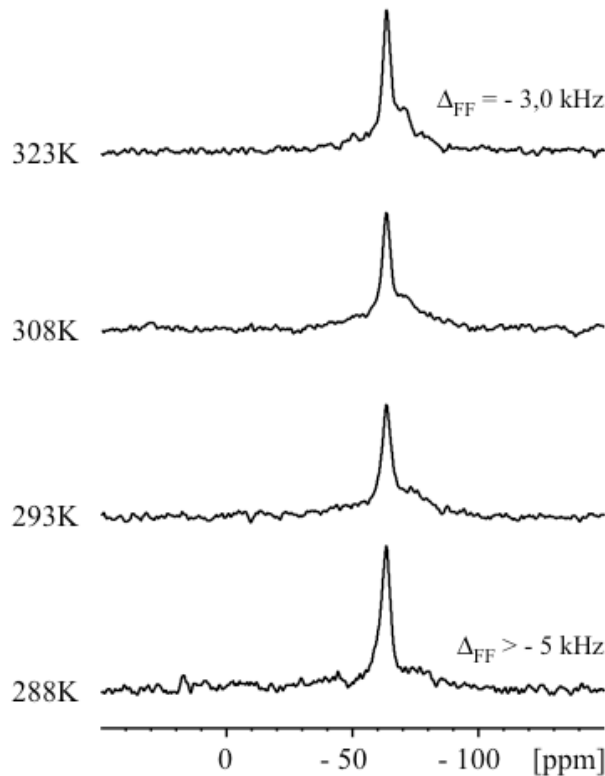
Figure 6.4 Solid state ^{19}F-NMR spectra of 13CF$_3$-Phg PGLa in suspensions of *M. luteus* membrane vesicles at high P/PL ratio (1/20) at different temperatures. Dipolar splitting at 323 K was estimated with an accuracy of 0,5 kHz.

6.2.3 13CF3-Phg PGLa in oriented erythrocyte membranes

13CF$_3$-Phg PGLa at high P/PL ratio (1/40) in oriented membranes of erythrocytes at 308 K exhibits broad lines with negative dipolar splittings at 0° as well as 90° tilt (Figure 6.5), as they are expected for unoriented immobilized peptide. However, as the line shapes are not identical, but a slight shift upon tilt and hence membrane-bound and oriented peptide was suspected, a temperature series was performed.

Figure 6.5 Solid state ^{19}F-NMR spectra of 13CF$_3$-Phg PGLa in oriented erythrocyte membranes at high P/PL ratio (1/40) at 308 K at 0° (upper) and 90° tilt (lower). Dipolar splittings are estimated with an accuracy of 0,5 kHz.

^{19}F-NMR spectra at high P/PL ratio (1/40) show a temperature-dependent change of line shape in the range from 308 K to 343 K (Figure 6.6). Broad negative dipolar splittings as shown in Figure 6.5, expected for unoriented immobilized peptide, persist throughout all temperatures. However, at elevated temperature, the evolution of positive dipolar splittings corresponding to a surface alignment of 13CF$_3$-Phg PGLa can also be observed (compare e.g. Figure 4.3, Figure 4.5).
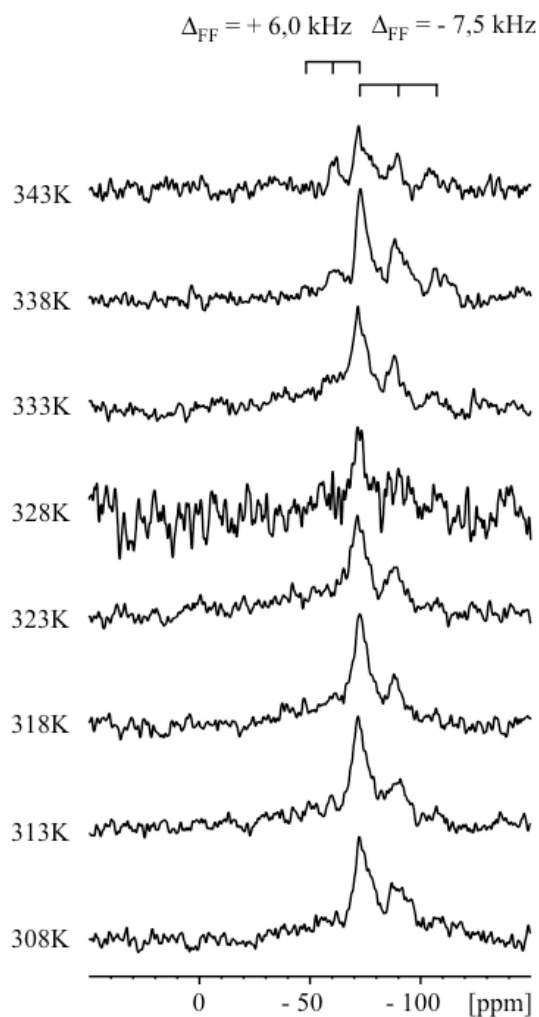
Figure 6.6 Solid state ^{19}F-NMR spectra of 13CF$_3$-Phg PGLa in oriented erythrocyte membranes at high P/PL ratio (1/40) at different temperatures. The spectra are measured with the membrane normal of the oriented sample aligned at 0° tilt with regard to the magnetic field. Dipolar splittings at 343 K are estimated with an accuracy of 0,5 kHz.

Solid state NMR spectra at lower P/PL ratios, i.e. 1/80, 1/100 and 1/300 at 308 K, exhibited comparable line shapes and similar dipolar splittings as those in Figure 6.5. However, due to the low amount of peptide, the signal-to-noise ratio of these spectra was poor (data not

shown). At elevated temperature for lower P/PL ratios, indications of positive dipolar splitting as those at the P/PL ratio of 1/40 (Figure 6.6) were found. A better-resolved spectrum at the low P/PL ratio of 1/300 at 308 K was obtained through a measurement with a larger number of scans. Due to the long measurement times needed, such experiments could not be performed for all temperatures at all P/L ratios.

In addition to a large negative dipolar splitting indicating unoriented immobilized peptide, the spectrum at the low P/PL of 1/300 exhibits positive dipolar splitting corresponding to a surface alignment of 13CF$_3$-Phg PGLa (Figure 6.7).

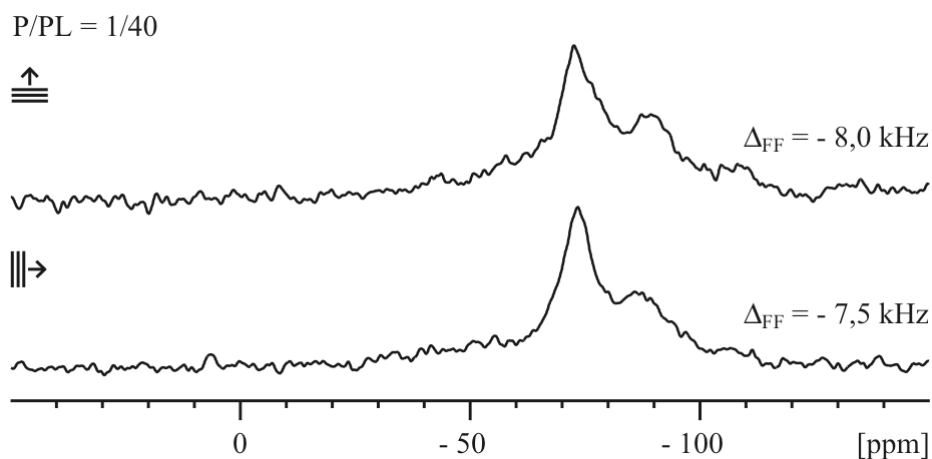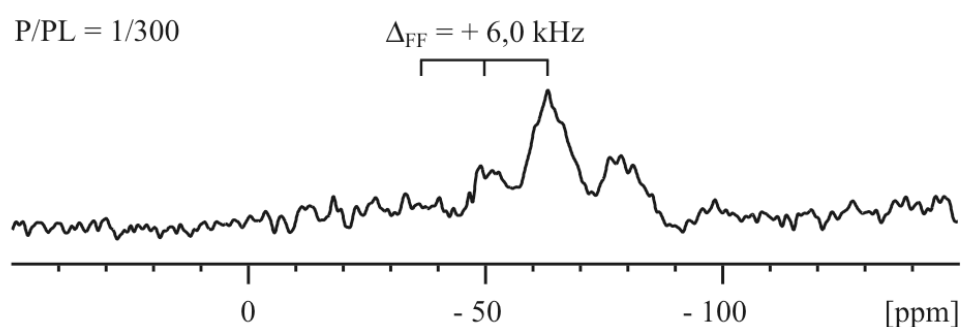**Figure 6.7 Solid state ^{19}F-NMR spectrum of 13CF$_3$-Phg PGLa in oriented erythrocyte membranes at low P/PL ratio (1/300) at 308 K.** Positive dipolar splitting was estimated with an accuracy of 0,5 kHz.

6.2.4 13CF$_3$-Phg PGLa in oriented *Micrococcus luteus* membranes

Solid state ^{19}F-NMR spectra of 13CF$_3$-Phg PGLa in oriented membranes of *M. luteus* at high P/PL ratio (1/40) do not show the line shape of unoriented immobilized peptide (Figure 6.8). Significantly different line shapes are obtained at 0° and 90° tilt at 308 K as well as at 338 K. Thus, the peptide can be concluded to be membrane-bound and oriented to a large extent. Signals are broad and not well-resolved. Yet a surface alignment of PGLa is indicated, as scaling of signal around the isotropic position upon tilt of sample by 90° at 308 K as well as at 338 K can be observed. Additionally, a broad signal with negative dipolar splitting is present at 308 K at 0° tilt, but does not scale around the isotropic position upon tilting. This broad unresolved component is absent at elevated temperature. At elevated temperature, an additional signal shows large negative dipolar splitting at 0° as well as 90° tilt. Similar line shapes with a large negative dipolar splitting suggest unoriented immobilized peptide. All spectra exhibit an isotropic component largely broadening to the base.

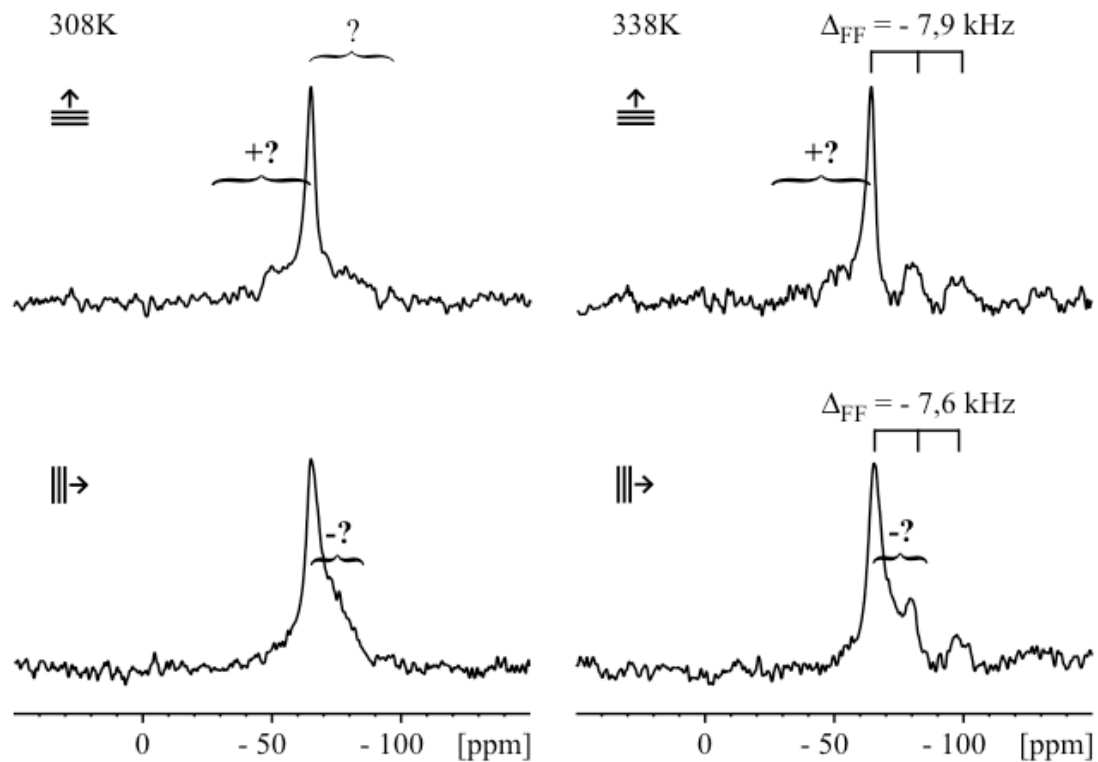**Figure 6.8 Solid state ^{19}F-NMR spectra of 13CF$_3$-Phg PGLa in oriented membranes of *M. luteus* at high P/L ratio (1/40) at 308 K (left column) and 338 K (right column). The samples are aligned with their membrane normals at 0° (upper row) and 90° (lower row) tilt with regard to the magnetic field.**

6.3   Discussion

In the present study, an AMP was observed for the first time directly in isolated cell membranes of human erythrocytes and the Gram-positive bacterium *M. luteus* by ^{19}F-solid state NMR spectroscopy. 13CF$_3$-Phg PGLa was investigated in vesicle suspensions as well as oriented samples of cell membranes to identify the alignment states of the peptide, which so far have been found in synthetic model membranes composed of few lipids. An attempt was made to identify the principle differences in both types of membranes, and to correlate them with the preference of the AMP for bacterial membranes.

Previous NMR spectroscopical investigations on AMPs in general and on PGLa in particular, restricted themselves to synthetic model membranes or bilayers composed of membrane lipid extracts. A previous study employed suspensions of live bacterial cells and focused on the behaviour of phospholipids upon application of AMPs (Chia 2000). However, as it could be demonstrated in this thesis, various additional sources of phosphorus from inside and outside the cell may severely influence ^{31}P-NMR spectra, thus hindering the interpretation (5.2).

Analysis of PGLa structure and alignment in synthetic model membranes (see 4) revealed that among the CF$_3$-Phg PGLa analogues, 13CF$_3$-Phg PGLa is the most appropiate peptide to apply to cell membranes. It demonstrates the most varied ^{19}F-NMR spectra for the three alignment states of the peptide. The solid state ^{19}F-NMR spectra from this peptide, measured in oriented samples and multilamellar vesicles, provided the reference set for the identification of the S-state, T-state and I-state (see the respective spectra in 4.2 and the corresponding discussion in 4.3).

As it can be judged from solid state ^{31}P-NMR spectra, none of the employed samples indicate perturbance of the cytoplasmic membranes due to the bound PGLa, in full correspondence to the peptide behaviour in synthetic lipid bilayers.

It could be demonstrated that multiple alignments of PGLa coexist in cell membranes of erythrocytes as well as of *M. luteus*. Thus, an unambiguous assignment of the states cannot be performed with only one labeled PGLa analogue, as this provides only limited (general) information. Yet this result it not surprising, as a similar tendency of multiple simultaneous alignments could already be observed for PGLa in the presence of magainin 2 in oriented lipid bilayers (4.2.7 and 4.3). Furthermore, in cell membranes, a much higher heterogenity of lipid species, as well as large amount and variety of protein components, are expected to exert

significant effects in this respect, i.e. by crowding. Another difficulty is the undefinable fluidity state of the overall cell membranes. As it was demonstrated in this study, PGLa alignment in lipid bilayers is strongly influenced by the phase behaviour. Correspondingly, different environments provided in cell membranes simultaneously may exert a severe influence on peptide behaviour.

Despite these difficulties, for all employed samples at the physiologically relevant temperature around 308 K, a surface alignment can be identified for PGLa.

The surface alignment is indicated in oriented erythrocyte membranes at the low P/PL ratio of 1/300. It is least pronounced at the high P/PL ratio of 1/40, though it is suggested upon tilt of sample by 90°, and it can be discriminated upon elevation of temperature. Both samples are dominated by a spectral component of unoriented immobilized peptide. Correspondingly, the surface alignment can be observed in vesicles, with a dominating isotropic signal instead, which is more pronounced at high P/PL ratio. It is thus reasonable to assign these obvious additional signals from both types of samples to each other. As solution ^{19}F-NMR spectroscopy demonstrated that PGLa was not dissolved in the media of vesicles, this population of peptide can be assumed to be bound to the membrane or its associated structures. The contribution of this population may be larger at higher P/PL ratio in both types of samples, as only a limited extent of peptide is accomodated by the lipid environment in a surface alignment. It cannot be determined if this residual PGLa is bound to some extramembraneous structure mobile in membrane suspension, but with restricted mobility in stacked membranes or resides in the lipid environment in a state exhibiting different behaviour under the conditions of vesicles and oriented membranes. The participation in the surfacial alignment, however, for high P/PL ratio was found to increase upon elevation of temperature.

Contrary to erythrocytes, at the physiologically relevant temperature around 308 K, no contribution of unoriented and immobilized peptide at high P/PL ratio to the spectra of oriented membranes of *M. luteus* can be identified. Surfacially aligned PGLa is indicated in vesicles and confirmed in oriented membranes upon tilt of sample by 90°. At the same time, in oriented membranes a broad negative signal does not scale around the isotropic position. The speculation that it may correspond to immobilized and strongly tilted peptide at least is not eliminated by vesicle samples. Overall, the extent of this PGLa fraction is found to decrease with increasing temperature, in favour of a surfacial alignment.

Among the physiologically most relevant systems investigated here, namely cell membrane vesicles at around 308 K, no indication for a major contribution of a stably inserted alignment can be found. Even beyond that, no clear evidence for this state can be identified. Yet it cannot be excluded for minor populations of PGLa, for reasons described above. However, the present results rather suggest a transient formation of pores.

Amongst others, the selectivity of natural linear positively charge amphipathic AMPs, including PGLa for bacterial over animal cells is attributed to the interaction with the negative or zwitterionic lipids of the respective cell membranes. Although there is no simple correlation between the peptide charge and the antimicrobial activity of an AMP, the reduction or addition of positive charge to a peptide was demonstrated to result in a loss or a gain of activity, respectively. These electrostatic interactions are supposed to play a major role in the initial attraction and the partitioning of AMPs into lipid bilayers (Dathe 1999). On the other hand, the presence of zwitterionic lipids and cholesterol, which are abundant in erythrocyte membranes, was demonstrated to contribute to the protection of lipid membranes from lysis by magainin 2 and related peptides (Matsuzaki 1995a). It may thus be speculated that PGLa may be accomodated to a larger extent by the membranes of *M. luteus* as compared to those of erythrocytes. Possibly, the fraction of peptide found in addition to the surfacially aligned PGLa in erythrocyte membranes represents peptide bound to some extracellular membrane compount, presumably the glycokalyx, whereas in *M. luteus* membranes, the major part of PGLa resides in the lipid environment.

7   Summary

For PGLa and magainin 2 separately, as well as together as a synergetic pair, toroidal pore formation is proposed as an explanation of the permeabilizing activity. Previously, by solid state NMR spectroscopy, PGLa was found to realign in synthetic lipid bilayers upon increase in peptide concentration from a monomeric flat surface-bound S-state to a tilted T-state, presumably forming homodimers. In the presence of equimolar quantity of magainin 2, PGLa was shown to adopt a membrane-inserted I-state, compatible with a pore structure.

In this study, to find out whether the observed alignment states (S, T and I) occur only in synthetic lipid bilayers or are relevant in vivo, PGLa alignment was studied by solid state NMR in cell membranes. The highly NMR-sensitive, and in biological samples background-free ^{19}F nucleus in form of a CF_3-group was used as a reporter for the peptide orientation.

Cell membranes from the Gram-positive bacterium *Micrococcus luteus* and from human erythrocytes were prepared by hypotonic lysis followed by extensive washing. After incubation of membranes with appropiate amounts of peptide, PGLa orientation was observed either in vesicle suspensions after collecting material by centrifugation, or in oriented membranes after drying and rehydration on glass support.

Solid state ^{31}P-NMR spectroscopy of phospholipids served to control the quality of the membrane preparations. Spectra showed a typical lamellar lipid phase of vesicles and alignment of lipids in oriented samples. The mosaic spread of aligned lipids was attributed to the complex lipid composition of cell membranes and high amount of protein. Correspondingly, this was larger for *M. luteus* membranes, containing higher amounts of protein compared to erythrocytes. Initial attempts to prepare membranes of *B. subtilis* delivered unsuitable material. Spectra of phospholipids were dominated by some large isotropic compound, presumably originating from teichoic acids. These are abundant in the envelope of most Gram-positive bacteria, however are luckily absent in *M. luteus*.

The complexity of real biomembranes required additional prior investigation of PGLa structure and orientation in the presence or absence of magainin 2 in synthetic lipid bilayers under different conditions. PGLa could be demonstrated to adopt each alignment state (S, T and I) individually, dependent on temperature and lipid bilayer phase. In presence of magainin 2, PGLa showed in principle the same temperature-dependent realignment. Yet, its behaviour was more complex. In the gel phase, in addition to the I-state, a surface aligned fraction of PGLa was found. Furthermore, magainin 2 stabilized a deeper inserted T-state into fluid lipid membranes. These results support models that explain permeabilizing activity of PGLa and PGLa/magainin 2 as a result of pore formation. Furthermore, the faster formation

of more stable transmembrane assemblies, served as an explanation to rationalize the enhanced functional activity of the synergetic heterodimer PGLa/magainin 2, may be attributed to the observed larger inclination and a presumably deeper immersion of the peptides.

For investigations in cell membranes, the PGLa analogue exhibiting the most pronounced difference in spectral appearance between the three alignment states found in synthetic model membranes was selected (13CF$_3$-Phg PGLa).

Hence, for the first time it was possible to observe an antimicrobial peptide directly in cell membranes by solid state ^{19}F-NMR spectroscopy. The coexistence of multiple alignment states could be demonstrated. This is not surprising, considering the heterogeneous composition and complex phase behaviour of real biomembranes. A similar tendency of multiple simultaneous alignments as well as a temperature-dependent behaviour could indeed be observed in synthetic lipid bilayers. Thus, an unambiguous assigment of all alignment states is not possible with one labeled PGLa analogue alone. However, a surface alignment could be identified irrespective of peptide concentration. On the contrary, an I-state was not indicated. If pore formation occurs in cell membranes, it appears to be a transient event. Yet it can be trapped and investigated under conditions of oriented samples.

8   Concluding remark and outlook

In the present study, an AMP was observed for the first time directly in cell membranes by solid state ^{19}F-NMR spectroscopy. Coexistence of different alignment states was indicated for PGLa in cell membranes of *M. luteus* and human erythrocytes of complex composition and undefined fluidity state. This behaviour was anticipated by preceding studies of PGLa and PGLa/magainin 2 on a smaller scale in simple synthetic lipid bilayers. Taken together, significant insight was gained not only with regard to a further factor affecting the realignment of these peptides, but towards a broader understanding of the activity of AMPs in real biomembranes.

Since the present study demonstrated the principle feasibility to observe AMPs directly in real cell membranes, this potential should be tapped in following studies, towards the understanding of the structure and orientation of PGLa in vivo. At first, protocols for the preparation of cell membranes should be optimized in terms of yield. Then, to overcome the overwhelming coexistence of alignment states, a limited range of appropiate experimental temperatures may be defined. For that purpose, the accurate determination of cell membrane properties is necessary, i.e. establishment of phase diagrams, determination of phase transition temperature(s), width(s) of the phase transition(s) or otherwise. For a refinement of PGLa structure and orientation in cell membranes, additional analogues need to be employed. In a simpler approach, appropiate analogues may be chosen to identify a particular alignment and to distinguish between different states, like 13CF3-Phg turned out to be the most appropiate one to identify a surface alignment among the others. Enzymatic digestion of extramembraneous components may help to differentiate between membrane- and non-membrane-bound fractions of peptide. Magainin 2 was already employed on bacterial membranes in initial experiments of this study. Yet due to lack of references then, results were ambiguous. With the results presented here, the implications are promising and systematic studies should be performed likewise.

9 Zusammenfassung

Für die membranpermeabilisierenden Eigenschaften der Peptide PGLa und Magainin 2, sowohl einzeln wie auch als synergetisches Paar, wird die Bildung einer toroidalen Pore angenommen. Mittels Festkörper-NMR-Spektroskopie konnte für PGLa an synthetischen Modellmembranen mit steigender Peptidkonzentration die Umorientierung von einem peripher gebundenen Zustand (S-state) zu einer schrägen Ausrichtung (T-state) gezeigt werden. In Anwesenheit von Magainin 2 wurde ein tief eingesenkter Zustand (I-state) entdeckt, welcher mit einer vorgeschlagenen Pore vereinbar wäre.

In dieser Studie wurde PGLa in Zellmembranen untersucht, um die Relevanz der beobachteten Orientierungen (S-,T- und I-state) für biologische Systeme zu prüfen. Mittels ^{19}F-NMR-Spektroskopie wurde die Orientierung des CF_3-markierten PGLa beobachtet.

Membranen des Gram-positiven Bakteriums *Micrococcus luteus* und menschlicher Erythrozyten wurden mittels hypotoner Lyse und ausgiebigem Waschen gewonnen und mit Peptid inkubiert. Die Ausrichtung des PGLa wurde in Membranvesikelsuspension und in orientierten Membranen beobachtet.

^{31}P-NMR-Spektroskopie an den Phospholipiden diente der Kontrolle der Präparatequalität und zeigte eine typische lamellare Lipidphase in Vesikeln und Ausrichtung der Lipide in orientierten Proben. Die Spreizung der Lipidsignale orientierter Proben wurde auf die komplexe Zusammensetzung und den hohen Proteingehalt der Zellmembranen zurückgeführt. Sie war erwartungsgemäss größer für Membranen von *M. luteus*, welche im Vergleich zu Erythrozyten erheblich mehr Protein enthalten. Anfängliche Membranpräparationen an *B. subtilis* lieferten kein geeignetes Material. Die ^{31}P-Spektren wurden von einem isotropen Signal beherrschte, welches vermutlich auf Teichonsäuren zurückzuführen ist. Diese sind üblicherweise in Gram-positive Bakterien vorhanden, wobei *M. luteus* eine Ausnahme darstellt.

Die Komplexität biologischer Membranen machte vorbereitende eingehendere Untersuchungen an PGLa mit und ohne Magainin 2 an synthetischen Lipidmembranen notwendig. In beiden Fällen konnte für PGLa eine Umorientierung in Abhängigkeit von Temperatur und Lipidphase gezeigt werden. Im Gelzustand der Lipidmembranen nahm PGLa einen I-Zustand an. In Anwesenheit von Magainin 2 konnte eine zusätzliche Peptidfraktion in einer peripheren Bindung gefunden werden. In der flüssigkristallinen Phase lag in beiden Fällen eine schräge Orientierung vor, welche jedoch bei Anwesenheit von Magainin 2 eine deutlich stärkere Neigung aufwies. Diese Ergebnisse stützen die Annahmen, dass die Permeabilisierung von Membranen durch PGLa und PGLa/Magainin 2 auf Porenbildung beruht. Als Erklärung für die synergetische Wirkung von PGLa/Magainin 2 wird eine schnellere Bildung langlebigerer Poren diskutiert. Dieses Verhalten könnte mit dem hier beobachteten stärkeren Neigungswinkel, welcher zu einem tieferen Einsenken der Peptide in die Lipidmembran führen sollte, teilweise erklärt werden.

Jenes PGLa Analogon, dessen ^{19}F-NMR-Spektren der drei Zustände (S, T und I) sich am stärksten unterschieden (13CF_3-Phg PGLa), wurde für weitere Untersuchungen an Zellmembranen herangezogen.

Somit konnte das erste Mal ein antimikrobielles Peptid mittels Festkörper-NMR-Spektroskopie am hochempfindlichen ^{19}F-Kern in biologischen Membranen beobachtet werden. Es konnte die gleichzeitige Anwesenheit unterschiedlicher Ausrichtungen des PGLa gezeigt werden. Dies ist insofern nicht überraschend, da Zellmembranen sehr komplex aufgebaut sind und nur ein wenig definiertes Phasenverhalten aufweisen. Bereits in Membranen synthetischer Lipide wurden tatsächlich zwei Zustände gleichzeitig gefunden. Zudem konnte gezeigt werden, dass das Verhalten des PGLa von der Lipidphase abhängt. Eine zweifelsfreie Zuordnung aller Ausrichtungen in Zellmembranen ist somit mit einem einzigen Analogon nicht möglich. Allerdings konnte eine periphere Bindung des PGLa an Zellmembranen identifiziert werden. Im Gegensatz dazu fand sich jedoch kein Hinweis auf eine Insertierung des PGLa entsprechend einer Pore. Sollte Porenbildung in Zellmembranen stattfinden, muss es sich um ein vorübergehendes Ereignis handeln. Dieses kann in orientierten Lipidmembranen festgehalten und untersucht werden.

10   Reference list

Afonin, S. (2003a). Structural studies on membrane-active peptides in lipid bilayers by solid state 19F NMR. Promotionsschrift, Friedrich Schiller Universität Jena.

Afonin, S., R. W. Glaser, et al. (2003b). 4-fluorophenylglycine as a label for 19F NMR structure analysis of membrane-associated peptides. Chembiochem 4(11): 1151-63.

Alberts, B., A. Johnson, et al. (2004). Molekularbiologie der Zelle. 4. Auflage. Weinheim, Wiley-VCH Verlag.

Ames, B. N. (1966). Assay of inorganic phosphate, total phosphate and phosphatases. Methods Enzymol 8: 115-118.

Ames, B. N., D. T. Dubin (1960). The role of polyamines in the neutralization of bacteriophage deoxyribonucleic acid. J Biol Chem 235: 769-75.

Andreu, D., H. Aschauer, et al. (1985). Solid-phase synthesis of PYLa and isolation of its natural counterpart, PGLa [PYLa-(4-24)] from skin secretion of Xenopus laevis. Eur J Biochem 149(3): 531-5.

Araki, Y., T. Nakatani, et al. (1972). Occurrence of N-nonsubstituted glucosamine residues in peptidoglycan of lysozyme-resistant cell walls from Bacillus cereus. J Biol Chem 247(19): 6312-22.

Atrih, A., G. Bacher, et al. (1999). Analysis of peptidoglycan structure from vegetative cells of Bacillus subtilis 168 and role of PBP 5 in peptidoglycan maturation. J Bacteriol 181(13): 3956-66.

Baake, M., A.Gilles (1994). Hämatologie. Theorie und Praxis für medizinische Assistenzberufe. Darmstadt, GIT Verlag GmbH.

Banerjee, S. K., E. Holler, et al. (1975). Reaction of N-acetylglucosamine oligosaccharides with lysozyme. Temperature, pH, and solvent deuterium isotope effects; equilbrium, steady state, and pre-steady state measurements. J Biol Chem 250(11): 4355-67.

Banerjee, S. K., I. Kregar, et al. (1973). Lysozyme-catalyzed reaction of the N-acetylglucosamine hexasaccharide. Dependence of rate on pH. J Biol Chem 248(13): 4786-92.

Baron, S. (Ed.) (1991) Medical Microbiology. Fourth Edition The University of Texas Medical Branch at Galveston.

Bechinger, B., K. Lohner (2006). Detergent-like actions of linear amphipathic cationic antimicrobial peptides. Biochim Biophys Acta 1758(9): 1529-39.

Bechinger, B. (1999). The structure, dynamics and orientation of antimicrobial peptides in membranes by multidimensional solid state NMR spectroscopy. Biochim Biophys Acta 1462(1-2): 157-83.

Bechinger, B., M. Zasloff, et al. (1998). Structure and dynamics of the antibiotic peptide PGLa in membranes by solution and solid state nuclear magnetic resonance spectroscopy. Biophys J 74(2 Pt 1): 981-7.

Bechinger, B., M. Zasloff, et al. (1993). Structure and orientation of the antibiotic peptide magainin in membranes by solid state nuclear magnetic resonance spectroscopy. Protein Sci 2(12): 2077-84.

Bechmann, W., Schmidt, J. (2000). Struktur- und Stoffanalytik mit spektroskopischen Methoden. Stuttgart Leipzig Wiesbaden, B. G. Teubner.

Begemann, H., J. Rastatter (Hrsg.) (1993). Klinische Hämatologie. 4., überarbeitete und erweiterte Auflage. Stuttgart New York, Georg Thieme Verlag.

Berditsch, M., S. Afonin, et al. (2007). The ability of Aneurinibacillus migulanus (Bacillus brevis) to produce the antibiotic gramicidin S Is correlated with phenotype variation. Appl Environ Microbiol 73(20): 6620-8.

Bligh, E. G., W. J. Dyer (1959). A rapid method of total lipid extraction and purification. Can J Biochem Physiol 37(8): 911-7.

Cao, M., J. D. Helmann (2004). The Bacillus subtilis extracytoplasmic-function sigmaX factor regulates modification of the cell envelope and resistance to cationic antimicrobial peptides. J Bacteriol 186(4): 1136-46.

Chia, B. C. S., Y.-H. Lam et al. (2000). A 31P NMR study of the interaction of amphibian antimicrobial peptides with the membranes of live bacteria. Letters in Peptide Science 7: 151-156.

Cullis, P. R., M. J. Hope, et al. (1986). Lipid polymorphism and the roles of lipids in membranes. Chem Phys Lipids **40**(2-4): 127-44.

Dathe, M., M. Schumann, et al. (1996). Peptide helicity and membrane surface charge modulate the balance of electrostatic and hydrophobic interactions with lipid bilayers and biological membranes. Biochemistry 35(38): 12612-22.

Dathe, M., T. Wieprecht (1999). Structural features of helical antimicrobial peptides: their potential to modulate activity on model membranes and biological cells. Biochim Biophys Acta 1462(1-2): 71-87.

de Bony, J., A. Lopez, et al. (1989). Transverse and lateral distribution of phospholipids and glycolipids in the membrane of the bacterium Micrococcus luteus. Biochemistry 28(9): 3728-37.

Denich, T. J., L. A. Beaudette, et al. (2003). Effect of selected environmental and physico-chemical factors on bacterial cytoplasmic membranes. J Microbiol Methods 52(2): 149-82.

Dockray, G. J, C. R. Hopkins (1975). Caerulein secretion by dermal glands in Xenopus laevis. J Cell Biol 64(3): 724-33.

Dodge, J. T., C. Mitchell, et al. (1963). The preparation and chemical characteristics of hemoglobin-free ghosts of human erythrocytes. Arch Biochem Biophys 100: 119-30.

Duerr, M. J. E. (2002). Solid state NMR spectroscopy. Principles and applications., Blackwell Science.

Dürr, U. (2005). Solid state 19F-NMR studies on fluorine-labeled model compounds and biomolecules. Dissertation, Universität Karlsruhe (TH).

Durst, U. N., E. Bruder, et al. (1991). Micrococcus luteus: a rare pathogen of valve prosthesis endocarditis. Z Kardiol 80(4): 294-8.

Epand, R. M., H. J. Vogel (1999). Diversity of antimicrobial peptides and their mechanisms of action. Biochim Biophys Acta 1462(1-2): 11-28.

Evans, W. H., J. M. Graham, (Hrsg.) (1991). Struktur und Funktion biologischer Membranen. Stuttgart New York, Georg Thieme Verlag.

Fields, G. B., R. L. Noble (1990). Solid phase peptide synthesis utilizing 9-fluorenylmethoxycarbonyl amino acids. Int J Pept Protein Res 35(3): 161-214.

Folch, J., M. Lees, et al. (1957). A simple method for the isolation and purification of total lipides from animal tissues. J Biol Chem 226(1): 497-509.

Ganz, T. (2001). Fatal attraction evaded. How pathogenic bacteria resist cationic polypeptides. J Exp Med 193(9): F31-4.

Gibson, B. W., L. Poulter, et al. (1986). Novel peptide fragments originating from PGLa and the caerulein and xenopsin precursors from Xenopus laevis. J Biol Chem 261(12): 5341-9.

Giovannini, M. G., L. Poulter, et al. (1987). Biosynthesis and degradation of peptides derived from Xenopus laevis prohormones. Biochem J 243(1): 113-20.

Glaser, R. W., C. Sachse, et al. (2005). Concentration-dependent realignment of the antimicrobial peptide PGLa in lipid membranes observed by solid state 19F-NMR. Biophys J 88(5): 3392-7.

Glaser, R. W., C. Sachse, et al. (2004). Orientation of the antimicrobial peptide PGLa in lipid membranes determined from 19F-NMR dipolar couplings of 4-CF3-phenylglycine labels. J Magn Reson 168(1): 153-63.

Glaser, R. W., A. S. Ulrich (2003). Susceptibility corrections in solid-state NMR experiments with oriented membrane samples. Part I: applications. J Magn Reson 164(1): 104-14.

Graham, J., M., Higgins, J., A. (1998). Molekularbiologische Membrananalyse. Heidelberg Berlin, Spektrum Akademischer Verlag GmbH.

Gröbner, G., A. Taylor, et al. (1997). Macroscopic orientation of natural and model membranes for structural studies. Anal Biochem 254(1): 132-8.

Hanahan, D. J., J. E. Ekholm (1974). The preparation of red cell ghosts (membranes). Methods Enzymol 31(Pt A): 168-72.

Hancock, R. E., D. S. Chapple (1999). Peptide antibiotics. Antimicrob Agents Chemother 43(6): 1317-23.

Hancock, R. E., H. G. Sahl (2006). Antimicrobial and host-defense peptides as new anti-infective therapeutic strategies. Nat Biotechnol 24(12): 1551-7.

Hanke W. H. R. (1997). Methoden der Membranphysiologie. Heidelberg Berlin, Spektrum Akademischer Verlag GmbH.

Hara, T., Y. Mitani, et al. (2001). Heterodimer formation between the antimicrobial peptides magainin 2 and PGLa in lipid bilayers: a cross-linking study. Biochemistry 40(41): 12395-9.

Hayashi, H., Y. Araki, et al. (1973). Occurrence of glucosamine residues with free amino groups in cell wall peptidoglycan from bacilli as a factor responsible for resistance to lysozyme. J Bacteriol 113(2): 592-8.

Helmerhorst, E. J., W. Van't Hof, et al. (1997). Synthetic histatin analogues with broad-spectrum antimicrobial activity. Biochem J 326 (Pt 1): 39-45.

Herbette, L., J. K. Blasie, et al. (1984). Phospholipid asymmetry in the isolated sarcoplasmic reticulum membrane. Arch Biochem Biophys 234(1): 235-42.

Hoffmann, D. (2000). NMR-Untersuchungen an Nanokapsel-Dispersionen. Dissertation, Gerhard-Mercator-Universität Duisburg.

Hoffmann, W., K. Richter, et al. (1983). A novel peptide designated PYLa and its precursor as predicted from cloned mRNA of Xenopus laevis skin. Embo J 2(5): 711-4.

Hrafnsdottir, S., J. W. Nichols, et al. (1997). Transbilayer movement of fluorescent phospholipids in Bacillus megaterium membrane vesicles. Biochemistry **36**(16): 4969-78.

Huang, H. W. (2000). Action of antimicrobial peptides: two-state model. Biochemistry 39(29): 8347-52.

James, T. (1998). Fundamentals of NMR. http://www.biophysics.org/education/james.pdf. (Nov 2007).

Kamysz, W., M. Okroj, et al. (2003). Novel properties of antimicrobial peptides. Acta Biochim Pol 50(2): 461-9.

Katsaras, J., T. Gutberlet (Eds.) (2001). Lipid Bilayers: Structure and interactions. Berlin Heidelberg New York, Springer-Verlag.

Kennedy, L. D. (1974). Teichoic acid synthesis in Bacillus stearothermophilus. Biochem J 138(3): 525-35.

Lewis, R. N., Y. P. Zhang, et al. (2005). Calorimetric and spectroscopic studies of the phase behavior and organization of lipid bilayer model membranes composed of binary mixtures of dimyristoylphosphatidylcholine and dimyristoylphosphatidylglycerol. Biochim Biophys Acta **1668**(2): 203-14.

Lommerse, P. H., H. P. Spaink, et al. (2004). In vivo plasma membrane organization: results of biophysical approaches. Biochim Biophys Acta 1664(2): 119-31.

Ludtke, S. J., K. He, et al. (1996). Membrane pores induced by magainin. Biochemistry 35(43): 13723-8.

Madigan, M. T., J. M. Martinko, et al. (2001). Brock Mikrobiologie. Heidelberg Berlin, Spektrum Akademischer Verlag GmbH.

Manno, S., Y. Takakuwa, et al. (2002). Identification of a functional role for lipid asymmetry in biological membranes: Phosphatidylserine-skeletal protein interactions modulate membrane stability. Proc Natl Acad Sci U S A 99(4): 1943-8.

Massiot, D., F.Fayon, et al. (2002). Modelling one- and two-dimensional Solid State NMR spectra.. Magnetic Resonance in Chemistry, 40: 70-76.

Matsuzaki, K. (1999). Why and how are peptide-lipid interactions utilized for self-defense? Magainins and tachyplesins as archetypes. Biochim Biophys Acta 1462(1-2): 1-10.

Matsuzaki, K., K. Sugishita, et al. (1998a). Relationship of membrane curvature to the formation of pores by magainin 2. Biochemistry 37(34): 11856-63.

Matsuzaki, K., Y. Mitani, et al. (1998b). Mechanism of synergism between antimicrobial peptides magainin 2 and PGLa. Biochemistry 37(43): 15144-53.

Matsuzaki, K., O. Murase, et al. (1996). An antimicrobial peptide, magainin 2, induced rapid flip-flop of phospholipids coupled with pore formation and peptide translocation. Biochemistry 35(35): 11361-8.

Matsuzaki, K., K. Sugishita, et al. (1995a). Molecular basis for membrane selectivity of an antimicrobial peptide, magainin 2. Biochemistry 34(10): 3423-9.

Matsuzaki, K., O. Murase, et al. (1995b). Translocation of a channel-forming antimicrobial peptide, magainin 2, across lipid bilayers by forming a pore. Biochemistry 34(19): 6521-6.

McLaughlin, A. C., P. R. Cullis, et al. (1975). Application of 31P NMR to model and biological membrane systems. FEBS Lett 57(2): 213-8.

Mookherjee, N., R. E. Hancock (2007). Cationic host defence peptides: innate immune regulatory peptides as a novel approach for treating infections. Cell Mol Life Sci 64(7-8): 922-33.

Moore, K. S., C. L. Bevins, et al. (1991). Antimicrobial peptides in the stomach of Xenopus laevis. J Biol Chem 266(29): 19851-7.

Neuhaus, F. C., J. Baddiley (2003). A continuum of anionic charge: structures and functions of D-alanyl-teichoic acids in gram-positive bacteria. Microbiol Mol Biol Rev 67(4): 686-723.

Nishida, M., Y. Imura, et al. (2007). Interaction of a magainin-PGLa hybrid peptide with membranes: insight into the mechanism of synergism. Biochemistry 46(49):14284-90.

Nultsch, W. (1996). Allgemeine Botanik. 10., neu bearbeitete und erweiterte Auflage. Stuttgart New York, Georg Thieme Verlag.

Otvos, L., Jr. (2005). Antibacterial peptides and proteins with multiple cellular targets. J Pept Sci 11(11): 697-706.

Owen, P., M. R. Salton (1975). A succinylated mannan in the membrane system of Micrococcus lysodeikticus. Biochem Biophys Res Commun 63(4): 875-80.

Pakkiri, L. S., B. A. Wolucka, et al. (2004). Structural and topological studies on the lipid-mediated assembly of a membrane-associated lipomannan in Micrococcus luteus. Glycobiology 14(1): 73-81.

Papo, N., Y. Shai (2003). Can we predict biological activity of antimicrobial peptides from their interactions with model phospholipid membranes? Peptides 24(11): 1693-703.

Park, C. B., K. S. Yi, et al. (2000). Structure-activity analysis of buforin II, a histone H2A-derived antimicrobial peptide: the proline hinge is responsible for the cell-penetrating ability of buforin II. Proc Natl Acad Sci U S A 97(15): 8245-50.

Pietiainen, M., M. Gardemeister, et al. (2005). Cationic antimicrobial peptides elicit a complex stress response in Bacillus subtilis that involves ECF-type sigma factors and two-component signal transduction systems. Microbiology 151(Pt 5): 1577-92.

Pless, D. D., A. S. Schmit, et al. (1975). The characterization of mannan of Micrococcus lysodeikticus as an acidic lipopolysaccharide. J Biol Chem 250(4): 1319-27.

Powell, D. A., M. Duckworth, et al. (1975). A membrane-associated lipomannan in micrococci. Biochem J 151(2): 387-97.

Prasad, A. L. G. Litwack (1965). Growth and Biochemical Characteristics of Micrococcus Lysodeikticus, Sensitive or Resistant to Lysozyme. Biochemistry 4: 496-501.

Prenner, E. J., M. Kiricsi, et al. (2005). Structure-activity relationships of diastereomeric lysine ring size analogs of the antimicrobial peptide gramicidin S: mechanism of action and discrimination between bacterial and animal cell membranes. J Biol Chem 280(3): 2002-11.

Reddy, K. V., R. D. Yedery, et al. (2004). Antimicrobial peptides: premises and promises. Int J Antimicrob Agents 24(6): 536-47.

Sandra, A., R. E. Pagano (1978). Phospholipid asymmetry in LM cell plasma membrane derivatives: polar head group and acyl chain distributions. Biochemistry 17(2): 332-8.

Sato, H., J. B. Feix (2006). Peptide-membrane interactions and mechanisms of membrane destruction by amphipathic alpha-helical antimicrobial peptides. Biochim Biophys Acta 1758(9): 1245-56.

Schlegel, H. G. (1992). Allgemeine Mikrobiologie. 7., überarbeitete Auflage. Stuttgart New York, Georg Thieme Verlag.

Schwoch, G., H. Passow (1973). Preparation and properties of human erythrocyte ghosts. Mol Cell Biochem 2(2): 197-218.

Seddon, J. M. (1990). Structure of the inverted hexagonal (HII) phase, and non-lamellar phase transitions of lipids. Biochim Biophys Acta 1031(1): 1-69.

Seifert, H., M. Kaltheuner, et al. (1995). Micrococcus luteus endocarditis: case report and review of the literature. Zentralbl Bakteriol 282(4): 431-5.

Shai, Y. (1999). Mechanism of the binding, insertion and destabilization of phospholipid bilayer membranes by alpha-helical antimicrobial and cell non-selective membrane-lytic peptides. Biochim Biophys Acta 1462(1-2): 55-70.

Singer, S. J., G. L. Nicolson (1972). The fluid mosaic model of the structure of cell membranes. Science 175(23): 720-31.

Sitaram, N., R. Nagaraj (1999). Interaction of antimicrobial peptides with biological and model membranes: structural and charge requirements for activity. Biochim Biophys Acta 1462(1-2): 29-54.

Somerharju, P., J. A. Virtanen, et al. (1999). Lateral organisation of membrane lipids. The superlattice view. Biochim Biophys Acta 1440(1): 32-48.

Soravia, E., G. Martini, et al. (1988). Antimicrobial properties of peptides from Xenopus granular gland secretions. FEBS Lett 228(2): 337-40.

Strandberg, E., P. Wadhwani, et al. (2006). Solid state NMR analysis of the PGLa peptide orientation in DMPC bilayers: structural fidelity of 2H-labels versus high sensitivity of 19F-NMR. Biophys J 90(5): 1676-86.

Strandberg, E., S. Ozdirekcan, et al. (2004a). Tilt angles of transmembrane model peptides in oriented and non-oriented lipid bilayers as determined by 2H solid state NMR. Biophys J 86(6): 3709-21.

Strandberg, E., A. S. Ulrich (2004b). NMR Methods for Studying Membrane-Active Antimicrobial Peptides. Concepts Magn Reson Part A 23A: 89–120.

Stryer, L. (1999). Biochemie. 4. Auflage. Heidelberg Berlin, Spektrum Akademischer Verlag GmbH.

Subczynski, W. K., A. Wisniewska (2000). Physical properties of lipid bilayer membranes: relevance to membrane biological functions. Acta Biochim Pol 47(3): 613-25.

Sures, I., M. Crippa (1984). Xenopsin: the neurotensin-like octapeptide from Xenopus skin at the carboxyl terminus of its precursor. Proc Natl Acad Sci U S A 81(2): 380-4.

Sutcliffe, I. C., N. Shaw (1991). Atypical lipoteichoic acids of gram-positive bacteria. J Bacteriol 173(22): 7065-9.

Tamm, L. K. (2005). Protein-lipid interactions: From membrane domains to cellular networks. Weinheim, Wiley-VCH Verlag.

Ting-Beall, H. P., M. J. Costello, et al. (1981). Ultrastructure of hemoglobin-depleted human erythrocyte resealed ghosts. Biochim Biophys Acta 640(3): 807-11.

Toke, O. (2005). Antimicrobial peptides: new candidates in the fight against bacterial infections. Biopolymers 80(6): 717-35.

Tremouilhac, P. (2007). Orientational behavior of the antimicrobial peptide PGLa in a lipid membrane environment studied by solid-state 2H-NMR spectroscopy. Dissertation, Universität Karlsruhe (TH).

Tremouilhac, P., E. Strandberg, et al. (2006a). Synergistic transmembrane alignment of the antimicrobial heterodimer PGLa/magainin 2. J Biol Chem

Tremouilhac, P., E. Strandberg, et al. (2006b). Conditions affecting the re-alignment of the antimicrobial peptide PGLa in membranes as monitored by solid state (2)H-NMR. Biochim Biophys Acta 1758(9): 1330-42.

Tristram-Nagle, S., Y. Liu, et al. (2002). Structure of gel phase DMPC determined by X-ray diffraction. Biophys J 83(6): 3324-35.

Ulrich, A. S. (2004). Solid state 19F-NMR methods for studying biomembranes. Progress in NMR spectroscopy(46): 1-21.

Voet, D., J. Voet, et al. (2002). Lehrbuch der Biochemie. Weinheim, Wiley-VCH Verlag.

Wallace, B. A. (2000). Common structural features in gramicidin and other ion channels. Bioessays 22(3): 227-34.

Welby, M., Y. Poquet, et al. (1996). The spatial distribution of phospholipids and glycolipids in the membrane of the bacterium Micrococcus luteus varies during the cell cycle. FEBS Lett 384(2): 107-11.

Westerhoff, H. V., M. Zasloff, et al. (1995). Functional synergism of the magainins PGLa and magainin-2 in Escherichia coli, tumor cells and liposomes. Eur J Biochem 228(2): 257-64.

Wieprecht, T., O. Apostolov, et al. (2000). Membrane binding and pore formation of the antibacterial peptide PGLa: thermodynamic and mechanistic aspects. Biochemistry 39(2): 442-52.

Wu, M., E. Maier, et al. (1999). Mechanism of interaction of different classes of cationic antimicrobial peptides with planar bilayers and with the cytoplasmic membrane of Escherichia coli. Biochemistry 38(22): 7235-42.

Yang, L., T. A. Harroun, et al. (2001). Barrel-stave model or toroidal model? A case study on melittin pores. Biophys J 81(3): 1475-85.

Yawata, Y. (2003). Cell membrane. The red blood cell as a model. Weinheim, Wiley-VCH Verlag.

Yeagle, P. L. (1982). 31P nuclear magnetic resonance studies of the phospholipid-protein interface in cell membranes. Biophys J 37(1): 227-39.

Zasloff, M. (2002). Antimicrobial peptides of multicellular organisms. Nature 415(6870): 389-95.

Zasloff, M. (1987). Magainins, a class of antimicrobial peptides from Xenopus skin: isolation, characterization of two active forms, and partial cDNA sequence of a precursor. Proc Natl Acad Sci U S A 84(15): 5449-53.

Zhang, W., H. R. Kaback (2000). Effect of the lipid phase transition on the lactose permease from Escherichia coli. Biochemistry 39(47): 14538-42.

Zwaal, R. F., D. R.A., et al. (1976). The lipid bilayer concept of cell membranes. TIBS: 112-114.

11   Appendices

11.1 List of abbreviations

AMP	antimicrobial peptide
CF$_3$-Phg	L-4-trifluoromethyl-phenylglycine
CSA	chemical shift anisotropy
DMDG	dimannosyldiacylglycerol
DMPC	dimyristoylphosphatidylcholine
DMPG	dimyristoylphosphatidylglycerol
DPG	diphosphatidylglycerol
dw	dry weight
FID	free induction decay
GPI	glycosyl-phosphatidylinositol
LPS	lipopolysacccharide
LTA	lipoteichoic acids
Mag 2	magainin 2
NMR	nuclear magnetic resonance
PAS	principal axes system
PC	phosphatidylcholine
PE	phosphatidylethanolamine
PG	phosphatidylglycerol
PGLa	peptidyl-glycine-leucine-carboxyamide
Phg	phenylglycine
PI	phosphatidylinositol
P/L	peptide to lipid (ratio)
P/PL	peptide to phospholipid (ratio)
PS	phosphatidylserine
RF	radio frequency
RMSD	root mean square deviation
SDH	succinic acid dehydrogenase
SM	sphingomyelin
TA	teichoic acids
v/v	volume by volume
v/w	volume by weight
wt	wild type
WTA	wall teichoic acids

11.2 Publication list

Articles

Afonin, S., Grage, S., Ieronimo, M., Wadhwani, P. and Ulrich, A. S. 2007. *Temperature-dependent transmembrane insertion of the amphiphilic peptide PGLa in lipid bilayers observed by solid state ^{19}F-NMR.* J. Am. Chem. Soc. (Submitted)

Strandberg, E., Tiltak, D., Ieronimo, M., Kanithasen, N., Wadhwani, P., and Ulrich, A. S. 2007. *Influence of C-terminal amidation on the antimicrobial and hemolytic activities of cationic alpha-helical peptides.* Pure Appl. Chem. 79(4): 717-728.

Wadhwani, P., Afonin, S., Ieronimo, M., Buerck, J. and Ulrich, A. S. 2006. *Optimized protocol for synthesis of cyclic Gramicidin S: starting amino acid is key to high yield.* J. Org. Chem. 71(1): 55-61.

Book chapters

Wadhwani, P., P. Tremouilhac, Strandberg, E., Afonin, S., Grage, S., Ieronimo, M., Berditsch, M., Ulrich, A. S. 2007. *Using Fluorinated Amino Acids for Structure Analysis of Membrane-Active Peptides by Solid state ^{19}F-NMR.* Current fluoroorganic chemistry : new synthetic directions, technologies, materials, and biological applications. V. A. Soloshonok, K. Mikami, T. Yamazaki, J. T. Welch and J. F. Honek. Washington, DC, American Chemical Society: 431-446.

Posters presented on conferences

Ieronimo, M., Afonin, S., Wadhwani, P., Zimmermann, K., Ulrich, A. S. *Solid state ^{19}F-NMR investigations of the antimicrobial peptide PGLa in native membranes from bacteria and erythrocytes.* At CFN Summer School on Nano-Biology. 2007. Bad Herrenalb, Germany.

Ieronimo, M., Afonin, S., Wadhwani, P., Ulrich, A. S. *^{19}F-NMR structure analysis of antimicrobial peptides in native membranes from bacteria and erythrocytes.* At 6th Annual Surface and Colloid Symposium (Lipid-Peptide Interactions and Biological Function. 2006. Lund, Sweden.

11.3 Curriculum vitae

Marco Ieronimo

Geburtsdatum	05.04.1975
Geburtsort	Baden-Baden
Staatsangehörigkeit	deutsch
Familienstand	ledig

Promotion

11/2004 – 02/2008	Promotion am Institut für Organische Chemie (Lehrstuhl Biochemie) der Universität Karlsruhe unter der Betreuung von Prof. A. S. Ulrich

Studium

09/2004	Diplom in Biologie
01/2004 – 09/2004	Diplomarbeit am Institut für Organische Chemie (Lehrstuhl Biochemie) der Universität Karlsruhe unter der Betreuung von Prof. A. S. Ulrich
10/1997 – 09/2004	Studium der Biologie an der Universität Karlsruhe

Berufsausbildung

09/1995 – 07/1997	Ausbildung zum Kaufmann im Groß- und Außenhandel (Fachrichtung Außenhandel) bei der Overlack Furniere GmbH, Rastatt (Abschluss IHK)

Schule

09/1995 – 06/1997	Ludwig-Erhard-Schule, Karlsruhe (Kaufmännische Berufsschule) (Abschluss)
08/1985 – 06/1995	Goethe-Gymnasium Gaggenau (Abschluss allgemeine Hochschulreife)

Berufstätigkeiten

11/2004 – 10/2007	Wissenschaftlicher Mitarbeiter am Institut für Organische Chemie (Lehrstuhl für Biochemie) der Universität Karlsruhe
04/2003 – 12/2003	Wissenschaftlicher Mitarbeiter am Institut für Organische Chemie (Lehrstuhl für Biochemie) der Universität Karlsruhe
09/1995 – 07/1997	Auszubildender bei der Overlack Furniere GmbH, Rastatt